Dipl.-Ing. Stefan Retschitzegger

High-temperature corrosion in biomass-fired fixed bed boilers

DOCTORAL THESIS

to achieve the university degree of

Doktor der technischen Wissenschaften

submitted to

Graz University of Technology

Supervisor

Dipl.-Ing. Dr.techn. Univ.-Doz. Prof., Ingwald Obernberger

Institute of Process and Particle Engineering

Graz, 2017

AFFIDAVIT

I declare that I have authored this thesis independently, that I have not used other than the declared sources/resources, and that I have explicitly marked all material which has been quoted either literally or by content from the sources used. The text document uploaded to TUGRAZonline is identical to the present doctoral thesis.

_____ _____

Date Signature

Acknowledgements

First of all, I would like to express my gratitude to my supervisor, Prof. Ingwald Obernberger, for his guidance.

I also wish to thank my day-to-day supervisor Thomas Brunner for his patience and for teaching me a great deal about biomass combustion.

Special thanks go to my colleagues at BIOENERGY 2020+, in particular to Thomas Gruber, who supported me with valuable discussions on corrosion processes and worked with me on the corrosion measurements. Further, I want to thank my dear friend and colleague Peter Sommersacher for the moral support he provided and for his professional input on fuel and ash chemistry.

Another thank you goes to Norbert Kienzl and his team in the laboratory of BIOENERGY 2020+. Thank you for the numerous chemical analyses over the last few years. I would also like to thank Angelika Reichmann for the SEM/EDX analyses included in this work and her help with the interpretation of the results.

Finally, I would like to give warmest thanks to my wife Regina and my children Florian and Elisabeth. I dedicate this work to you. Thank you for your never-ending patience and encouragement (and the occasional home-baked cake for moral support).

Abstract

High-temperature corrosion in biomass-fired boilers is a major problem affecting heat exchanger surfaces which may cause a substantial reduction of their service life as well as unexpected shutdowns of plants. In order to minimize the risk of high-temperature corrosion, steam temperatures in biomass CHP plants based on water-tube steam boilers are typically kept at rather moderate levels, which results in decreased electrical efficiencies. In order to improve the efficiency of future biomass CHP plants at acceptable high-temperature corrosion risks, systematic investigations of high-temperature corrosion in biomass-fired fixed bed boilers using online corrosion probes were performed for the first time.

First, investigations were conducted in real-scale biomass-fired grate furnaces with water-tube steam boilers. Here, the online corrosion probes were applied over a period of several months in the radiative sections of a 28 MW_{NCV} CHP plant firing chemically untreated wood chips, and in a 58 MW_{NCV} CHP plant firing waste wood (A1-A4 in accordance with German standards). Within these test runs, proof of the applicability of online corrosion probes for biomass-fired boilers was furnished.

The test runs were performed using the superheater material 13CrMo4-5. In the process, the probe surface temperatures were varied between 400°C and 550°C, and flue gas temperatures ranging from 710°C to 950°C were investigated. The measurement data showed a clear dependence of the corrosion rate on the probe surface temperature for both test runs. A distinctive influence of flue gas temperatures on the corrosion rates could only be determined during the test runs in the wood chips fired CHP plant. In this case, the data were evaluated over extended periods (weeks) and were used to establish a correlation between flue gas temperatures and corrosion rates. The data obtained in the waste wood fired CHP plant showed increasing corrosion rates for increasing flue gas temperatures, too. However, a clear trend was only found for short intervals (days). When using longer intervals (weeks) for the evaluation, only a minor influence of the flue gas temperature was established. A possible explanation can be found in the fuel composition, which differed significantly during the test run. These changes most likely resulted in different corrosion rates at constant probe and flue gas temperatures. Since the influence of the probe surface temperature was more distinct, it was still possible to determine a trend over longer periods whereas this was not possible for the flue gas temperature. For flue gas velocity no measurable influence on the corrosion rate was established.

These measurements provided real-life data on corrosion processes, but they were gained during operations with varying fuel compositions and boiler loads. Furthermore, control of certain parameters of interest was not possible.

Therefore, online corrosion probe measurements were also conducted in lab-scale experiments at a test rig (50 kW grate furnace coupled with an electrically heated drop tube). Here, the use of more homogenous fuels as well as control of single parameters of interest were possible. However, online corrosion probes require a conductive layer on their surface to perform the measurements. This layer is formed from ash deposits and corrosion products as soon as the probe is exposed to the flue gas. When a fully developed layer has been formed, the measurement signal represents the real corrosion rate. However, during the build-up of this layer (the initial phase), the measurement signal does not represent the actual corrosion rate. Since the corrosion rate is calculated based on the measurement signal subsequent to the test run and uses the integral over the whole measurement signal, the wrong signal during the initial phase will cause an error in the corrosion rate determination.

This “start-up” error can be neglected during long-term measurements lasting several 1000 h but it can significantly influence results during short-term measurements lasting only several 100 h. Therefore, a methodology based on the parallel application of a mass loss probe and an online corrosion probe was developed. This methodology allowed the calculation of the start-up error and enabled a proper evaluation of short-term online corrosion probe measurements.

Based on this new methodology, test runs using different superheater steels (13CrMo4-5 (1.7335), P91 (1.4903) and 1.4541)) were conducted using chemically untreated wood chips as well as waste wood (A1–A3 in accordance with German standards) as fuels. The short-term test runs lasted for about 500 h and showed that the start-up error was not constant but differed significantly between the individual test runs. Hence, determination of the start-up error during short-term measurements is necessary for a proper comparison of corrosion rates from different test runs.

The measurements performed for the combustion of chemically untreated wood chips showed comparable corrosion rates for 13CrMo4-5 and P91 at low flue gas temperatures up to 750°C. At flue gas temperatures exceeding 800°C, the corrosion rates of P91 were lower indicating better corrosion resistance at these flue gas temperatures. In waste wood combustion, 1.4541 had a significantly better corrosion resistance than P91 for all probe surface and flue gas temperatures investigated.

In order to gain relevant information regarding the dominating corrosion mechanisms, the deposits and corrosion products on the online corrosion probe were investigated by means of SEM/EDX subsequent to the test runs. Furthermore, deposits sampled with a deposit probe were also analysed by means of SEM/EDX. Since the chemical compositions of deposits on the online corrosion probe and the deposits sampled with the deposit probe differed significantly, it was concluded that variations of the probe surface temperature altered the chemistry of deposits and corrosion products on the online corrosion probe.

Despite the alteration due to temperature variation, the analyses of online corrosion probes and deposit samples were used to deduce possible corrosion mechanisms. For the combustion of wood chips it was concluded that Cl-induced active oxidation as well as oxidation of the steel by oxygen from the flue gas are relevant corrosion mechanisms. For the combustion of waste wood it was concluded that Cl-induced active oxidation as well as hot corrosion (due to molten deposits) are relevant corrosion mechanisms.

To sum up, the investigations conducted proved the applicability of online corrosion probes for the determination of high-temperature corrosion rates in biomass-fired fixed bed boilers. Furthermore, a methodology was developed enabling lab-scale short-term measurements with online corrosion probes and a proper evaluation of the resulting corrosion rates. These methods, and the data generated, provide a tool for plant manufacturers to evaluate corrosion rates for future plants in advance. The aim is the application of increased steam parameters leading to increased electrical efficiencies at acceptable high-temperature corrosion risks.

.

Kurzfassung

Hochtemperaturkorrosion von Wärmetauschern stellt ein nach wie vor unzureichend erforschtes Problem in Biomassefeuerungsanlagen dar. Es ist bekannt, dass sowohl die Materialtemperatur von Wärmetauschern als auch die Materialwahl von Wärmetauschern und die Art des Biomassebrennstoffes Hochtemperaturkorrosion beeinflusst. Die Problematik betrifft insbesondere KWK-Anlagen auf Wasserrohr-Dampfkesselbasis, da hier der Dampf in Überhitzern auf hohe Temperaturen gebracht wird wodurch hohe Materialtemperaturen der Überhitzer bedingt sind. Um Korrosionsprobleme zu vermeiden, wird deshalb zumeist eine konservative Auslegung der Endtemperatur des überhitzen Dampfes gewählt, was in weiterer Folge zu keiner vollen Ausnutzung des Potentials bezüglich des elektrischen Wirkungsgrades führt. Zur Steigerung der elektrischen Effizienz von zukünftigen Biomasse-KWK-Anlagen ist es notwendig die Dampftemperaturen zu erhöhen. Um das damit einhergehende Korrosionsrisiko bewerten zu können, wurden erstmal Online-Korrosionssonden zur systematischen Untersuchung von Hochtemperaturkorrosion in Biomasse-Rostfeuerungen durchgeführt.

Die Untersuchungen wurden zuerst in Biomasse-Rostfeuerungen mit Wasserrohr-Dampfkesselanlagen (Großanlagen) als Langzeitmessungen über mindestens 3000 h durchgeführt. Dabei wurden Online-Korrosionssonden in den Strahlungszügen einer 28 MW_{NCV} KWK-Anlage, welche mit chemisch unbehandeltem Hackgut befeuert wird, sowie in einer 58 MW_{NCV} KWK-Anlage, welche mit Altholz (A1-A4 nach deutscher Altholzverordnung) befeuert wird, eingesetzt. Bei diesen Untersuchungen konnte die Anwendbarkeit von Online-Korrosionssonden in Biomassefeuerungen nachgewiesen werden.

Die Korrosionsuntersuchungen in den Großanlagen wurden mit dem Überhitzermaterial 13CrMo4-5 durchgeführt. Hierin wurden die Oberflächentemperaturen der Korrosionssonden von 400°C bis 550°C variiert und es wurde Rauchgastemperaturen im Bereich von 710°C bis 950°C untersucht. Die Messdaten zeigten in beiden Anlagen eine klare Abhängigkeit der Korrosionsrate von der Oberflächentemperatur der Korrosionssonde. Eine Korrelation der Korrosionsrate mit der Rauchgastemperatur konnte über längere Zeiträume bei den Messungen in der Hackgut-befeuerten Anlage abgeleitet werden, wobei der Einfluss der Rauchgastemperatur jedoch deutlich geringer als jener der Oberflächentemperatur war. Bei den Messungen in der Altholz-befeuerten Anlage konnte eine Abhängigkeit der Rauchgastemperatur nur über kurze Zeiträume (Tage) festgestellt werden. Bei Auswertung längerer Zeiträume (Wochen) wurde nur ein sehr geringer Einfluss festgestellt. Als mögliche Ursache wurde eine stark schwankende Brennstoffzusammensetzung während der Messungen identifiziert. Dadurch sind Schwankungen der Korrosionsrate bei gleicher Sonden-Oberflächentemperatur und Rauchgastemperatur möglich. Da der Einfluss der Rauchgastemperatur auf die Korrosionsrate deutlich geringer als jener der Oberflächentemperatur war, konnte dieser über längere Zeiträume nicht mehr detektiert werden. Die Rauchgasgeschwindigkeit zeigte in keiner der Untersuchungen einen messbaren Einfluss auf die Korrosionsrate.

Diese Messungen lieferten Messdaten unter realen Randbedingungen für Korrosionsprozesse. Allerdings mussten bei derartigen Feldmessungen Schwankungen der Brennstoffzusammensetzung sowie der Kessellast in Kauf genommen werden. Weiters konnten gewisse, relevante Einflussparameter nicht gezielt gesteuert bzw. untersucht werden, wodurch sich eine gewisse Schwankungsbreite bzw. Unsicherheit der Messdaten ergab.

Deshalb wurden Online-Korrosionsmessungen auch an einer Versuchsanlage im Technikumsmaßstab (50 kW Rostfeuerung gekoppelt mit einem elektrisch beheizten Fallrohr) durchgeführt. Hier waren die Verwendung von homogeneren Brennstoffen sowie eine gezielte Steuerung einzelner Einflussparameter möglich. Allerdings benötigen die Online-Korrosionssonden zur Messung der Korrosionsrate eine leitfähige Schicht auf deren Oberfläche, welche nach dem Einbringen der Sonden in das Rauchgas durch Depositionen und Korrosionsprodukte gebildet wird. Während des Aufbaus dieser Schicht entspricht das Messsignal noch nicht der realen Korrosionsrate. Dieses fehlerbehaftete Signal wird als "Anfangsfehler" bezeichnet. Der Anfangsfehler wird bei Langzeitmessungen, die mehrere 1000 h dauern, vernachlässigbar klein. Bei Kurzzeitmessungen die nur einige 100 h dauern, wie sie typischerweise im Technikumsmaßstab durchgeführt werden, kann dieser jedoch nicht vernachlässigt werden.

Um den Anfangsfehler bestimmen und korrigieren zu können, wurde eine Methodik basierend auf einer Masseverlustsonde entwickelt, welche parallel zu der Online-Korrosionssonde eingesetzt werden kann. Basierend auf dieser Methodik wurden mehrere Überhitzermaterialien (13CrMo4-5 (1.7335), P91 (1.4903) und 1.4541)) untersucht, wobei ebenfalls wie bei den Feldmessungen chemisch unbehandeltes Hackgut sowie Altholz (A1-A3 nach deutscher Altholzverordnung) als Brennstoffe eingesetzt wurden. Die Kurzzeitmessungen (ca. 500 h) im Technikumsmaßstab zeigten, dass der Anfangsfehler kein konstanter Wert ist, sondern zwischen den einzelnen Testläufen deutlich variiert. Daraus resultiert, dass die Bestimmung des Anfangsfehlers notwendig ist, um derartige Testläufe vergleichbar durchzuführen.

Die Korrosionsmessungen mit chemisch unbehandeltem Hackgut zeigten eine vergleichbare Korrosionsresistenz von P91 gegenüber 13CrMo4-5 bei geringen Rauchgastemperaturen bis 750°C. Bei erhöhten Rauchgastemperaturen größer als 800°C wurden für P91 jedoch geringere Korrosionsraten bestimmt. Bei der Verbrennung von Altholz zeigte 1.4541 eine deutlich höhere Korrosionsresistenz gegenüber P91 bei allen untersuchten Sonden-Oberflächentemperaturen und Rauchgastemperaturen.

Um Rückschlüsse auf die vorherrschenden Korrosionsmechanismen ziehen zu können, wurden Depositionen und Korrosionsprodukte auf den Korrosionssonden nach den Testläufen mittels SEM/EDX untersucht. Weiters wurden Depositionsproben mit einer Depositionssonde gezogen und ebenfalls mittels SEM/EDX untersucht. Da sich die Zusammensetzungen der Depositionen auf den Korrosionssonden deutlich von jenen, die mit den Depositionssonden gezogen wurden unterschieden, wurde der Schluss gezogen, dass durch die Variationen der Sondentemperaturen die Zusammensetzung von Depositionen und Korrosionsprodukten verändert wurde. Dadurch wurden konkrete Schlussfolgerungen hinsichtlich der vorherrschenden Korrosionsmechanismen erschwert.

Basierend auf den Analysen wurden, unter Berücksichtigung der Einschränkungen durch die Temperaturvariationen, die wahrscheinlichsten Korrosionsmechanismen ermittelt. Für Hackgutverbrennung wurde der Schluss gezogen, dass Cl-induzierte aktive Oxidation und direkte Oxidation des Stahls durch den Sauerstoff im Rauchgas wahrscheinliche Korrosionsmechanismen darstellen. Für Altholzverbrennung wurden Cl-induzierte aktive Oxidation und Korrosion durch geschmolzene Depositionen (hot corrosion type II) als wahrscheinlichste Mechanismen identifiziert.

Zusammenfassend zeigten die Untersuchungen, dass Online-Korrosionssonden in Biomasse-Rostfeuerungen einsetzbar sind um Hochtemperaturkorrosion in Echtzeit zu untersuchen.

Weiters wurde eine neue Methodik entwickelt, um Kurzzeitmessungen mit Online-Korrosionssonden im Technikumsmaßstab durchführen zu können und plausibel bewerten zu können. Diese Methoden sowie die ermittelten Daten stellen ein Werkzeug für Kesselhersteller dar, um Korrosionsraten von Überhitzern in zukünftigen Anlagen vorab abschätzen zu können. Damit soll ermöglicht werden, die Dampftemperaturen und damit die elektrische Effizienz bei bekanntem Korrosionsrisiko zu steigern.

List of publications

This thesis is based on the work contained in the following papers:

I. S. Retschitzegger, T. Brunner, I. Obernberger and B. Waldmann, “Assessment of Online Corrosion Measurements in Combination with Fuel Analyses and Aerosol and Deposit Measurements in a Biomass Combined Heat and Power Plant” *Energy & Fuels,* vol. 27, no. 10, pp. 5670-5683, 2013.

II. S. Retschitzegger, T. Gruber, T. Brunner and I. Obernberger, “Short term online corrosion measurements in biomass fired boilers. Part 1: Application of a newly developed mass loss probe” *Fuel Processing Technologies,* vol. 137, pp. 148-156, 2015.

III. S. Retschitzegger, T. Gruber, T. Brunner and I. Obernberger, “Short term online corrosion measurements in biomass fired boilers. Part 2: Investigation of the corrosion behavior of 13CrMo4-5, P91 and 1.4541 for two biomass fuels” *Fuel Processing Technologies,* vol. 142, pp. 59-70, 2016.

IV. T. Gruber, S. Retschitzegger, R. Scharler and I. Obernberger, “Dominating high temperature corrosion mechanisms in low alloy steels in wood chips fired boilers,” *Energy & Fuels*, vol. 30 (3), pp. 2385–2394, 2016.

Author's contributions

Paper I

Retschitzegger performed the experimental work. The results of the experiments and the analyses were carried out by Retschitzegger in collaboration with the co-authors. Retschitzegger was the main author of the paper.

Paper II

Retschitzegger developed the methodology in collaboration with the co-authors. The experimental tests were conducted by Retschitzegger and Gruber. The evaluation of the test run results was performed by Retschitzegger together with the co-authors. Retschitzegger was the main author of the paper.

Paper III

Retschitzegger conducted the experiments together with Gruber. The test run results and the analyses were evaluated by Retschitzegger in collaboration with the co-authors. Retschitzegger was the main author of the paper.

Paper IV

Gruber was the main author of the paper. He planned and performed the measurements with support from Retschitzegger. Retschitzegger also supported the data evaluation.

Related publications not included in the thesis:

Papers in peer reviewed journals

I. S. Retschitzegger, T. Brunner, and I. Obernberger, “Low-Temperature Corrosion in Biomass Boilers Fired with Chemically Untreated Wood Chips and Bark” *Energy & Fuels*, vol. 29 (6), pp. 3913–3921, 2015.

Conference proceedings

I. S. Retschitzegger, T. Brunner, I. Obernberger and B. Waldmann, “Assessment of Online Corrosion Measurements in Combination with Fuel Analyses and Aerosol and Deposit Measurements in a Biomass Combined Heat and Power Plant,” in *Proceedings: Impacts of Fuel Quality on Power Production and Environment*, Puchberg, Austria, 2012.

II. S. Retschitzegger, T. Gruber, T. Brunner and I. Obernberger, “Improvement of the accuracy of short-term corrosion probe measurements by addition of a mass-loss probe,” in *Proceedings: Impacts of Fuel Quality on Power Production and Environment*, Snowbird, Utah, USA, 2014.

Table of Contents

List of Figures

List of Tables

Nomenclature

Abbreviations

ASTM	American Society for Testing and Materials
CHP	combined heat and power
d.b.	dry basis
EDX	energy dispersive X-ray
MSW	municipal solid waste
NCV	net calorific value
ppmv	part per million related to volume
SEM	scanning electron microscopy
vol.%	volume percentage
wt.%	weight percentage
w.b.	wet basis

Symbol	Unit	Description
b	[(mm/1000h)·(V/mA)]	factor between l_P and k
C_l	[m]	linear constant
C_p	[m]	parabolic constant
C_{pl}	[m]	paralinear constant
g	[mm]	radial mass loss
k	[mm/1000h]	corrosion rate
k_{MLC}	[mm/1000h]	mass loss corrected corrosion rate
k_l	[m/h]	linear rate constant
k_p	[m²/h]	parabolic rate constant
l_P	[mA/V]	linear polarization resistance
t	[h]	time

T_{FG}	[°C]	temperature of flue gas
T_S	[°C]	temperature of probe surface
x	[m]	material loss

Chemical formulas

Al	aluminium
C	carbon
Ca	calcium
Cl	chlorine
Cr	chromium
Cu	copper
Fe	iron
H	hydrogen
K	potassium
Mn	manganese
Mo	molybdenum
N	nitrogen
Na	sodium
Ni	nickel
O	oxygen
P	phosphorus
Pb	lead
S	sulphur
Si	silicon
Zn	zinc

1 Introduction and Objectives

1.1 Introduction

World energy consumption is constantly increasing. At the beginning of 2015, the European Commission issued the "Energy Union Package" to achieve secure, sustainable, competitive and affordable energy for Europe [1]. In this package, the EU set a target of at least 27 % for the share of renewable energy consumed in the EU in 2030. Amongst other sources, energetic biomass utilisation will play an important role in providing energy from renewable resources.

The most common technology for energetic biomass utilisation is combustion, for which several technologies are available. The most common ones in large-scale or industrial applications are fixed bed combustion (grate furnaces), fluidised bed combustion (bubbling fluidised beds and circulating fluidised beds) and pulverized fuel combustion (dust burners). The main applications of energetic biomass utilisation are the production of hot water, steam and electricity. For these purposes, the combustion technologies listed above are coupled with hot water, thermal oil or steam boilers.

Although combustion is a technologically mature process, the combustion of biomass is often linked to ash-related problems, such as particulate emissions, as well as in-plant problems due to ash deposit formation and corrosion. Corrosion is a major problem affecting heat exchanger surfaces and may cause a significantly reduced boiler service life as well as unexpected shutdowns [2], [3], [4].

Corrosion processes in biomass combustion plants occur in the high-temperature section of a plant, where evaporators and superheaters are attacked, as well as in the low-temperature section, where economizers, air pre-heaters and downstream equipment (e.g. filters) are affected. This work focused on the high-temperature section and did not consider corrosion in the low-temperature section, since the corrosion mechanisms differ significantly and they have to be treated separately. Within the high-temperature section, different types of corrosion attack occur. Evaporator tubes are typically attacked under reducing conditions, which are present in the furnace itself. The corrosion of heat exchangers downstream the furnace typically occurs under oxidising conditions. The latter is referred to as "high-temperature corrosion" within this thesis, since the corrosion occurs at significantly higher material temperatures.

High-temperature corrosion is mainly relevant at heat exchanger surface temperatures above 400°C. In hot water boilers, no heat exchangers with these surface temperatures are present, and in thermal oil boilers typical maximum temperatures of the operating media are 300°C – 320°C. Therefore, they are not discussed in this thesis. In steam boilers, the superheated steam reaches temperatures in the range of 400°C – 540°C. Consequently, the issue of high-temperature corrosion is of relevance in CHP plants as well as in biomass combustion plants for power-only production based on steam boilers.

For these reasons, the work presented in this thesis focused on corrosion processes affecting superheaters in steam boilers. Within this thesis only fixed bed combustion systems were considered, since these are the most relevant ones regarding number of installations.

1.2 Background

Research on high-temperature corrosion in biomass-fired boilers was already performed in the last decade. An overview can be found in [3], [5], [6], [7] or [8]. The work mainly focused on high-temperature corrosion for the combustion of specific fuels such as biomass fuels rich in chlorine [9], [10], [11], [5], [12], [13], [14], [15], [16], [17], [18], [19] or heavy metals [7], [20], [21], [22]. Furthermore, plants firing chemically untreated wood fuels were investigated, which are at risk of high-temperature corrosion when applying increased steam parameters [8].

This research suggests that high-temperature corrosion rates as well as corrosion mechanisms are influenced by a number of factors. In the conditions investigated within this work the most relevant factors are:

- the steel surface temperature of the superheater [2], [23], [24], [25]
- the flue gas temperature [24], [26], [27]
- the flue gas velocity [24], [28]
- the chemical composition of ash deposits and the flue gas [5], [6], [29]
- the material used for the superheater tubes [3], [30]

As stated above, high-temperature corrosion processes depend on the temperature prevailing. Therefore, the temperature on the surface of superheaters, where the corrosion process occurs, is of special relevance. On the inside of superheaters, the heat transfer coefficient between the superheated steam and the tube material is typically at values of 10^3 W/(m²·K), whereas on the flue gas side it is typically in the range of 30-100 W/(m²·K). The significantly higher heat transfer coefficient on the steam side compared to the flue gas side causes a superheater material temperature very close to the steam temperature. Since the thermal conductivity of superheater steels is rather high, with a typical value of 38 W/(m·K) (for 13CrMo4-5 at 20°C [31]), only a minor temperature drop between the steam side and flue gas side of the superheater tube occurs. Therefore, the outside surface temperature of a superheater tube, where the corrosion process occurs, is mainly defined by the steam temperature.

Hence, the highest risk of high-temperature corrosion occurs at the final superheater, where the steam reaches its maximum temperature. To minimize high-temperature corrosion, maximum steam temperatures are usually kept at rather moderate levels. Although this strategy generally ensures failure-free operation, it has the drawback that the plants are operated at reduced electrical efficiencies.

In order to determine the current state of technological development, a survey was performed considering steam temperatures and superheater steels applied in 94 biomass

CHP plants in Europe from 1985 to 2012 [32]. Since biomass is a rather inhomogeneous fuel, and the chemical composition can vary significantly with different biomass fuels, combustion of different biomass fuels results in different chemical compositions of the flue gas as well as of the deposits formed on heat exchanger tubes. Therefore, the type of fuel is a relevant influencing factor regarding high-temperature corrosion. Consequently, different biomass fuels (chemically untreated woody biomass, waste wood as well as mixtures of chemically untreated woody biomass with waste wood and straw) were treated separately in the survey.

Time-related development of steam temperatures

Figure 1 presents steam temperatures of biomass CHP plants in relation to the start of operation from 1985 to 2012 for the different biomass fuels mentioned.

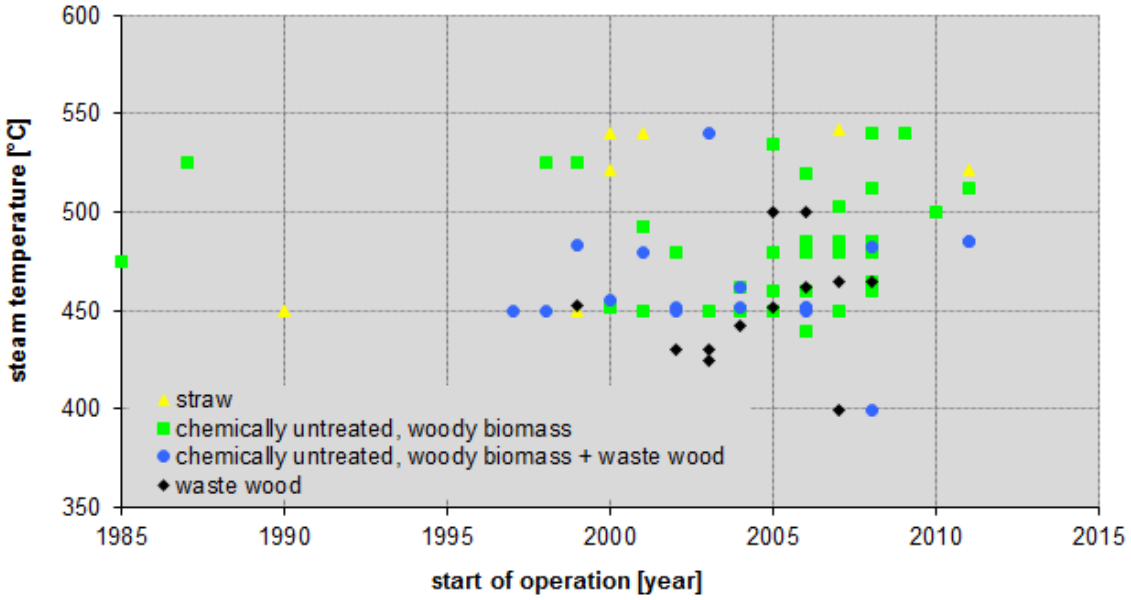

Figure 1: Steam temperatures of biomass CHP plants (adapted from [32])

The data show that steam temperatures in plants firing chemically untreated woody biomass range from 450°C – 540°C. There is a trend towards increasing temperatures, especially for plants established after 2008 which are operated above 500°C. However, 540°C was the upper limit in 2012. Plants firing waste wood as well as mixtures of chemically untreated woody biomass and waste wood are mainly operated at steam temperatures ranging from 400°C – 500°C.

For straw-firing plants, an increase in the steam temperature from 450°C to 520°C – 540°C in the year 2000 is evident. This was achieved by the operation of the superheaters in "slagging mode". In this case, the superheaters are made from austenitic steel (which to a large degree is resistant to corrosive salts) and mounted in the first and second ducts, hanging from the ceiling, and they are not cleaned during operation. Here, a certain amount of slag forms and builds up to a layer where the surface temperature is high enough for the slag to melt, and then it drips from the layer [7], [33].

Regarding steam temperatures, the study concluded that 540°C constituted the maximum steam temperature applied for plants using chemically untreated woody biomass as well as straw. For waste wood firing plants, maximum steam temperatures were at 500°C. Comparable results have also been published by Skrifvars et al. [34].

State-of-the-art coal-fired CHP plants are operated at steam temperatures of up to 600°C resulting in electrical efficiencies up to 47 % (NCV basis) [35]. Due to the lower steam parameters in biomass CHP plants, their electrical efficiencies currently only amount to 34 % (at a steam temperature of 540°C without reheating). In order to improve the competitiveness of energetic biomass utilisation compared with fossil fuel utilisation, a further increase of the steam temperature would be necessary.

Superheater steels

Within the survey, the steels used for the final superheaters in 51 biomass CHP plants were determined. According to the data, low alloyed steels as well as stainless steels are currently used as superheater materials. As presented in Figure 2, according to the survey 88 % of the final superheaters (in 45 of 51 plants) are currently made from low alloyed steels such as 16Mo3 (1.5415), 13CrMo4-5 (1.7335) and 10CrMo9-10 (1.7380). The stainless steel X6CrNiNb18-10 (1.4550) is used in five plants which are fired with straw. The stainless steel X6NiCrNbCe32-27 (1.7380) is only used in one plant which uses a mixture of bark, forestry wood, wood chips and peat as fuel.

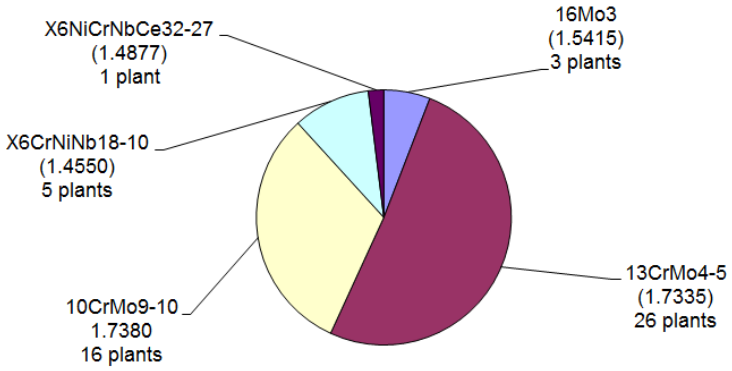

Figure 2: Steels used for the final superheater including the number of plants where this steel is used
Explanations: steels are referred to by their EN steel names and their EN steel numbers in accordance with EN 10027-2.

Since the vast majority of the final superheaters are made from low alloyed steels, it can be concluded that plant manufacturers mainly apply the superheater steels they have experience of. Furthermore, these steels are cheaper than stainless steels.

A correlation between the superheater steels and steam temperature is presented in Figure 3. It shows that the steam temperature is limited to 500°C when applying low alloyed steels. Although only few data on superheater materials for plants applying steam temperatures above 500°C are available, the data in Figure 3 show that with the

application of higher alloyed superheater steels, such as X6CrNiNb18-10 and X6NiCrNbCe32-27, steam temperatures up to 540°C are realizable. This finding is consistent with results from lab-scale research (e.g. [21], [34], [36]), showing an increased corrosion resistance of higher alloyed steels compared to traditionally used low alloyed steels.

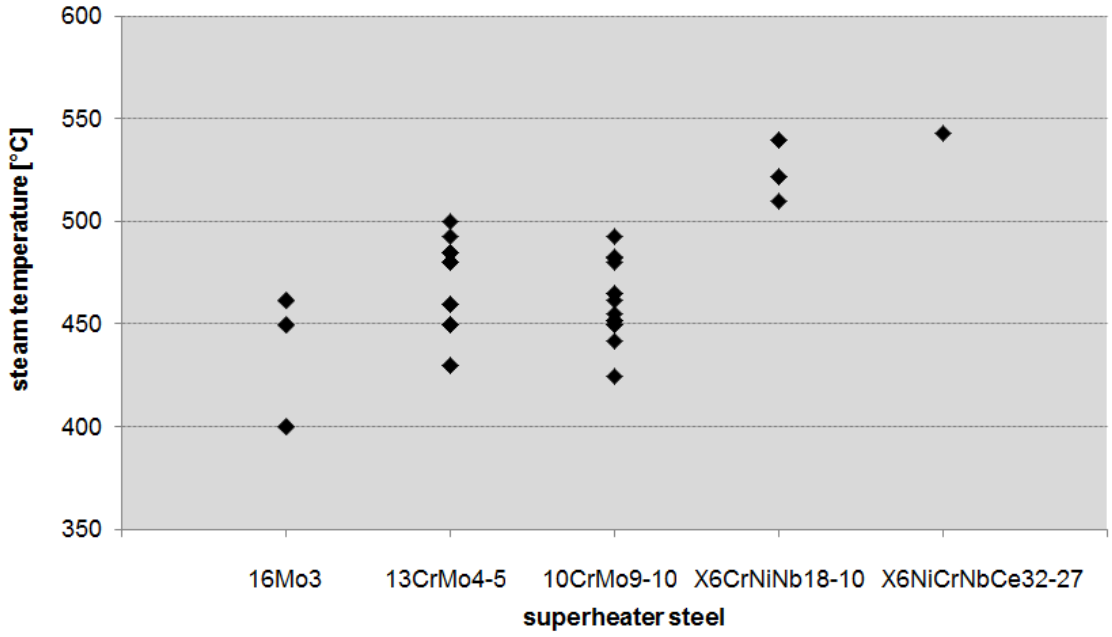

Figure 3: Correlation of steam temperatures with superheater steels (adapted from [32])

Conclusions from survey

The survey showed that, in 2012, 540°C constituted the upper limit of the steam temperature in biomass fired CHP plants. The majority of plants were equipped with superheaters made from low alloyed superheater steels and operated with a maximum steam temperature of 500°C. Within the study, no medium alloyed superheater steels (with a Cr content of 8 – 10 wt.%) were found to be currently applied. However, according to plant manufacturers, these steels have already been considered for application. Furthermore, the increased application of already applied stainless steels would be meaningful in order to allow an increase in the steam temperature.

The survey suggested that plant manufacturers tend to stick to the superheater steels they currently use since they have vast experience in processing the materials as well as in their operational behaviour. Changes in the use of superheater steels as well as an increase of the steam temperature in biomass CHP plants are often based on a trial-and-error basis. Furthermore, higher alloyed steels are more expensive, and their application has to be justified by plant manufacturers. Therefore, further research is necessary to provide the basis for the application of increased steam parameters at acceptable corrosion risks.

Knowledge of actual corrosion rates for superheater steels contingent on influencing parameters such as material temperature would be an essential step towards this goal. These data would allow a targeted selection of superheater materials and the avoidance of the trial-and-error approach. However, these data are not available yet for biomass fired boilers.

Recently developed high-temperature online corrosion probes allow the determination of corrosion rates of superheater steels dependent on influencing parameters. Already, these probes have successfully been applied in municipal solid waste (MSW) incinerators [37], [38], [39] as well as in fossil fuel fired boilers [40], [41], [42]. In biomass fired boilers their applicability has not been proven but they are considered a suitable tool for the determination of the missing corrosion rate data.

1.3 Objectives

Based on the results available in literature and found in the survey, the aim of this thesis was a detailed investigation of parameters influencing high-temperature corrosion in biomass fired CHP plants based on grate combustion by means of newly developed online corrosion probes.

- The steel surface temperature of the superheater tube was of special interest. As already stated, it is a main influencing parameter on the corrosion rate. Since it is mainly defined by the steam temperature, it is highly relevant to the electrical efficiency of a CHP plant. Within this thesis, steel surface temperatures ranging from 400°C to 560°C were investigated.
- The flue gas temperature at the superheaters of a boiler is also known to influence high-temperature corrosion rates. It is defined by numerous factors such as evaporator arrangement, superheater arrangement, boiler design, boiler control and boiler load. Therefore, a broad range of flue gas temperatures is of relevance, and one goal was to apply online corrosion probes at different flue gas temperatures.
- Since the flue gas velocity is also known to influence the high-temperature corrosion rate, an additional task was to perform measurements at varying flue gas velocities.
- As already stated, different biomass fuels result in different chemical compositions of the flue gas and of the deposits responsible for high-temperature corrosion. Therefore, test runs with forest wood chips and waste wood were performed.
- Finally, different superheater steels are characterised by different resistances to high-temperature corrosion. Therefore, three different steels (13CrMo4-5, P91 (X10CrMoVNb9-1) and 1.4541 (X6CrNiTi18-10)) were used for online corrosion probe test runs.

In order to meet these objectives, online corrosion probes were applied in two real-scale, grate-fired biomass CHP plants. Since these probes had never been applied in biomass combustion plants so far, the first task was to test the applicability of the probes (***Paper I***). With these measurements a detailed investigation of superheater corrosion and its

influencing factors was targeted. These real-scale measurements were performed in one plant firing forest wood chips (nominal fuel power input: 28 MW_{NCV}) and in a plant using waste wood as fuel (nominal fuel power input: 58 MW_{NCV}).

Measurement campaigns in real-scale plants usually last a number of months, and operating conditions as well as fuel compositions can vary significantly. In order to determine corrosion rates with online corrosion probes quicker and in a more controllable environment, additional lab-scale test runs using online corrosion probes should be conducted. However, online corrosion probes require a conductive layer on their surface, which is formed from ash deposits and corrosion products during the measurement stage. Therefore, the corrosion signal during the initial stages of a measurement campaign – the build-up phase of the conductive layer – is inaccurate. This inaccuracy can be disregarded in long-term measurements lasting more than several 1000 h, which are usually performed in real-scale plants, but it may significantly influence results during short-term measurements. It follows from this that, if short-term measurements lasting about 500 h are to reflect or come close to real-life conditions, this "start-up" effect cannot be ignored. To this end, a methodology was developed enabling the reliable determination of corrosion rates with online corrosion probes during short-term test runs (***Paper II***).

The methodology development as well as subsequent short-term test runs (***Paper III***) were conducted at a 50 kW_{NCV} test rig. The test rig consists of a packed bed reactor (biomass grate furnace equipped with air staging and flue gas recirculation) coupled with a vertical tube, which can be electrically heated (a so-called drop tube). At the exit of the drop tube the measurement ports for the corrosion measurements are located.

The test rig was also used for additional test runs to identify the dominating corrosion mechanism when using 13CrMo4-5 as superheater steel, and chemically untreated wood chips as fuel (***Paper IV***).

Based on the results of these test runs, corrosion rates dependent on the main influencing factors were determined which should enable more efficient CHP plant designs in the near future in terms of increased electrical efficiencies at moderate or acceptable corrosion rates. The data should provide the basis for selecting the correct material for superheater tubes as well as for setting appropriate steam parameters.

2 High-temperature corrosion: chemical background

According to DIN 50900 [43] high-temperature corrosion is the “oxidation of metals in hot gases under formation of a covering layer which allows the flow of electrons and ions”. Shreir [44] defines high-temperature corrosion as a chemical attack on a metal by gases, solid or molten salts as well as molten metals. This attack typically takes place at temperatures above 400°C.

Corrosion of superheaters in biomass CHP plants takes place on the flue gas side of the tubes under ash deposits. Hence, the chemical composition of the deposits as well as the chemical composition of the flue gas are relevant to the corrosion process. Also, the time-dependency of corrosion processes is a relevant influencing factor on high-temperature corrosion, due to time-dependent variations regarding the deposit shapes and chemical compositions.

2.1 High-temperature corrosion mechanisms

The most relevant corrosion mechanisms are direct oxidation of the metal, Cl-induced active oxidation and molten salt corrosion (also known as “hot corrosion”).

2.1.1 Oxidation of metals

Besides high-temperature corrosion due to deposits, also direct oxidation of metals is of relevance to superheaters in biomass-fired CHP plants. Since only iron-based superheater steels were considered in this thesis, the chemical background of oxidation is explained on the basis of iron or iron oxides. During high-temperature corrosion three different iron oxides are formed, depending on the temperature and the partial pressure of O_2 [45]:

- **FeO (wustite)**
  is formed at temperatures above 570°C. Wustite has a rather loose structure compared to other iron oxides and therefore does not form a protective layer. Hence low alloyed, iron-based steels are usually not used at temperatures above 570°C.
- **Fe_3O_4 (magnetite)**
  is formed at temperatures below 570°C and typically forms homogenous, dense structures. Therefore, magnetite provides a protective layer which helps to reduce the corrosion rate.
- **Fe_2O_3 (hematite)**
  is also formed at temperatures below 570°C but contains more O compared with Fe. Therefore, it is usually present in higher O_2 concentrations compared with magnetite.

When using low-alloyed iron-based steels at temperatures below 570°C the formation of magnetite and hematite is usually of relevance in the early stages as long as no other corrosion process is dominating. Also, when deposits are being removed, e.g. by soot blowers, direct oxidation becomes relevant.

When using higher alloyed steels, Cr is the most important element to increase corrosion resistance. Due to its higher affinity to oxygen compared with iron, it diffuses to the surface faster and forms Cr_2O_3. For Cr contents above 10 wt.% a very thin but compact passive layer of Cr_2O_3 is formed on the steel surface. This so-called passive layer provides a high resistance against corrosion since it prohibits the diffusion of corrosive species into the material as well as the diffusion of steel elements (e.g. Fe) outwards.

Ni is also commonly used as an alloying element. It is typically used in corrosion-resistant stainless steels which contain about 18 % Cr and 10 % Ni. Therefore, a passive layer of Cr_2O_3 is formed on the surface of the steel and Ni does not directly react with the oxygen, but it generally enhances the corrosion resistance of Fe-based steels and increases hardness, toughness and ductility.

A more detailed discussion of the oxidation of metals can be found in [6], [25], [45], [46], [47] and [48]. Superheater steels are usually chosen in such a manner that their corrosion rate due to oxidation is reduced to a value that does not affect the service life of a superheater. However, if the protective oxide scales are penetrated or dissolved, severe corrosion rates can occur.

2.1.2 Cl-induced active oxidation

Biomass fuels typically contain relevant concentrations of the alkali species K and Na as well as S and Cl. Especially waste wood also contains relevant concentrations of Pb and Zn. These elements are partly released to the gas phase during combustion [49] and form alkali- and heavy metal chlorides and sulphates which may later on be deposited on heat exchanger surfaces.

The alkali and heavy metal salts formed in the hot zone of the combustion process are gaseous and condense when either the flue gas temperature is below the dew point of the salts or when the gaseous salts get in contact with cooled heat exchanger surfaces. Therefore, deposits on heat exchanger surfaces are formed by direct condensation of ash vapours as well as the deposition of solid particles.

The metals and Cl released during combustion form gaseous chlorides almost immediately, whereas the released S mainly forms SO_2 and SO_3 as soon as an excess of O is available. SO_2 and SO_3 may subsequently react with alkali metal chlorides and release gaseous HCl. This reaction can be described according to Vaughan et al. [50] like this, using KCl as an example:

$$2\ KCl + SO_2 + ½\ O_2 + H_2O \rightarrow 2\ HCl + K_2SO_4 \qquad \textbf{Eq. 1}$$

The reaction described in Eq. 1 depends on the availability of water in the flue gas. If no water is available, the reaction is possible nonetheless, but results in the formation of gaseous Cl_2, according to Kautz [51]:

$$2\ KCl + SO_2 + O_2 \rightarrow Cl_2 + K_2SO_4 \qquad \textbf{Eq. 2}$$

HCl in the flue gas is known to enhance high-temperature corrosion, but detailed research was only carried out for HCl concentrations above 250 ppmv, which are typical concentrations prevalent in municipal solid waste incinerators [46], [52]. In biomass combustion plants, the concentrations of HCl are typically lower. Especially with chemically untreated wood fuels, HCl concentrations are about 10 ppmv [53]. For these rather low concentrations, it is assumed that gaseous HCl in the flue gas does not strongly enhance high-temperature corrosion (details are included in ***Paper IV***).

However, also low concentrations of gaseous chlorine may cause severe corrosion, if the chlorine is released in the deposits on the surface of superheater tubes. So, the risk of Cl-induced active oxidation depends not only on the release of chlorine itself but also on the location where the reaction occurs. The sulphation process can already take place upstream the superheaters (with gaseous or solid chlorides) resulting in the release of chlorine at a safe distance from superheater tubes. Hence, the chlorine released is assumed to pass the superheater tubes with the flue gas flow and does not cause severe corrosion. The sulphates formed are almost inert when deposited on the superheaters [3]. However, when molten ash fractions containing sulphates are formed on the superheater surface, they can cause severe corrosion (e.g. hot corrosion type II, Section 2.1.3)

Since the release of S and Cl into the gas phase during biomass combustion is rather constant (80 – 90 % for S and > 90 % for Cl [54]), it is possible to evaluate the risk of the deposition of alkali chlorides on superheaters and hence the risk of Cl-induced active oxidation based on the fuel composition. For this purpose, the fuel index 2S/Cl was developed [55], which is calculated on a molar basis and evaluates the possibility of the sulphation of chlorides before they are deposited [54]:

- For fuels with 2S/Cl ratios > 8 only minor risks of Cl-induced active oxidation have to be expected, since a protective sulphate layer is formed on the tube surfaces.
- For 2S/Cl ratios < 4 severe risks of Cl-induced active oxidation have to be expected, since chlorides are likely to be deposited on superheater tubes.

If alkali chlorides are deposited on superheater tubes and sulphated later on, the chlorine released is assumed to cause the severe corrosion known as Cl-induced active oxidation. This process is schematically presented in Figure 4.

The schematic mechanism explains the process based on iron as tube material. However, the general concept of the process also applies to iron-based alloys, Cr and Ni [30]. Within the Cl-induced active oxidation process, the chlorine released on the surface or in the deposit layer (ash layer) can penetrate through the iron oxide layer to the corrosion front. There, chlorine reacts with iron and forms iron chlorides. These chlorides are stable at low O_2 concentrations, which can prevail below the oxide layer.

Due to their low vapour pressure, the iron chlorides can evaporate depending on the temperature, which is mainly defined by the steam temperature inside the superheater tube. Evaporated iron chlorides diffuse outwards towards the flue gas and will eventually

reach zones with higher O_2 concentrations. There, iron oxides are formed and chlorine is released again whereby it partly can diffuse towards the corrosion front again. In this way, a catalytic process is maintained which can result in rather high corrosion rates. More detailed descriptions of the process are summarized in [5], [30], [37] and [56].

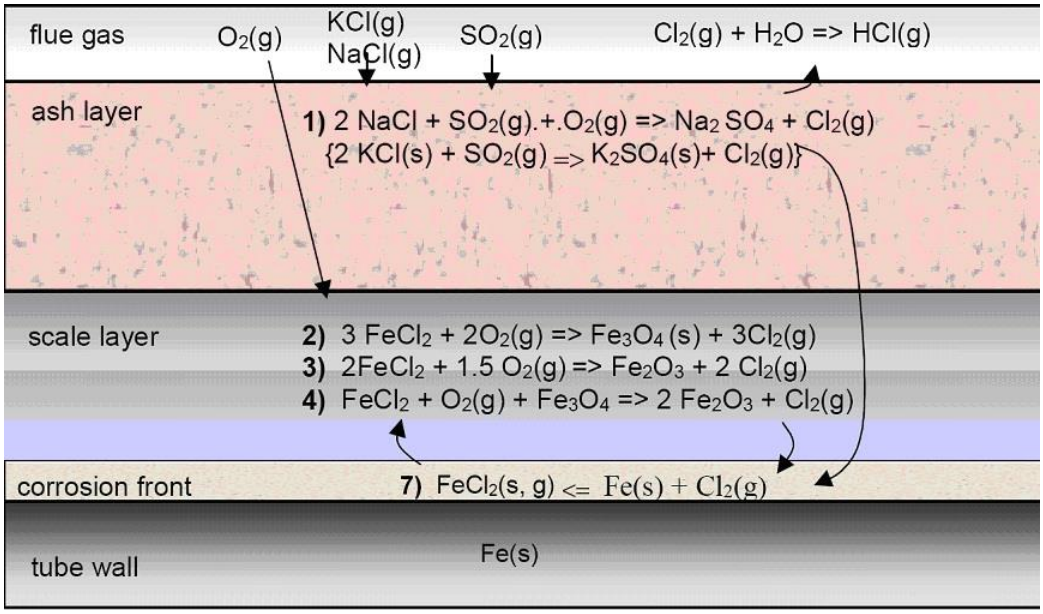

Figure 4: Schematic mechanism of Cl-induced active oxidation (adapted from [57])

2.1.3 Molten salt corrosion

Salt melts on superheater tubes typically increase the corrosion rates [5]. On the one hand, this is due to the fact that chemical reactions as well as diffusion processes are faster in melts compared with solid-solid reaction. On the other hand, melts provide an electrolyte for ionic charge transfer for an electrochemical attack [30].

Molten sulphates (especially alkali sulphates) are the most common reason for molten salt corrosion. Their melting points are typically around 800°C. Two mechanisms are considered to be especially important when molten salts are present:

- **Hot corrosion type I**
  occurs when single molten alkali sulphates are present and it therefore occurs in the temperature range between 800°C – 1000°C [7]. Since such high temperatures in deposits do not prevail in biomass fired boilers due to maximum steam temperatures of 540°C (see section 1), this corrosion process is not relevant and therefore not further discussed.

- **Hot corrosion type II**
  occurs below the melting temperature of sulphates [7]. Melting occurs typically in the presence of small concentrations of SO_3 as well as in the presence of heavy metal chlorides. These components cause the formation of eutectic mixtures which can have melting points significantly below the melting points of pure

sulphates. According to Spiegel [58], this may occur even below 500°C. Especially heavy metals (Zn, Pb) in deposits can lead to such low melting temperatures. Therefore, biomass CHP plants firing waste wood, which often contains elevated heavy metal concentrations, are facing a higher risk of hot corrosion type II.

The molten sulphates cause increased corrosion rates because they can dissolve an already formed protective oxide layer. Besides iron oxides, also nickel and chromium oxides are attacked by molten sulphates. Therefore, also high alloyed steels are at increased risk of high-temperature corrosion when salt melts containing sulphates occur. The corrosion process itself is caused by the formation of pyrosulphates and the formation of alkali metal trisulphates. Both compounds can dissolve the protective oxide scales. Details on hot corrosion can be found in [4], [5], [30], [59] and [60].

2.2 Rate laws

During the corrosion process, a layer of corrosion products is formed on the surface of the metal. This layer may influence the corrosion process, therefore corrosion processes are often time-dependent. Since reaction partners participating in the corrosion process have to pass this layer and since, often, multiple chemical and/or physical steps are necessary, the slowest process is the rate-determining step. Here, the rate law is determined, which describes the corrosion process dependent on time. Figure 5 shows the most relevant rate laws that apply to high-temperature corrosion processes. In this figure the corrosion process is described as material loss of the metal. Although other laws exist, they only play a minor role and can be neglected, according to Gellings [45].

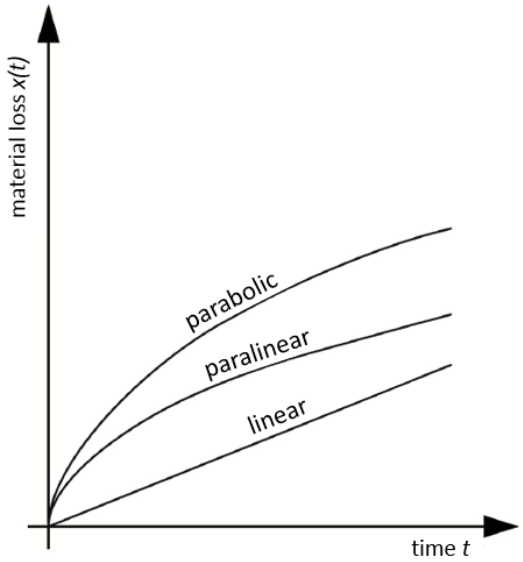

Figure 5: High-temperature corrosion rate laws (adapted from [61])
Explanations: x(t): material loss dependent on time in [m]

2.2.1 The linear rate law

A linear rate law describes a constant corrosion rate over time and can be formulated as:

$$x = k_l \cdot t + C_l \qquad \textbf{Eq. 3}$$

Explanations: x: material loss in [m]; k_l: linear rate constant [m/h]; t: time [h]; C_l: constant [m]

This rate law describes a time-independent corrosion rate. The rate-limiting step of such a process can be a surface reaction at the phase boundaries metal / covering layer or covering layer / gas phase [62].

2.2.2 The parabolic rate law

A parabolic rate law can be formulated as:

$$x^2 = k_p \cdot t + C_p \qquad \textbf{Eq. 4}$$

Explanations: x: material loss in [m]; k_p: parabolic rate constant [m^2/h]; t: time [h]; C_p: constant [m^2]

This rate law applies if the corrosion products form a compact, adherent layer on the surface of the metal. The rate-determining step in this case is the diffusion of reaction partners through the corrosion layer. The corrosion rate *dx/dt* decreases with time since the growing corrosion layer results in longer ways for the diffusion of the reaction partners [62].

2.2.3 The paralinear rate law

During corrosion processes the rate-determining step may change with time. Such a process can be described by combining two rate laws, for instance the linear rate law and the parabolic rate law. The resulting paralinear rate law can be described in a simplified form as:

$$x = k_l \cdot t + \sqrt{k_p \cdot t} + C_{pl} \qquad \textbf{Eq. 5}$$

Explanations: x: material loss in [m]; k_l: linear rate constant [m/h]; k_p: parabolic rate constant [m^2/h]; t: time [h]; C_{pl}: constant [m]

The paralinear rate law applies to a corrosion process which forms a compact, adherent corrosion layer in the beginning phases, which is described by the parabolic law. With time, the outer side of the corrosion layer is transformed into a porous layer which does not provide protection against corrosion. Hence, after a certain time the corrosion rate follows a linear rate law [45].

3 Methodology

In order to generate the basic data for the investigation of influencing parameters on high-temperature corrosion, test runs with online corrosion probes in biomass combustion plants were performed. During long-term measurements (several months) in a grate-fired CHP plant with a water-tube steam boiler, fired with chemically untreated forest wood chips, the applicability of online corrosion probes was tested and validated for biomass combustion processes (***Paper I***). The common superheater steel 13CrMo4-5 (1.7335) was tested within these measurements. For this purpose, the material temperature was varied via cooling of the online corrosion probe to determine its influence on the corrosion rate. In order to investigate the influence of the flue gas temperature on the corrosion rate, two probes were applied in parallel at different positions in the radiative section of the boiler. The measurements at the CHP plant were accompanied by regular fuel analyses as well as deposit probe measurements close to the positions of the online corrosion probes in order to identify the framework conditions of the long-term test runs. Furthermore, relevant temperatures measured in the plant were recorded. The continuous flue gas analyses data were also recorded to monitor and evaluate the combustion quality of the plant. Detailed results are given in ***Paper I;*** in this thesis only the most relevant results are included.

A second long-term test campaign was conducted in a grate-fired CHP plant with a water-tube steam boiler fired with a mix of waste wood and chemically untreated wood chips, using also 13CrMo4-5 as superheater steel for the corrosion test. In this test run, the influence of another chemical environment resulting from the change in fuel was investigated. The test run was accompanied by the same additional measurements and data recordings as the first one.

The long-term measurements in the two plants showed that online corrosion probes are well applicable to biomass CHP plants. The data from the online corrosion probes gave a valid indication of the influence of the steel surface temperature as well as of the flue gas temperature on the corrosion rate. However, as the fuel analyses showed, in real-scale plants the fuel composition varies to a certain extent, which influences the corrosion rates. Furthermore, the boiler load, and therefore also the flue gas temperature at the positions of the online corrosion probes, changed significantly during the test runs. Additionally, unexpected plant shutdowns occurred, which also influenced the accuracy of the measurements.

Therefore, additional test runs were performed at a lab-scale 50 kW_{NCV} test rig. It consists of a packed bed reactor (biomass grate furnace equipped with air staging and flue gas recirculation) coupled with a vertical tube, which can be electrically heated (a so-called drop tube). This test rig allowed the operation at well-defined conditions, and also the use of more homogeneous biomass fuels was possible. Additionally, the targeted variations of single parameters of interest such as flue gas temperature were possible. Consequently, this test rig allowed a more detailed investigation of influencing parameters on high-temperature corrosion compared with a real-scale CHP plant.

However, online corrosion probes require a conductive layer on their surface to perform the measurements. This layer is formed from ash deposits and corrosion products as soon as the probe is exposed to the flue gas. When a fully developed layer has been formed, the measurement signal represents the real corrosion rate. However, during the build-up of this layer (the initial phase), the measurement signal does not represent the actual corrosion rate. Since the corrosion rate is calculated from the measurement signal subsequent to the test run and uses the integral over the whole measurement signal, the wrong signal during the initial phase causes an error in the corrosion rate determination. This "start-up" error can be neglected during long-term measurements lasting several 1000 h but it can significantly influence results during short-term measurements lasting only several 100 h. Since the online corrosion probe measurements at the test rig lasted for about 500 h, a methodology for the correction of the start-up error had to be developed for these measurements (***Paper II***). This was achieved by the construction of a mass loss probe which was applied in combination with the online corrosion probe.

Using this methodology, the superheater steels 13CrMo4-5, X10CrMoVNb9-1 (P91, 1.4903) and X6CrNiTi18-10 (1.4541) were investigated at the test rig (***Paper III***). 13CrMo4-5 and P91 were tested during combustion of chemically untreated wood chips, and P91 and 1.4541 were tested during the combustion of waste wood. These measurements were also accompanied by regular fuel analyses, deposit probe measurements as well as continuous flue gas analyses.

Additionally, test runs with the newly developed mass-loss probe were conducted at the test rig in order to determine the dominating high-temperature corrosion mechanisms. For this purpose, the superheater steel 13CrMo4-5 was tested during the combustion of wood chips as well as during the combustion of natural gas (***Paper IV***). However, these results are discussed only briefly in this thesis since they are included in detail in the PhD thesis of the first author of ***Paper IV***.

Next, the fuels investigated, the reactors used, as well as the experimental methods and equipment used within the scope of this thesis will be elaborated.

3.1 Biomass fuels investigated

Biomass fuels comprise solid, liquid and gaseous biomass. In this thises only solid fuels are considered. The most relevant solid biomass fuels can be classified as woody biomass (e.g. forest wood chips, industrial wood chips, bark, waste wood), as herbaceous biomass (e.g. straw, cereals, grass) or as fruit biomass (e.g. kernels, shells). In this thesis, forest wood chips and waste wood were used for the corrosion investigations.

3.2 Reactors

3.2.1 Real-scale reactors (CHP plants)

First measurements were performed at a biomass CHP plant located in Austria, which is fired with chemically untreated forest wood chips (henceforward referred to as "wood chips"). The plant consists of a grate-fired combustion unit with a 4-path water-tube

steam boiler consisting of two radiative sections followed by a convective section which contains three superheater bundles and five economizer bundles (steam parameters: 32 t/h at 480°C and 63 bar). The nominal fuel power input is 28 MW_{NCV}, corresponding to an electric capacity of 5 MW and a thermal capacity of 18 MW (district heat supply). The plant is operated in heat controlled mode and covers the base load of the district heating network. A multi-cyclone and an electrostatic precipitator are applied for flue gas cleaning. Figure 6 shows the scheme of the plant, fuel sampling and corrosion measurement positions as well as relevant temperature and flue gas measurement points.

The online corrosion probes were applied in the radiative section of the boiler. At these positions, no soot blowers were installed. Therefore, soot blowing did not affect the online corrosion probe measurements.

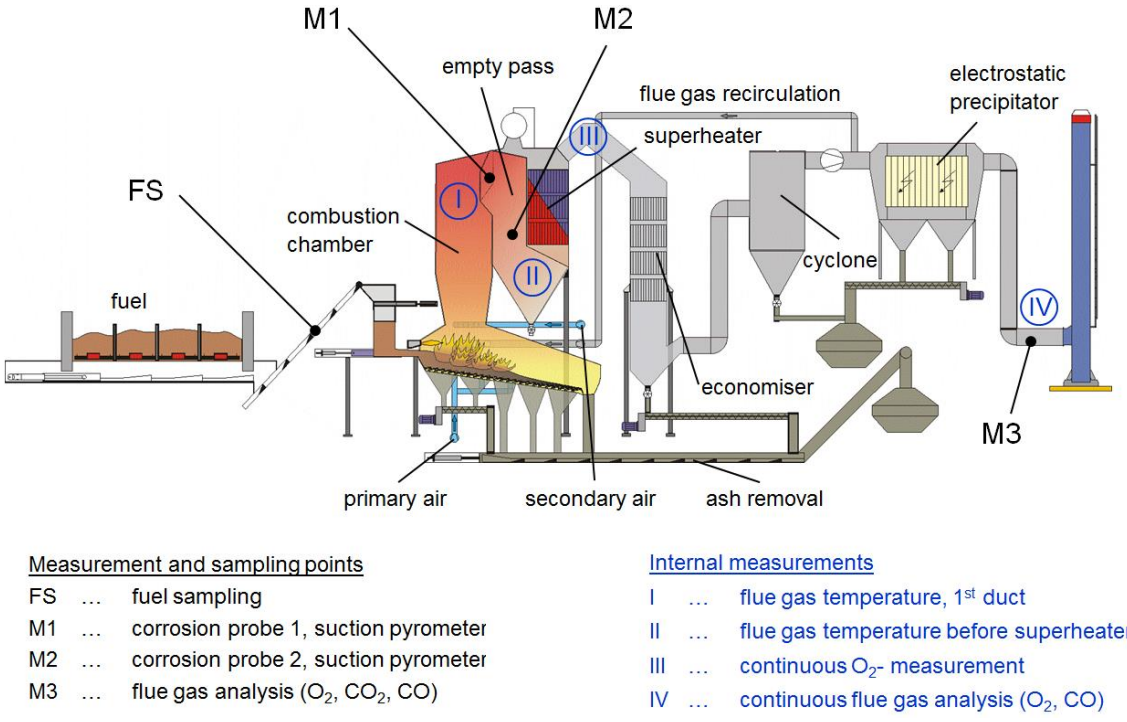

Figure 6: Scheme of the forest wood chips fired CHP plant including relevant measurement points (adapted from Paper I)

A second measurement campaign was performed in a CHP plant in Germany. The fuel mix used in this plant consisted of 50 % chemically untreated wood chips, 45 % waste wood of categories A1-A3 and 5 % waste wood of category A4 in accordance with German standards. The plant consists of a grate furnace with a 4-path water-tube steam boiler comparable to the first plant. The boiler produces 64 t/h steam at 450 °C and 79 bar with a nominal fuel power input of 58 MW_{NCV} producing 9.6 MW_{el} of electricity as well as heat. The heat is delivered to the local district heating network.

For NO_x reduction, urea is injected (SNCR) in the 1st path and the 2nd path. The flue gas cleaning system consists of a cyclone and a filter unit applying blast furnace coke and lime

hydrate for dry sorption (HCl, SO_2, Hg emission reduction) as well as fabric filters for particle separation. The scheme of the plant as well as relevant measurements points are shown in Figure 7. The online corrosion probes were applied in the radiative section of the boiler, similar to the wood chips fired CHP plant. In the waste wood plant, also no soot blowers were installed in the radiative section. Therefore, soot blowing did not affect the online corrosion probe measurements.

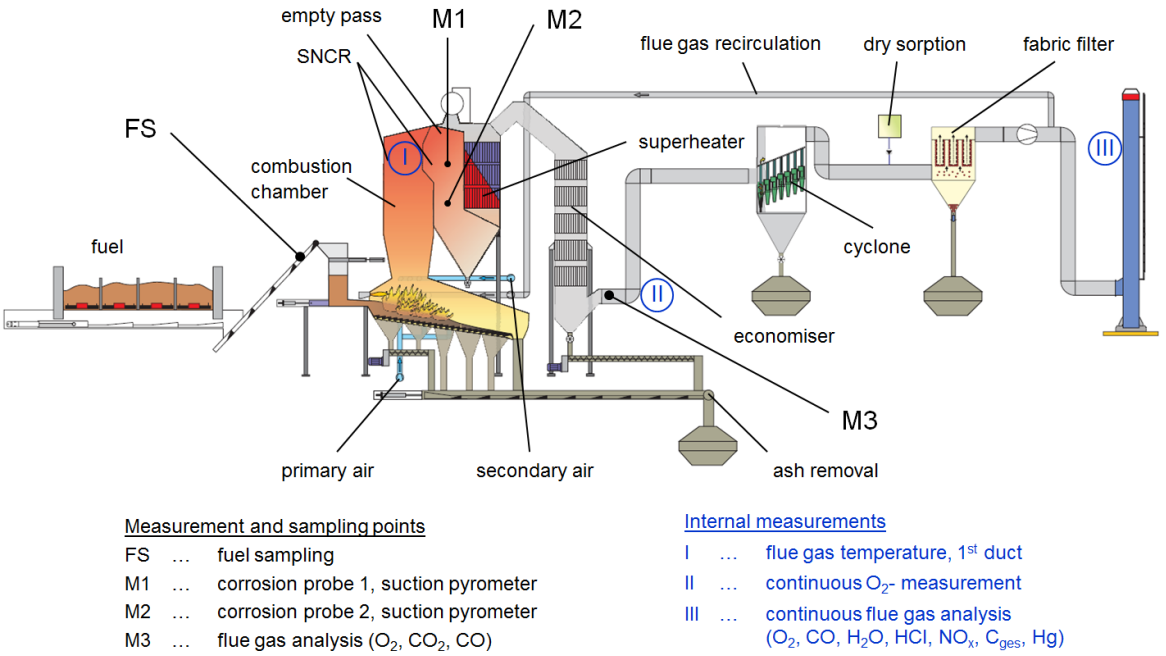

Figure 7: Scheme of the waste wood fired CHP plant including relevant measurement points
Explanations: SNCR: selective non-catalytic reduction (urea injection)

3.2.2 Lab-scale reactor (test rig)

The test rig (Figure 8) consists of a packed bed reactor (biomass grate furnace equipped with air staging and flue gas recirculation) coupled with a vertical tube which can be electrically heated (the so-called drop tube). At the exit of the drop tube, the measurement ports for the online corrosion probe and the mass loss probe are located. The grate furnace can be operated between 12–50 kW fuel input power (related to the net calorific value) and the drop tube has an electrical input power of up to 60 kW.

The grate furnace provides a flue gas composition typical of biomass combustion systems. The electrically heated drop tube allows for well-defined flow and temperature conditions at the measurement ports. With this combination, typical conditions at the superheater of a CHP plant can be achieved.

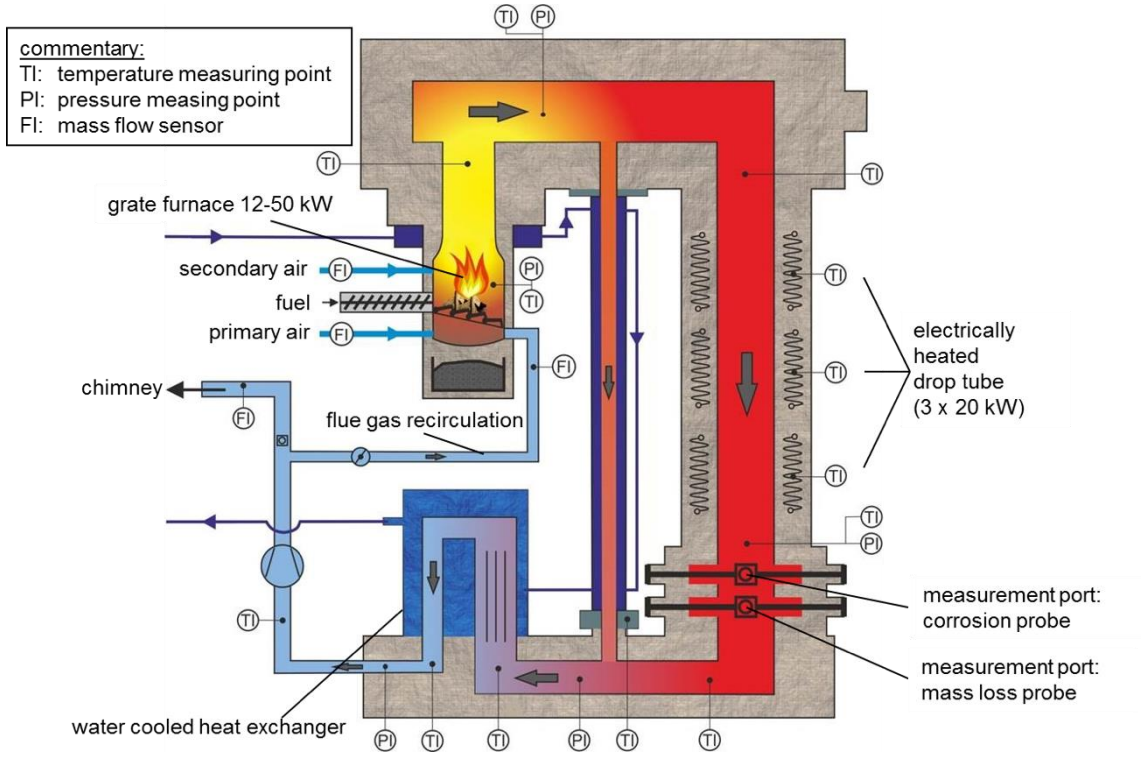

Figure 8: Scheme of the test rig (combined packed bed / drop tube reactor). Adapted from Paper II

3.3 Superheater steels investigated

The purpose of a superheater is to raise the steam temperature to generate power. Superheater tubes in biomass CHP plants are exposed to steam pressures typically ranging from 40 bar up to 310 bar and typical steam temperatures between 400°C and 540°C. On the one hand, the steels have to be heat-resistant to withstand the pressure at high-temperatures. On the other hand, they have to be resistant to corrosion on the flue gas side of the tube.

Besides low alloyed heat resistant steels, different grades of alloyed Fe-based steels as well as Ni-based materials are nowadays used to prevent corrosion of superheater tubes. Cr is one the most important alloying elements for Fe-based steels to enhance corrosion resistance. Since Cr has a very high affinity to O, it forms a thin, compact layer of Cr_2O_3 on the surface of the steel. This passive layer prohibits the diffusion of corrosive agents such as O into the steel as well as the diffusion of steel elements (e.g. Fe) outwards towards a corrosive agent. Therefore, the passive layer significantly reduces the corrosion rate. Ni is used as an alloying element since it enhances the corrosion resistance of Fe-based steels and increases the hardness, toughness and ductility. Typical corrosion-resistant stainless steels contain about 18 % Cr and 10 % Ni.

Based on the results of the study regarding steam parameters and superheater steels (see section 1.2), three superheater steels were selected for the corrosion investigations. To

ensure readability of the text, the most common denotations for the steels are used henceforward (bold letters in Table 1):

Table 1: Superheater steels selected for corrosion investigations

EN steel name	EN steel number	Trade name
13CrMo4-5	1.7335	-
X10CrMoVNb9-1	1.4903	**P91**
X6CrNiTi18-10	**1.4541**	-

The chemical compositions of the three steels are given in Table 2.

Table 2: Chemical compositions of the superheater steels in weight percent

Steel	C	Si	Mn	P	S	Al	Cu	Cr	Mo	Ni	Fe
13CrMo4-5	0.14	0.35	0.55	0.025	0.02	0.04	0.30	0.93	0.50	0.30	rest
P91	0.10	0.35	0.45	0.02	0.01	0.04	-	8.75	0.95	0.40	rest
1.4541	0.08	1.00	2.00	0.04	0.015	-	-	18	-	10.5	rest

13CrMo4-5 is a common superheater steel used in CHP plants firing chemically untreated wood chips but also in plants firing waste wood. The steel is among the low-alloy steels with a total alloy content below 5 wt.%. According to steel manufacturers, the temperature limit for continuous use is 560°C, but the steel is currently only used for steam temperatures up to 500°C in biomass-fired CHP plants.

According to plant manufacturers, there are plans to apply P91 as superheater steel in future plants firing chemically untreated wood chips at higher superheater temperatures (e.g. 520°C).

1.4541 is a high-alloyed steel which is to be used if necessary due to a high risk of high-temperature corrosion. Comparable steels with 18 wt.% Cr and 10 wt.% Ni are currently used for superheaters in straw-fired plants.

3.4 Online corrosion probes

The online corrosion probes applied in this thesis are based on a system which was developed at the Institute of Physics, Augsburg University. The probes were provided by Corrmoran GmbH and Babcock Borsig Steinmüller GmbH. The system is designed to simulate a superheater tube in the flue gas of a combustion system. The probes allow for online corrosion measurements which respond virtually in real time to changes in the corrosion rate [63], [64].

3.4.1 Principle

The corrosion rate measurement is performed by a sensor which consists of 3 electrodes as well as a mass loss ring, which are separated by ceramic isolators. (Figure 9 b). This temperature-controlled sensor is placed on the top of a water-cooled carrier-lance, which

is about 200 cm long (Figure 9 a). For the measurements, the corrosion probe is inserted into the flue gas of a combustion plant via an opening in the boiler casing. The sensor on top of the corrosion probe is cooled by air to a defined temperature. When exposed to the flue gas, a layer consisting of deposits and corrosion products is formed on the sensor surface. This layer represents an electrolyte and allows the measurement of the corrosion rate. The system is based on the measurement of a linear polarization resistance.

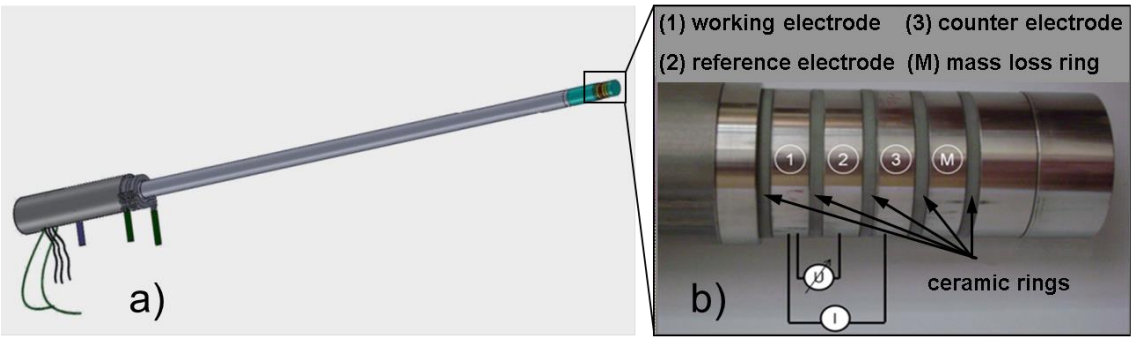

Figure 9: Scheme of the online corrosion probes (Paper I, II & III)
Explanations: a) Corrosion probe; b) sensor with three electrodes (1 - 3) and the mass loss ring (M); source: [38]

For the measurement, a voltage is applied between the working electrode and the counter electrode resulting in a current between the two electrodes. The voltage applied cannot be accurately measured between the two electrodes due to the chemical corrosion reactions on the electrodes. Therefore, the reference electrode is connected to the working electrode via a high-resistance voltage metering device and hence not influenced by the corrosion processes. Between the reference electrode and the working electrode the unbiased voltage can be measured.

The voltages applied are shifted around a value of zero, which results in different currents and allows the recording of a current-voltage-characteristic. The linear content of the gradient of the characteristic is called the linear polarization resistance l_P [mA/V], which is proportional to the actual corrosion rate k [mm/1000h] according to Eq. 6. The factor b [(mm/1000h)·(V/mA)] describing the relation between l_P and k is determined subsequent to the test run using the mass loss g of a mass loss ring. To determine this mass loss, the ring is weighed before being exposed to the flue gas. After the test run, the corrosion products are removed in accordance with ASTM G1-03 [65] (details in section 3.8.2) and the ring is weighed again. For the calculation of b (Eq. 7), g is calculated as the radial material loss of the mass loss ring in [mm]. A more detailed description of the online corrosion probe can be found in [37], [38].

$$k = l_P \cdot b \qquad \textbf{Eq. 6}$$

$$b = \frac{g}{\int l_P \, dt} \qquad \textbf{Eq. 7}$$

3.4.2 Start-up error

Since the conductive layer on the surface of the online corrosion probe starts to form as soon as the probe is exposed to the flue gas, the corrosion signal starts at zero and increases gradually. When a fully developed layer is formed on the surface, the corrosion signal l_P is proportional to the corrosion rate in accordance with Eq. 6. During this time (the initial phase), the corrosion signal does not represent the actual corrosion rate, which generally follows a paralinear trend [30], [45]. For the determination of the calibration factor *b,* the integral over the measurement signal is used in accordance with Eq. 7 (grey area in Figure 10). The wrong corrosion signal in the initial phase causes this integral (Figure 10 left) to be lower than the real one (Figure 10 right), which results in a too high calibration factor. This wrong calibration factor leads to an overestimation of the actual corrosion rate.

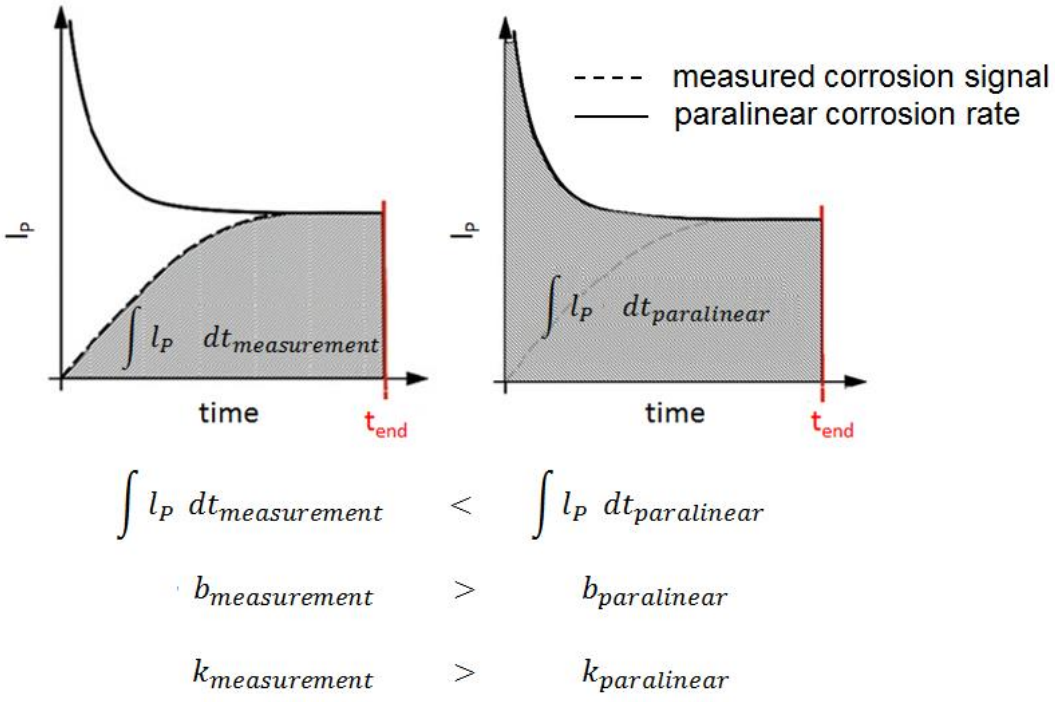

Figure 10: Schematic explanation of the measurement error occurring in the initial phase (adapted from Paper II)
Explanations: l_P: corrosion signal

This error can be neglected during long-term measurements conducted at real-scale plants which last more than several 1000 h. But in short-term measurements lasting about 500 h the error may significantly influence results, and if such measurements are to reflect or come close to real-life conditions, they cannot be neglected. Consequently, to be able to correct this “start-up” effect, a methodology was developed which combines results of parallel measurements of an online corrosion probe and a mass loss probe.

3.5 Mass loss probe

The mass loss probe consists of a carrier-lance with five test rings on top (Figure 11) which is cooled by air and is inserted into the flue gas. The temperature of the test rings is measured with a thermocouple located on the inside of the first test ring. A PID controller is used to control the cooling airflow.

For the measurement, the mass loss probe is exposed to the flue gas next to the online corrosion probe with the same surface temperature. Individual test rings are removed from the probe after different times to gain time-related mass losses. The mass loss is determined gravimetrically in accordance with ASTM G1-03 [65] (details in section 3.8.2) and expressed as a radial material loss in [mm].

By means of this procedure it is possible to establish a mass loss trend. The derivate of the trend towards time represents the trend of the real corrosion rate during the initial phase.

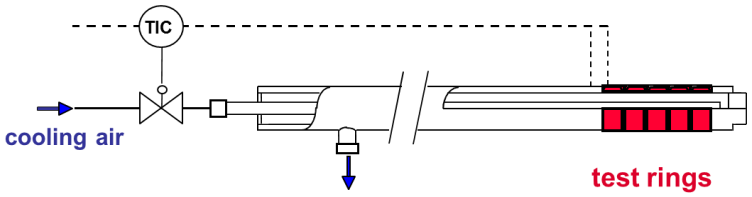

Figure 11: Scheme of the mass loss probe (adapted from Paper II)

3.6 Evaluation methodology for the combination of corrosion probe and mass loss probe

The evaluation methodology is described in detail in ***Paper II*** and is summarized at this point. The online corrosion probe and the mass loss probe are simultaneously exposed to the flue gas at the measurement ports. Both probes are operated at the same temperatures throughout the whole test run. Therefore, the corrosive attack should be similar for both probes. For the combination of the data from the two probes the test run is divided in two phases: the initial phase and the variation phase. During the initial phase, the operating conditions of the biomass reactor as well as the temperatures of the two probes are kept constant. During this phase a conductive layer forms on the online corrosion probe, and the trend of the corrosion rate is determined with the mass loss probe. At the end of the initial phase a fully developed layer exists on the online corrosion probe, and the measured corrosion signal I_P is proportional to the actual corrosion rate.

At this point, the variation phase is started, where the flue gas temperature and the probe surface temperatures are varied. Their influence on the corrosion rate is determined with the online corrosion probe.

To obtain the calibration factor for the calculation of corrosion rates from the corrosion signal, the mass loss occurring at the mass loss probe during the variation phase is used. The mass loss is combined with the integral over the measurement signal of the online

corrosion probe during the variation phase to calculate the calibration factor in accordance with Eq. 7. This calibration factor allows a correct calculation of the corrosion rates in accordance with Eq. 6 since it does not take the wrong online corrosion probe data from the initial phase into account. An example of this procedure is shown in section 4.2.1.

3.7 Deposit probe measurements

The deposit formation of ashes on heat exchanger surfaces was investigated using a deposit probe (Figure 12). This deposit probe consists of a carrier lance with a test ring on top, which is temperature-controlled by cooling air. The temperature of the test ring is measured with a thermocouple which is applied on the inside of the carrier lance close to the test ring. The carrier lance as well as the test rings are made of the high-alloyed steel X15CrNiSi25-20 to preclude corrosion processes.

For the measurement, the deposit probe is exposed to the flue gas for a certain time at a certain test ring temperature of interest. The test ring is weighed before and after the exposure. By means of this procedure, the deposit build-up rate can be calculated. This rate is expressed in relation to the surface of the test ring and the exposure time resulting in the unit [g/(m^2·h)].

The possibility to control the test ring temperature allows the simulation of heat exchanger tubes at different steam temperatures. By varying the exposure time, the time dependency of the deposit formation process can be investigated. Furthermore, the chemical composition as well as the structure of the deposits sampled can be analysed by means of SEM/EDX (Scanning Electron Microscopy / Energy Dispersive X-ray Spectroscopy) analyses.

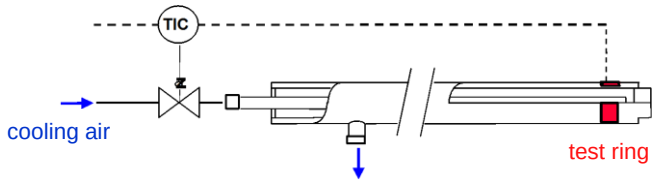

Figure 12: Scheme of the deposit probe
Explanations: TIC … temperature measurement and control; source: [2]

3.8 Analytical methods

3.8.1 Fuel analyses

The moisture content was determined in accordance with European Norm EN 14774-1 [66]. For further analyses, the samples were prepared in accordance with EN 14780 [67]. The determination of the ash contents was carried out in accordance with EN 14775 [68]. The C, H, and N-contents were determined in accordance with EN 15104 [69]. The determination of major and minor ash forming elements was carried out in accordance with EN 15290 [70] and 15296 [71].

3.8.2 Determination of mass loss from mass loss probe rings and online corrosion probe rings

To determine the mass loss of the test rings, the rings were weighed before being exposed to the flue gas. After the test run, the corrosion products were removed in accordance with ASTM G1-03. For this procedure, the corroded test rings were placed in an acidic solution in an ultrasonic bath for 10 minutes. Afterwards the rings were dried in a desiccator and weighed. This procedure was repeated until all corrosion products were removed. The accuracy of the method will be discussed in section 4.2.2.2.

3.8.3 SEM/EDX analyses of deposit probe samples and corrosion probe electrode rings

SEM/EDX was used to determine the chemical compositions of deposits sampled with the deposit probe. The deposit samples were coated with carbon before the analyses. The carbon coating ensures conductance of the surface and, hence, prevents the samples from charging during the analyses. The analyses were performed using a Zeiss Gemini 982 (SEM-system) and a Noran Voyager (EDX-system).

The deposit samples were analysed at three positions of the rings (windward, windward +50°, leeward) which are illustrated in Figure 13. The three positions were chosen due to differences in the deposit formation process which is explained in detail by Lauren [72] as well as in ***Paper III***.

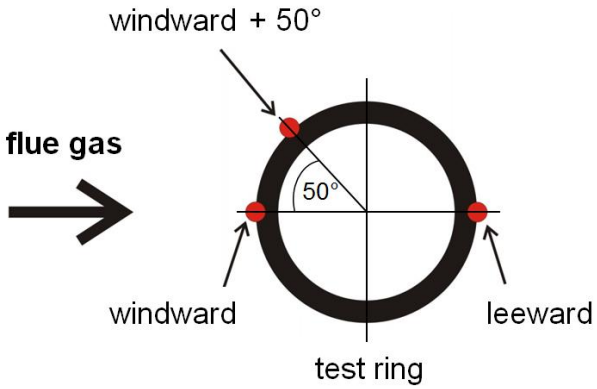

Figure 13: Scheme of the analyses positions for SEM/EDX

The electrodes of the online corrosion probes were analysed subsequent to the test runs using SEM/EDX to investigate the structure and chemical composition of the deposits and corrosion products. For preparation, the electrode rings were embedded in resin and ground with sand papers without using any fluid in order to avoid the dissolution of sample species. Then the samples were coated with carbon. The analyses were performed using a Zeiss Ultra 55 (SEM-system) equipped with an EDAX Pegasus (EDX-system). Analyses of the electrodes of the online corrosion probes were conducted at the windward position and the leeward position.

All analyses were performed using a voltage of 12 kV, which allows the determination of the most relevant elements without influencing the probe surface during the analyses.

However, at 12 kV, the EDX lines of Na and Zn overlap. Therefore, these two elements cannot be accurately separated in the analyses.

The SEM/EDX analyses were conducted at the Institute for Electron Microscopy and Nanoanalysis (FELMI) at Graz University of Technology and at the Graz Centre for Electron Microscopy (ZFE) at Austrian Cooperative Research (ACR).

4 Results

4.1 Real-scale measurements

Within this thesis online corrosion probe test runs were performed in a biomass CHP plant fired with chemically untreated forest wood chips (henceforward referred to as "wood chips") for the first time. Furthermore, measurements were conducted in a biomass CHP plant using a mixture of 50 % chemically untreated wood chips, 45 % waste wood of categories A1-A3 and 5 % waste wood of category A4 in accordance with German standards (henceforward referred to as "waste wood").

In order to characterise the fuels fired in these plants, fuel samples were taken at regular intervals during dedicated measurement campaigns at the plants and forwarded to chemical analyses. In Table 3 the fuel compositions of the wood chips as well as of the waste wood are presented.

Table 3: Fuel compositions of wood chips (Paper I) and waste wood
Explanations: w.b.: wet basis, d.b.: dry basis

		Wood chips 14 samples		**Waste wood 14 samples**	
		mean	std.-dev.	mean	std.-dev.
moisture content	wt.% w.b.	31.6	3.9	38.4	2.1
ash content (550°C)	wt.% d.b.	2.7	1.2	9.0	2.7
C	wt.% d.b.	48.1	0.4	45.7	1.1
H	wt.% d.b.	6.0	0.1	5.6	0.2
N	wt.% d.b.	0.3	0.1	1.2	0.2
S	mg/kg d.b.	262	70	944	217
Cl	mg/kg d.b.	117	71	1 141	625
Ca	mg/kg d.b.	4 723	1 207	13 018	3 187
Si	mg/kg d.b.	3 654	3 009	20 100	6 276
Mg	mg/kg d.b.	614	193	1 681	531
Al	mg/kg d.b.	615	424	2 122	570
Na	mg/kg d.b.	128	92	3 396	1 682
K	mg/kg d.b.	1 875	449	2 140	323
Fe	mg/kg d.b.	313	237	2 370	1 297
P	mg/kg d.b.	242	71	364	44
Mn	mg/kg d.b.	88	26	211	43
Zn	mg/kg d.b.	14.8	5.4	409.0	403.0
Pb	mg/kg d.b.	4.1	4.6	126.8	62.5
2S/Cl	mol/mol	6.0	2.4	2.2	0.9

The fuel analyses of the wood chips samples showed rather uniform fuel compositions. Although Ca, Si and Al showed comparably high standard deviations, they were within a normal range for biomass fuels. The most relevant elements regarding corrosion (K, S, Cl) were within typical variation ranges. Heavy metal concentrations (e.g. Zn) were small as expected in chemically untreated wood fuel. Therefore, the fuel was representative of

forest wood chips, and the most relevant elements for high-temperature corrosion were rather homogenous during the test run campaign. Hence, relevant impacts by fuel quality variations on the results were not likely.

The waste wood composition varied strongly, which is in agreement with the high variability of waste wood compositions reported i.e. by Krook et al. [73] and Edo et al. [74] for Swedish recovered waste wood comparable to A1-A4 in accordance with German standards. In order to evaluate the representative character of the waste wood, the composition presented in Table 3 is discussed briefly in comparison with compositions of waste wood A1-A4 obtained within BIOASH [75] and in comparison with the Swedish recovered waste wood reported by Edo et al. [74]:

- S and Cl contents were comparable to the values reported within BIOASH (S: 1500 mg/kg d.b.; Cl: 1200 mg/kg d.b.) and reported by Edo et al. (S: 1000 mg/kg d.b., Cl ranging from 700 – 1300 mg/kg d.b.)
- Mean values of K and Na were comparable to data from BIOASH (K: 2 500 mg/kg d.b.; Na: 2700 mg/kg d.b.) but higher than the values by Edo et al. (K ranging from 900 – 1400 mg/kg d.b., Na ranging from 800 – 1300 mg/kg d.b.).
- Regarding corrosion, also heavy metals such as Zn and Pb are of significant relevance. Their mean values were typical of waste wood compared with data from BIOASH (Zn: 800 mg/kg d.b, Pb: 140 mg/kg d.b) and from Edo et al. (Zn ranging from 300 – 600 mg/kg d.b., Pb ranging from 2 – 2900 mg/kg d.b.).

In conclusion, the the composition of the the waste wood used within the test runs for this thesis was within typical ranges for waste wood A1–A4 in accordance with German standards. However, the deviation in K and Na from the results of Edo et al. showed that waste wood is a very inhomogeneous fuel, and waste wood used in different plants may vary strongly in composition. Furthermore, different countries have different laws governing the use of wood preservatives and coatings. Therefore, the comparison of waste wood compositions originating from different countries is difficult.

As shown in section 2.1.2, the molar ratio of 2S/Cl is an indicator of the high-temperature corrosion risk due to Cl-induced active oxidation. For wood chips, the mean value of the 2S/Cl ratios of the fuel samples analysed was calculated at 6.0. Therefore, only a minor risk of Cl-induced active oxidation was to be expected. For waste wood, the mean value was 2.2, resulting in a significantly higher risk for Cl-induced active oxidation. Furthermore, the waste wood contained significantly higher concentrations of the heavy metals Zn and Pb. Therefore, the formation of eutectic salt mixtures with low melting temperatures was more likely compared with wood chips. This means that for waste wood the risk of high-temperature corrosion due to molten salts (see section 2.1.3) was significantly higher.

4.1.1 Test run in a CHP plant fired with wood chips (Paper I)

In an Austrian CHP plants firing wood chips, two corrosion probes were applied in parallel in the radiative section of the boiler to determine the applicability of the probes in

biomass-fired boilers. For this test run, the superheater steel 13CrMo4-5 was used on the online corrosion probes. In order to use the correct (radiation free) flue gas temperatures for the test run evaluation, suction pyrometer measurements were performed at the positions of the online corrosion probes. These measurement data were correlated with the data measured with thermocouples which were used to measure the flue gas temperature over the whole test run. The suction pyrometer measurements as well as the correlations with the thermocouples are presented in ***Paper I***. Henceforward only suction pyrometer corrected flue gas temperatures are used within this thesis.

Figure 14 shows weekly mean values as well as the standard deviations of relevant plant operating data. The plant was operated in rather stable conditions except for weeks 15 and 16 when an unexpected plant shutdown took place. This shutdown affected the corrosion probe measurements to the effect that after the re-start of the plant the corrosion signals were rather unstable and it took about three weeks to regain a stable and meaningful corrosion signal.

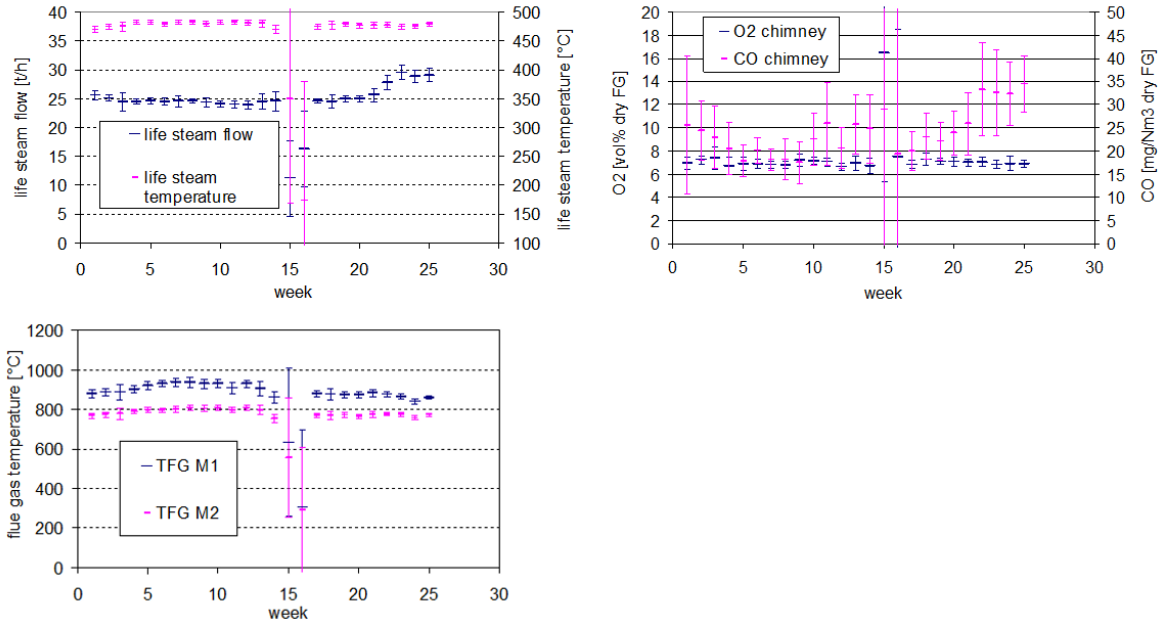

Figure 14: Operating data of the wood chips fired CHP plant during the test run (adapted from Paper I).
Explanations: operating data were recorded at 1-minute intervals, mean values of one week are shown, and the corresponding standard deviations; TFG: flue gas temperature; CO emissions related to dry flue gas and 13 vol.% O_2; M1: measurement position 1; M2: measurement position 2 (see Figure 6)

In weeks 21 to 25 the boiler load was increased due to an increased demand from the district heating network, as can be seen in the life steam flow. The life steam flows of 25.1 t/h (week 2) and 29.0 t/h (week 25) correspond to boiler outputs of 21.4 MW and 24.7 MW. The increased boiler load in weeks 21 to 25 resulted in increased flue gas flow rates, but the mean values of the flue gas temperatures remained almost the same as at lower boiler load. Consequently, for the whole corrosion measurement period, stable and

well comparable conditions regarding flue gas temperatures prevailed. The continuous O_2-measurements show largely constant values; the variations of the CO-concentrations can be caused by variations of the fuel moisture content, the fuel composition and the boiler output as well as by inhomogeneous distribution of the fuel on the grate. In general, a very good flue gas burnout was achieved.

4.1.1.1 Online corrosion probe measurements

For the corrosion probe measurements a stable corrosion signal needs to be established at the beginning of a test run (see section 3.4.2). For this period, a probe temperature of 480°C was chosen, since this also represents the steam temperature of the CHP plant where the test run was performed. After the establishment of a stable signal, the probe temperatures were varied stepwise in the range between 400°C and 560°C for certain times. The dependence of the corrosion rate on the flue gas temperature was determined by the variations in the flue gas temperatures due to changes in the boiler load. Figure 10 shows selected results of the corrosion probe measurements at position M1 to illustrate the correlations found. Detailed results are presented in ***Paper I***. Figure 15 a) shows a clear trend of increasing corrosion rates with increasing probe temperatures. In Figure 15 b) it can be seen that increasing flue gas temperatures results in increasing corrosion rates, too. The data indicate that the corrosion rates immediately follow variations of the probe surface temperature and the flue gas temperature.

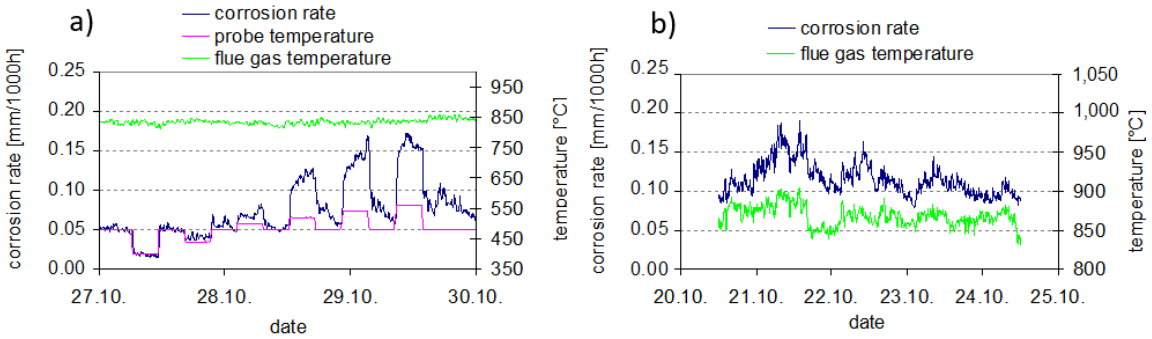

Figure 15: a) Corrosion signal of the corrosion probe at position M1 dependent on the probe temperature at rather constant flue gas temperatures; b) Corrosion rates of the corrosion probe at position M1 dependent on the flue gas temperature at constant surface temperatures of the corrosion probe (adapted from Paper I)

The data gained from the online corrosion probes were evaluated by calculating mean values at certain flue gas temperatures (+/- 10°C) and certain corrosion probe temperatures (+/- 1°C). This evaluation is presented in Figure 16 and shows the resulting corrosion rates for both corrosion probes dependent on the probe surface temperature and the flue gas temperature. The flue gas temperatures at the two measurement positions overlapped to a certain extent at 810°C. This overlap allowed a first evaluation whether the data of the two probes matched for similar flue gas temperatures. Figure 16 shows that the data of the two corrosion probes nearly agree. This means that by the

application of multiple corrosion probes in parallel, a wider range of flue gas temperatures can be investigated.

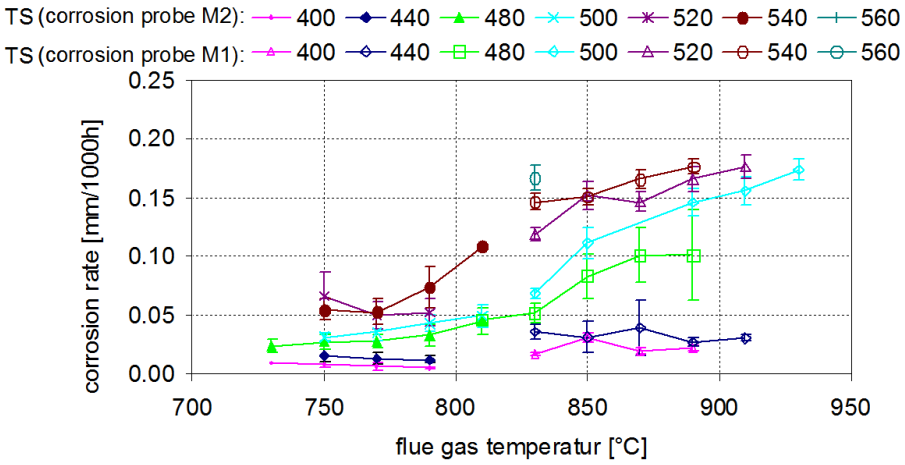

Figure 16: Comparison of corrosion rates of corrosion probes M1 and M2 dependent on the flue gas temperature for certain probe surface temperatures (adapted from Paper I).
Explanations: T_S: surface temperature of corrosion probe; error bars show the standard deviations

High-temperature corrosion rates determined in waste incineration plants [24] showed exponential dependencies on probe surface temperatures and the flue gas temperatures. This behaviour was described using an Arrhenius function, which is based on the assumption that the dissolution of the metal into the oxide layer is the rate-determining step. The rates determined within this thesis only showed an exponential dependency on the probe surface temperature from 400°C to 520°C (presented in detail in ***Paper I***). For higher probe surface temperatures, the gradient of the corrosion rates decreased, which indicates that another mechanism had become rate-determining. However, these mechanisms were not investigated in more detail within this work. The dependency on the flue gas temperature is usually caused by the reactions in the outer layers of the deposits [38]. The most common reaction here is the release of gaseous chlorine by the sulphation of chlorides, which leads to Cl-induced active oxidation. Within this thesis, the dependency on the flue gas temperature was not investigated in more detail.

Test runs in waste incineration plants conducted by Maisch [38], as well as test runs at the test rig (see section 3.2.2) performed by Gruber et al. [76], showed a dependency of the corrosion rate on flue gas velocity. In order to investigate a possible influence of the flue gas velocity on the corrosion rates in the wood chips fired CHP plant, corrosion rate data obtained during a period with a constant probe surface were used. Since variations of the flue gas temperature occurred throughout the test run, the influence of the flue gas temperature on the corrosion rate had to be mathematically eliminated. For this purpose, a reduced corrosion rate was calculated, which refers to a constant flue gas temperature at a constant probe surface temperature. Therefore, variations caused by the flue gas velocity should be identifiable. The methodology for the calculation of the reduced corrosion rate is illustrated in ***Paper I***.

The flue gas velocity at the positions of the online corrosion probes was calculated based on the air flow measurements from the process control system and CFD simulations performed for a comparable biomass CHP plant. Details regarding this procedure are elaborated in ***Paper I***.

Figure 17 a) shows the corrosion rates as well as flue gas temperatures and flue gas velocities (divided by 50 to fit on the primary axis) for corrosion probe M1. In Figure 17 b), the reduced corrosion rates are plotted against the flue gas velocities. Since this data show corrosion rates for a constant probe surface temperature and a constant flue gas temperature (mathematically calculated), an influence of the flue gas velocity would be detectable here. From Figure 17 b) it can be seen that no clear correlation between the corrosion rate and the flue gas velocity can be identified.

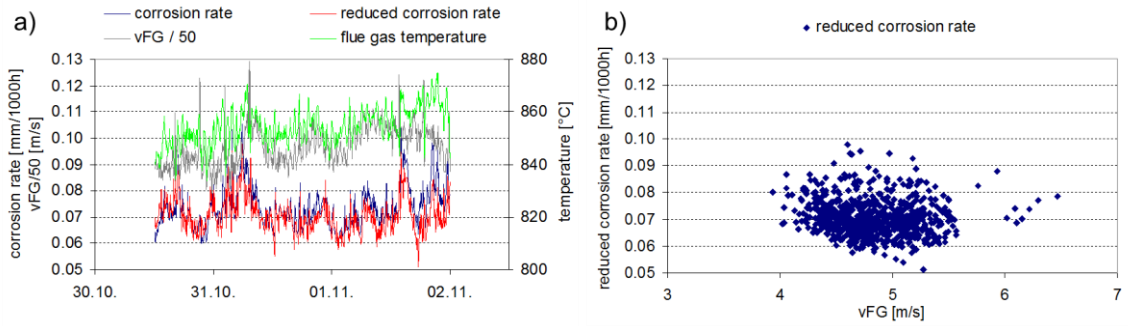

Figure 17: (a) Corrosion rates at a constant probe temperature of 480°C as well as flue gas temperatures and flue gas velocities. Flue gas velocities were divided by a factor of 50 to fit on the primary axis of the figure. (b) Reduced corrosion rates (adapted from Paper I)

A possible reason for the discrepancy vis-à-vis the results of Maisch and Gruber is the variation in flue gas velocity. Maisch used corrosion rate data for flue gas velocities of 0.5 m/s and 9.5 m/s for her observations, whereas Gruber varied the flue gas velocity from 2 – 8 m/s. The data shown in Figure 17 b) range mainly from 4 – 5.5 m/s. Gruber reported only a minor influence of the flue gas velocity on the corrosion rate. Therefore, the narrow variation range might not be enough to identify a possible correlation. Furthermore, the corrosion rates fluctuated more strongly compared with the data of Gruber. Therefore, the identification of small influencing factors is more difficult or impossible in the case at hand.

The corrosion rates determined within this test run ranged from 0.01 to 0.18 mm/1000h. For a probe surface temperature of 480°C, which was also the final steam temperature of the CHP plant, the rates ranged from 0.03 to 0.10 mm/1000h. If one assumes an operating time of 8000 h per year, the total corrosion would result in 0.24 – 0.8 mm per year. Based on the experience of the plant operator, no measureable corrosion occurred at the final superheater of the plant over the period from 2006 (commissioning) to 2011. This means that the absolute values from the online corrosion probe measurements cannot be applied in practice directly. However, the trends of the influencing factors on the corrosion rates can be applied. Most likely, the variations of the probe surface temperature cause too high corrosion rates. Due to these temperature variations,

spallation of the corrosion layers and deposits occurs which enables corrosive species to attack the ground material multiple times. Therefore, the function of a protective layer, which is typically formed at constant operating conditions (as described in section 2.1.1), is destroyed.

4.1.1.2 Deposit probe measurements

In addition to the online corrosion probe measurements, deposit probe measurements were performed to investigate the deposit formation process. For this purpose, deposits were sampled at probe surface temperatures of 480°C and 560°C over a period of 2 h. The measurements were conducted in week 4 during partial boiler load, and during week 23 during increased boiler load (see Figure 14). Subsequent to the sampling, the deposits were analysed by means of SEM/EDX at three positions of the rings. The three positions were chosen on account of differences in the deposit formation process which is explained in detail by Lauren [72] as well as in ***Paper III*** (see also section 3.8.3). Figure 18 shows the results of the analyses of the deposits sampled at measurement position M1 (see Figure 6).

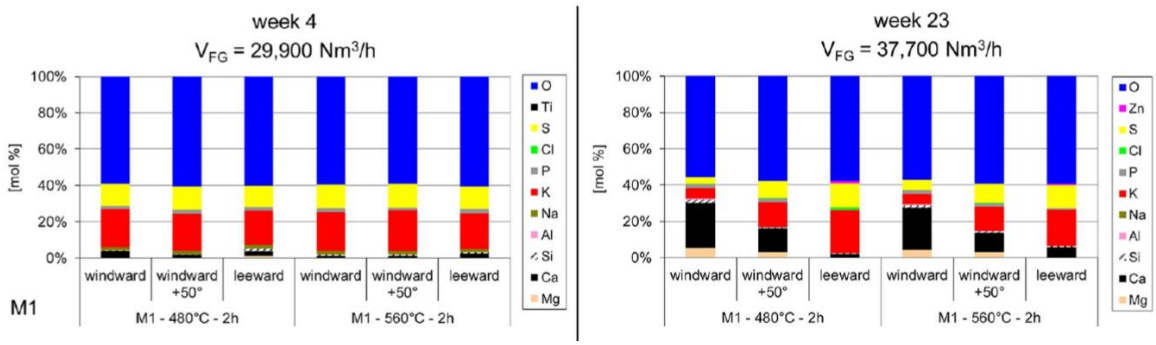

Figure 18: Results of SEM/EDX analyses of the deposits sampled at the positions of the corrosion probes. (adapted from Paper I).
Explanations: The caption of each analysis characterizes the sampling point, the surface temperature of the test ring and the sampling time, e.g., M1 at 480°C for 2 h

The analyses of the deposits sampled (Figure 18) generally show that the variation in the surface temperatures of the test rings did not significantly influence the chemical composition of the deposits. At low boiler load, the deposits mainly consisted of K and S independent of the point analysed. The ratio of K and S indicates K_2SO_4 as the main component of the deposits. With increased boiler load, increased ratios of Ca and Mg were found in the deposits, especially on the windward side. Since deposits on the windward side are mainly formed by inert impaction [72], this result indicates a higher entrainment rate of ash from the grate.

Cl was generally only found in small quantities in the deposits during the corrosion test run, with a maximum concentration of 1.0 wt.% (week 23, M1 – 480°C – 2h, leeward). The Cl concentrations found were higher at a probe surface temperature of 480°C compared with 560°C. This result can be explained by higher condensation rates of gaseous

chlorides due to the lower probe surface temperature. More details on the deposits probe measurements are presented in ***Paper I*.**

4.1.1.3 Analyses of online corrosion probe rings

Subsequent to the test runs, the electrode rings from the online corrosion probes were analysed by means of SEM/EDX. Figure 19 shows a macro image of a corroded electrode ring from corrosion probe M1 as well as the corresponding SEM picture of the relevant layers.

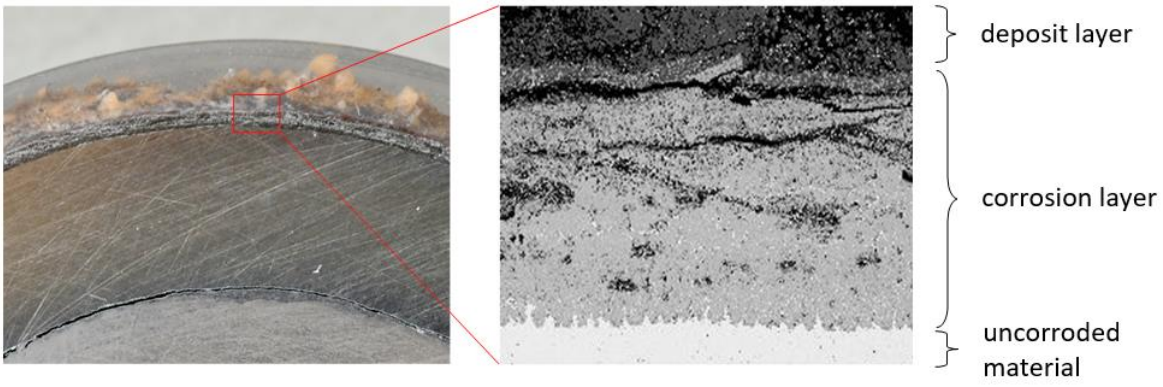

Figure 19: Scheme of SEM / EDX analyses: exemplarily on one ring from corrosion probe M1 *Explanations*: position: windward (Paper I)

The element mappings presented in Figure 20 show that on the windward as well as on the leeward side, deposits mainly consisted of K, S and Ca. This indicates the presence of K_2SO_4 and $CaSO_4$. The corrosion layer mainly consisted of Fe, Cr and O, which indicates that it was only formed of oxides from the ring material. The corrosion layer shows some cracks or spallation, which is most likely the result of the variations in the probe surface temperature.

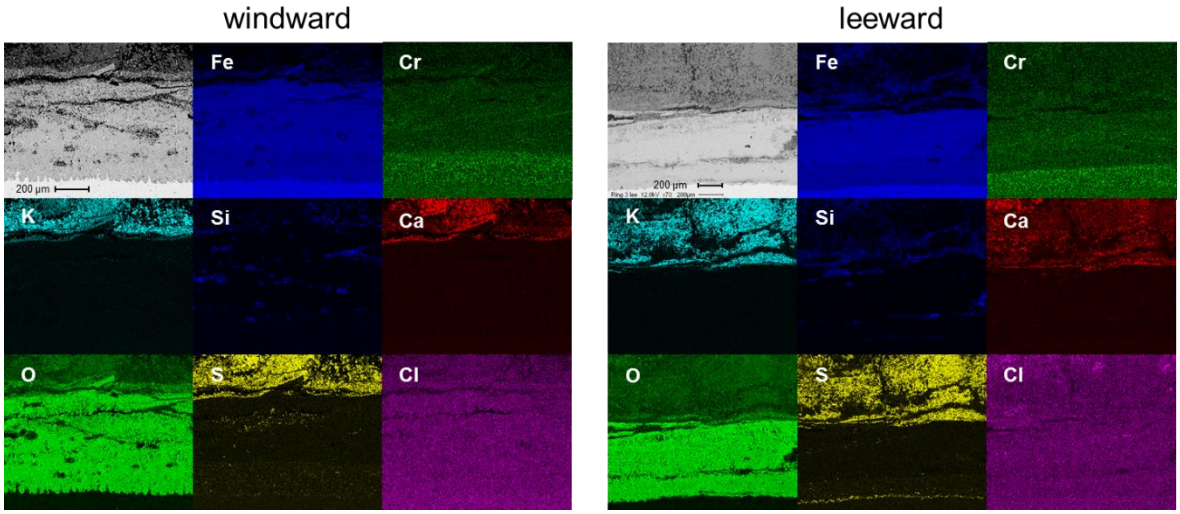

Figure 20: EDX-mappings of one ring from the corrosion probe at position M1 (adapted from Paper I)

At the corrosion front on the leeward side, an enrichment of S was found. Comparable results were also found during test runs with online corrosion probes in lab-scale experiments using wood chips as fuel [76]. There it was concluded that the S enrichment consists of iron sulphides. Their formation was already investigated in the past (see [77], [78]) and was explained by the reaction of SO_2 with the steel [3]. Furthermore, S may be present as FeS or FeS_2 due to the sulphation of metal chlorides resulting from Cl-induced active oxidation [79], [80]).

On the windward side as well as on the leeward side, no Cl was found at the corrosion front, which would indicate that Cl-induced corrosion was a relevant corrosion mechanism. Although Cl was found in the deposit probe samples at a probe surface temperature of 480°C, no Cl was found on the corrosion probe rings. Therefore, certain differences in the chemical compositions of the deposits sampled with the deposit probe and the deposits on the online corrosion probe are evident.

As pointed out in detail in ***Paper IV***, the analyses of the corrosion probes were conducted after variations of the probe surface temperature in the range of 400°C to 560°C. These variations may have produced two effects. First, at high probe surface temperatures, already deposited chlorides and active Cl may have evaporated. Second, at times of low probe surface temperatures increased condensation of chlorides may have occurred. This Cl could have been active for some time until the temperature was increased again and Cl would have disappeared. Based on these results, Cl-induced corrosion cannot be excluded as a corrosion mechanism for the wood chips test runs. Besides Cl-induced active oxidation, also the oxidation of steel by oxygen in the flue gas may play a relevant role in the case, as discussed in ***Paper IV.***

The difference between the deposits sampled with the deposit probe and the deposits on the online corrosion probe shows that SEM/EDX analyses of the online corrosion probes allow a general investigation of the chemistry of deposits and corrosion products. However, a detailed investigation of the corrosion mechanism in not possible due to the variations of the probe surface temperature. For this purpose, a test run at a constant temperature would be more meaningful.

4.1.2 Test runs in a CHP plant fired with waste wood

In addition to the measurements in the wood chips firing CHP plant, a testing campaign in a German CHP plant firing a mix of waste wood (A1-A4 in accordance with German standards) and chemically untreated wood chips was conducted. Two corrosion probes were applied in the radiative section of the boiler (see Figure 7). Similar to the measurements in the wood chips firing CHP plant, 13CrMo4-5 was used for the investigation, and probe surface temperatures were varied between 400°C and 560°C.

The corrosion probe measurements lasted for four months in total, with three dedicated measurement weeks on site for fuel sampling and deposit probe measurements. Although the plant was operated at mainly stable conditions, four unplanned shutdowns occurred (weeks 1/2, 12/13, 14, 15/16) during the 4 months. Figure 21 presents relevant

operating data of the plant. The data recorded during the shutdowns (criteria: O_2 in the flue gas > 18 vol.%) were removed for the evaluation presented in Figure 21. The operating data show a reduced steam flow in weeks 13 – 16 due to the plant shutdowns. With the exception of the shutdowns, the plant was operated at nominal boiler load. The evaluation of the flue gas analyses data shows that CO emissions were usually below 50 mg/Nm³ (dry flue gas at 11 % O_2). Therefore, complete combustion was achieved. Mean flue gas temperatures at the positions of the corrosion probes were 869°C at position M1, and 799°C at position M2.

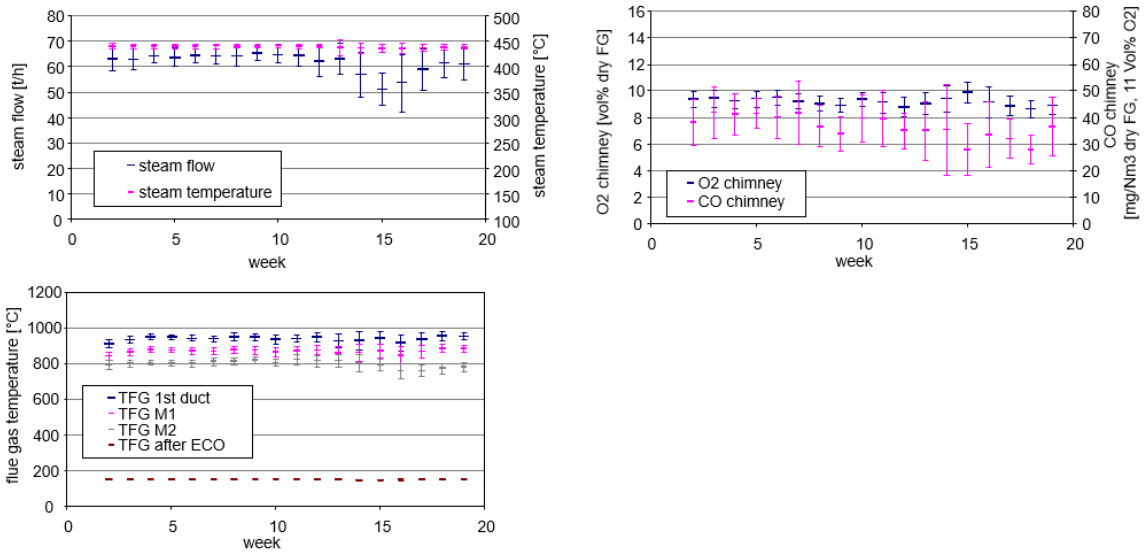

Figure 21: Operating data of the waste wood fired CHP plant during the test run.
Explanations: operating data were recorded at 1-minute intervals, mean values of one week are shown, and the corresponding standard deviations; TFG: temperature of the flue gas; ECO: economizer; CO emissions related to dry flue gas and 11 vol.% O_2

4.1.2.1 Online corrosion probe measurements

Similar to the measurement procedures in the wood chips fired CHP plant, a stable corrosion signal was established at a probe temperature of 480°C. After the stable signal was obtained, variations of the probe temperatures were started. Variations in the flue gas temperature occurred due to changes in the boiler load.

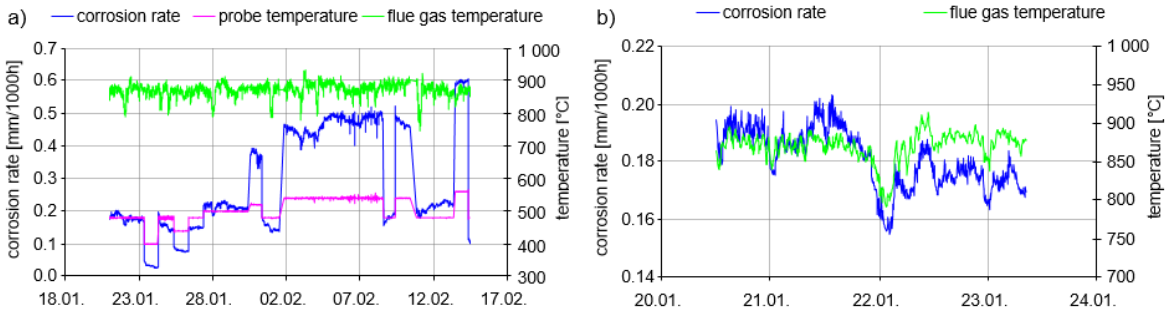

Figure 22: Corrosion signal of the corrosion probe at position M1 dependent on the probe temperature at rather constant flue gas temperatures; b) Corrosion rates of the corrosion probe at position M1 dependent on the flue gas temperature at constant surface temperatures of the corrosion probe

Figure 22 shows that changes in the probe surface temperature (Figure 22 a) as well as in the flue gas temperature (Figure 22 b) resulted in immediate, plausible changes of the corrosion rate. This shows that online corrosion probes are also applicable to the determination of high-temperature corrosion rates in plants firing waste wood.

The evaluation of the corrosion rates dependent on the probe temperature and the flue gas temperature was performed by means of a similar procedure as used for the data obtained in the wood chips fired CHP plant. Mean values of the corrosion rates at certain flue gas temperatures (+/- 10°C) and certain corrosion probe temperatures (+/- 1°C) were calculated. The results are presented in Figure 23.

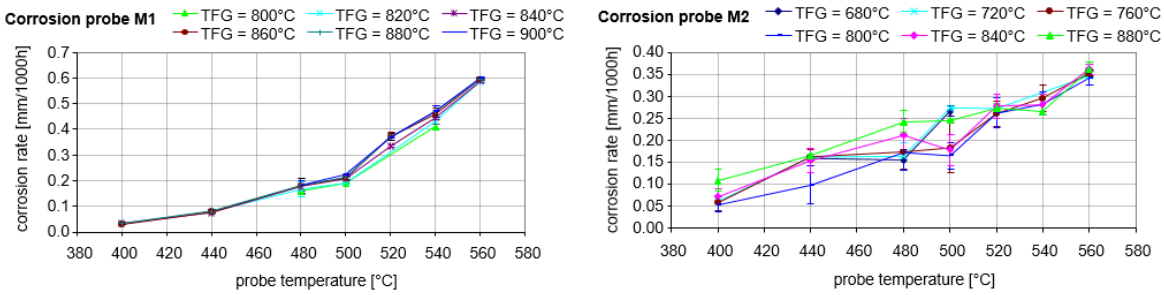

Figure 23: Comparison of corrosion rates of corrosion probe M1 and M2 dependent on the probe temperature for certain flue gas temperatures.
Explanations: TFG: flue gas temperature; error bars show the standard deviations

The data in Figure 23 show a clear dependence of the corrosion rate on the probe temperature, but only a minor or not replicable dependence on the flue gas temperature. It can be seen that only a slight influence of the flue gas temperature is measureable which is not as distinctive as found for shorter intervals, as presented in Figure 22 b). Possible reasons are, for instance, changing fuel compositions, as is to be expected for a plant firing waste wood. These will result in different corrosion rates at similar probe and flue gas temperatures. Additionally, the detaching of deposit and corrosion layers on the corrosion probes influences the measurement signal. SEM/EDX analyses (see section 4.1.2.3) show multiple corrosion layers, which point to a detachment during the

measurements. Such detachments were also reported during laboratory high-temperature corrosion measurements conducted by Westen-Karlsson [81].

Figure 24 shows a plot of the corrosion rates of both corrosion probes dependent on the flue gas temperature. It shows that the corrosion rates obtained by the two corrosion probes do not overlap as was the case with the measurements in the wood chips fired CHP plant (see section 4.1.1.1). The corrosion rates determined within the test runs ranged from 0.03 mm/1000h to 0.6 mm/1000h. For the evaluation regarding the applicability of the data, the corrosion rates for a probe surface temperature of 440°C are used, since the steam temperature of the plant is 450°C. Hence, the corrosion rates should be comparable to the experience of the plant operator. The corrosion rate at a probe surface temperature of 450°C is between 0.08 and 0.09 mm/1000h. If one assumes an operating time of 8000 h per year, the total corrosion would amount to 0.64 – 0.72 mm per year. Since typical superheater tubes have a wall thickness 4 to 5 mm, this would result in a maximum operating time of 6 – 7 years. According to the experience of the plant operator, no measureable corrosion occurred at the final superheater of the plant over the period from 2004 (commissioning) until 2012. Therefore, absolute values of the corrosion rates determined with the online corrosion probes are not directly applicable.

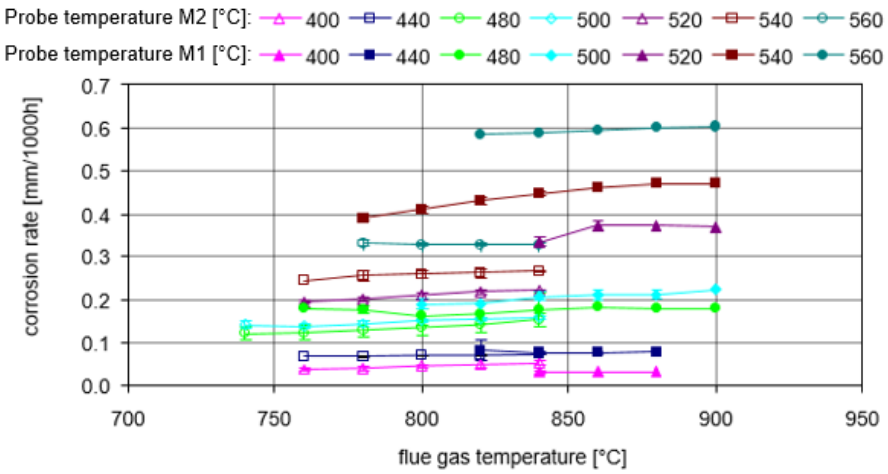

Figure 24: Comparison of corrosion rates of corrosion probe M1 and M2 dependent on the flue gas temperature for certain probe temperatures.
Explanations: error bars show the standard deviations

This overestimation of corrosion rates was also found and already discussed for the measurements in the CHP plant firing wood chips. Since the methodology regarding the temperature variations was similar, most likely the same reasons for the too high corrosion rates apply (section 4.1.1.1).

4.1.2.2 Deposit probe measurements

Deposit probe measurements were conducted in addition the corrosion probe measurements close to the positions of the online corrosion probes (see Figure 7). Similar

to the measurements in the wood chips fired CHP plants, probe surface temperatures of 480°C and 560°C were used for deposit sampling. Figure 25 presents the results of SEM/EDX analyses of the deposits sampled in weeks 8 and 11 at position M1. In both weeks, the boiler load was similar, with mean steam flow rates of 64 t/h, which is the nominal boiler load.

The fuel analyses presented in Table 3 showed significant standard deviations in the fuel composition, as is to be expected for waste wood. Therefore, it was expected that the deposit compositions would vary within a noticeable range. However, the analyses of the deposit probe samples (Figure 25) show comparable compositions for weeks 8 and 11. From the results of these analyses it was concluded that the deposit compositions were constant enough to provide a good basis for the evaluation of corrosion rates during long-term corrosion probe measurements.

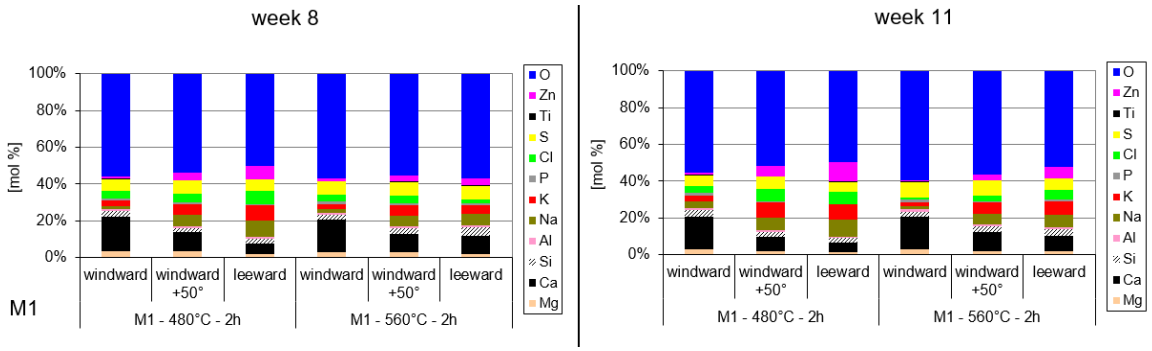

Figure 25: Results of SEM/EDX analyses of the deposits sampled at the positions of the corrosion probes.
Explanations: The caption of each analysis characterizes the sampling point, the surface temperature of the test ring, and the sampling time, e.g., M1 at 480°C for 2 h

Deposits on the windward side mainly consisted of elements typically found in coarse fly ashes (Ca, Si, Mg). Furthermore, K, Na as well as S and Cl were found, indicating the presence of alkali metal sulphates and chlorides. Additionally, Zn was found in relevant concentrations. On the leeward side, significantly lower concentrations of Ca, Si and Mg were found. Instead, the shares of alkali metals and Zn as well as S and Cl were higher.

Coarse fly ash particles are typically deposited by impaction. Therefore, they are mainly found on the windward side. Alkali metal chlorides and sulphates are usually deposited by direct condensation from the gas phase as well as thermophoresis if they are already solid. Zn can be found as ZnO, which is deposited by thermophoresis, or as $ZnCl_2$, which condenses from the gas phase on the cooled surface. It has to be kept in mind that an accurate separation of Zn and Na is not possible by EDX analyses at 12 kV. However, since Zn was found in noticeable concentrations, it is very likely that Zn occurred in the deposits. The lower shares of coarse fly ash particles on the leeward side result in increased shares of the other elements.

The measurements at two different probe surface temperatures (480°C and 560°C) revealed increased shares of chlorides at 480°C. Lower probe surface temperatures lead

to increased condensation rates, which result in increased concentrations of these compounds.

4.1.2.3 Analyses of online corrosion probe rings

The electrode rings from the online corrosion probes were analysed by means of SEM/EDX in a similar manner as for the test runs in the wood chips fired CHP plant. In contrast to the results from the wood chips fired CHP plant, the corrosion layers are significantly more spalled and more separated from the uncorroded ground material.

The EDX mappings on the windward and the leeward sides show that the outside deposit layers mainly consist of K, Na (Zn) and Cl. This indicates the presence of KCl and NaCl. Zn can be present as $ZnCl_2$ or as ZnO. However, Na and Zn could not be separated during the analyses as pointed out in section 3.8.3. Towards the inside, the deposits consist of Ca, Si and S as well as lower concentrations of K. These elements indicate Ca- and K-sulphates as well as Si-oxides. On the windward side, there are separate corrosion layers with elements of deposits (Na, K, S, Cl) between the corrosion layers. This indicates a detachment during the test run resulting from the shutdowns on the one hand and from the temperature variations on the other [82].

At the corrosion front, only a minor enrichment of S and Cl was found on the windward side. Such enrichments would indicate the participation of the elements in the corrosion process. However, since significant concentrations of Cl were found in the deposits, Cl-induced corrosion is very likely to be a dominant corrosion mechanism.

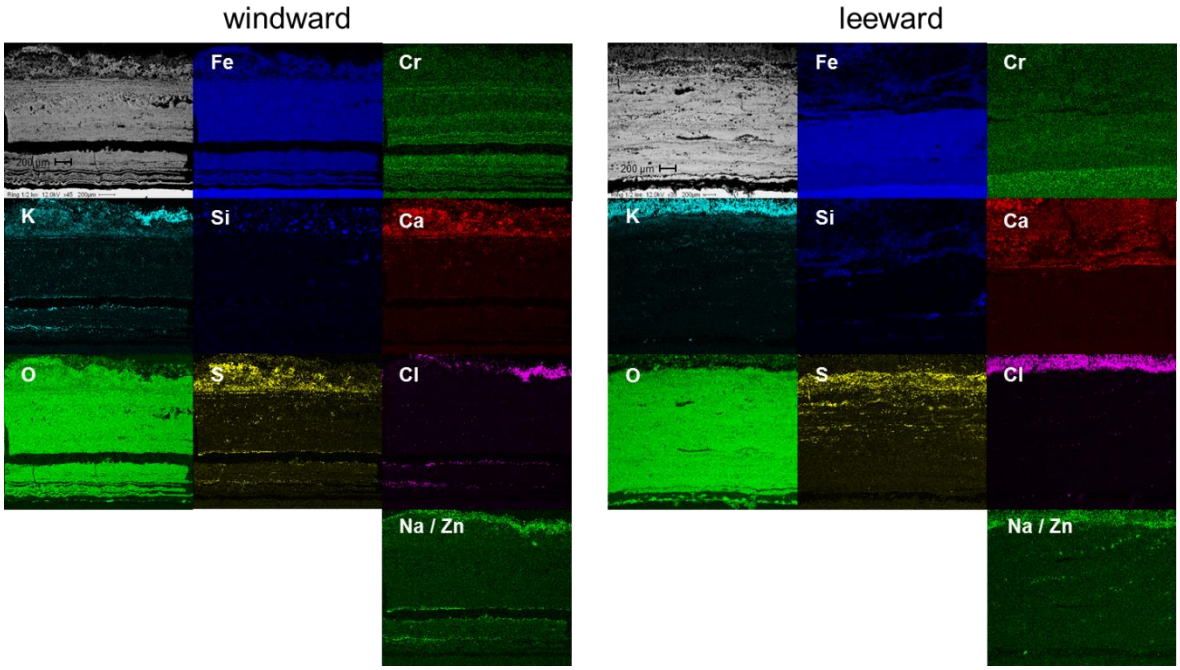

Figure 26: EDX-mappings of one ring from the corrosion probe at position M1

The results of the SEM/EDX analyses of the corrosion probe rings closely agree with those of the deposits sampled with the deposit probe, although the surface temperature of the online corrosion probe was varied between 400°C and 560°C. Since the deposits sampled with the online corrosion probe at 480°C and 560°C showed no significant differences in chemical composition it was concluded that the variations did not alter the chemical compositions significantly either.

4.2 Lab-scale measurements

The results of the test runs in real-scale plants showed the applicability of online corrosion probes in biomass-fired boilers and provided useful data on corrosion rates. However, access to the boiler is often only possible at certain points in some distance to the superheaters. Here, flue gas conditions (temperatures and chemical environment) can deviate from conditions at the actual superheaters. Furthermore, operating conditions and fuel compositions can vary, and unexpected shutdowns can interfere with the measurements.

For these reasons, online corrosion probe measurements were applied at a test rig, which can be operated at well-defined conditions and allows the use of more homogeneous fuels. Additionally, parameters of interest such as flue gas temperature or flue gas velocity can be arbitrarily defined. Due to the possibility of constant and stable operating conditions, test runs for the investigation of a set of probe surface and flue gas temperatures can be performed in significantly shorter time compared to a real-scale test run. Consequently, a test rig allows the determination of the influence of single parameters on high-temperature corrosion in more detail.

4.2.1 Application of a mass loss probe (Paper II)

In ***Paper II***, the methodology for the combination of a newly developed mass loss probe with an online corrosion probe is described in detail. In this thesis, the methodology as well as the main results are briefly summarized.

In order to perform short-term online corrosion probe measurements, a methodology for the correction of the start-up error (see section 3.4.2) was developed. This was achieved by the application of a mass loss probe (section 3.5) which is applied in combination with an online corrosion probe. The development and validation of this methodology was performed using forest wood chips as fuel and 13CrMo4-5 as superheater steel.

The evaluation test run lasted for 480 h. The first 334 h were used to determine the corrosion kinetics with the mass loss probe (initial phase) and the remaining 146 h were used to determine corrosion rates for certain influencing parameters (variation phase). During the initial phase, the mean flue gas temperature at the measurement ports was held at a constant level of 745°C (standard deviation: 12.9°C).

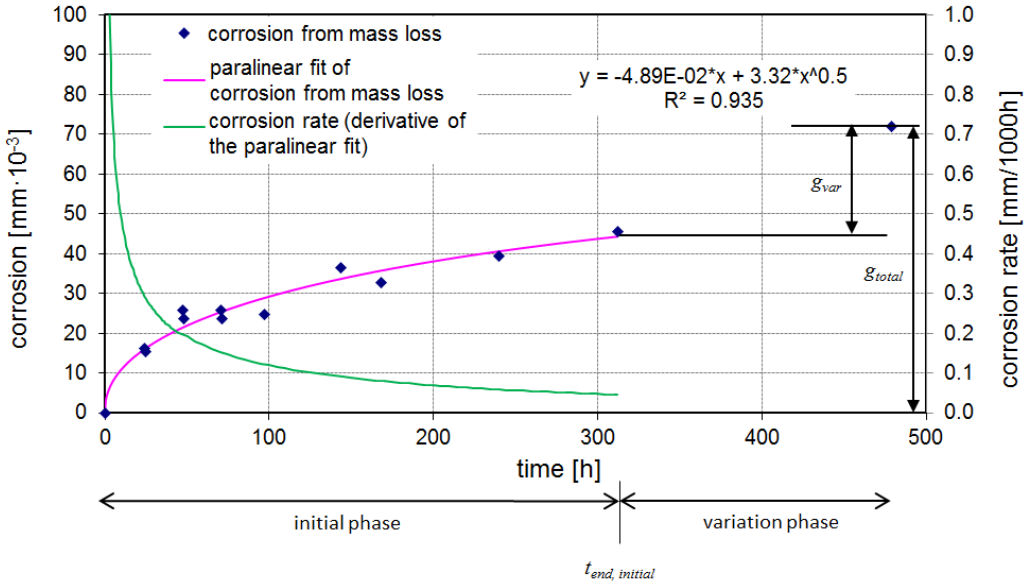

Figure 27: Results from the mass loss probe and a paralinear fit of the mass loss during the initial phase (adapted from Paper II)

The online corrosion probe and the mass loss probe were operated at a mean constant surface temperature of 480°C (standard deviation: 0.1°C). The resulting mass losses are presented in Figure 27. Here, a distinction is made between the initial phase and the variation phase. In the initial phase, high values of the corrosion rate prevail in the beginning, which decrease with time. The data obtained were fitted using a paralinear equation (see section 2.2.3). The total mass loss at the end of the test run, g_{total} was determined with the mass loss ring on the online corrosion probe. The mass loss during the variation phase g_{var} was determined using the paralinear fit at the end of the initial phase ($t_{end, initial}$).

Figure 28 shows the measurement signal of the online corrosion probe over the time. It can be seen that the trend of the corrosion signal starts from zero and steadily increases to a rather constant level at 315 h. However, this trend does not reflect the real corrosion rate trend, which is shown in Figure 27 (green line).

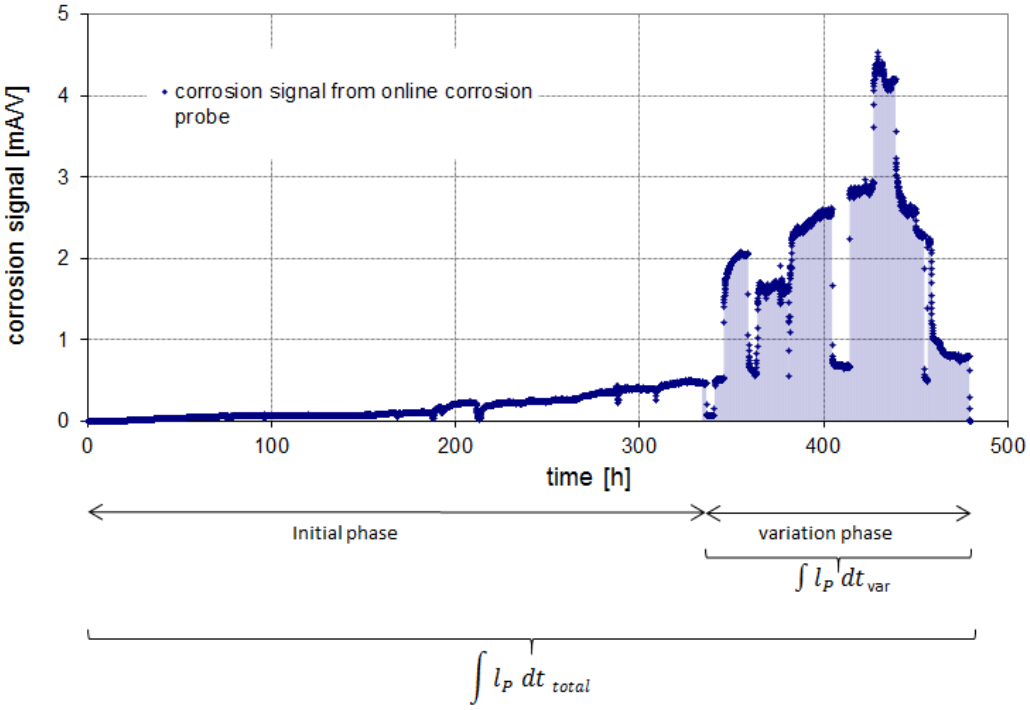

Figure 28: Measurement signal from corrosion probe (adapted from Paper II)
Explanations: $\int l_P\, dt_{var}$: integral over the measurement signal during variation phase (blue area); $\int l_P\, dt_{total}$: integral over the measurement signal of the whole test run

The mass losses shown in Figure 27 and the integrals over the measurement signal shown in Figure 28 were used to calculate the calibration factors in accordance with Eq. 7. While in the original methodology, applied during the real-scale test runs, g_{total} and $\int l_P\, dt_{total}$ were used to calculate the calibration factor (see Eq. 8), in the modified methodology only g_{var} and $\int l_P\, dt_{var}$ were used. (see Eq. 9).

$$b_{total} = \frac{g_{total}}{\int l_P\, dt_{total}} \qquad \textbf{Eq. 8}$$

$$b_{var} = \frac{g_{var}}{\int l_P\, dt_{var}} \qquad \textbf{Eq. 9}$$

The values used for Eq. 8 and Eq. 9 and the resulting calibration factors are given in Table 4. The data show that the calibration factor determined with the mass loss probe (b_{var}) is 55 % lower than the calibration factor determined without the mass loss probe (b_{total}).

Table 4: Comparison of calibration factors determined without and with mass loss probe

	mass loss [mm]	integral over measurement signal [(mA/V)·1000h]	calibration factor [(V/mA)·(1000h/mm)]
without mass loss probe	$g_{total} = 72.0 \cdot 10^{-3}$	$\int I_P \, dt_{total} = 386 \cdot 10^{-3}$	$b_{total} = 186 \cdot 10^{-3}$
with mass loss probe	$g_{var} = 26.6 \cdot 10^{-3}$	$\int I_P \, dt_{var} = 321 \cdot 10^{-3}$	$b_{var} = 83 \cdot 10^{-3}$

Using these calibration factors, the corrosion rates during the variation phase were calculated. Here, the corrosion rates determined with the original methodology without the mass loss probe are denoted as "original corrosion rates (k_{orig})" and are calculated in accordance with Eq. 10. The corrosion rates derived by means of the new methodology with the mass loss probe are denoted as "mass loss corrected corrosion rates (k_{MLC})" and are calculated in accordance with Eq. 11 (with mass loss probe). The results are plotted in Figure 29.

$$k_{orig} = I_P \cdot b_{total} \qquad \textbf{Eq. 10}$$

$$k_{MLC} = I_P \cdot b_{var} \qquad \textbf{Eq. 11}$$

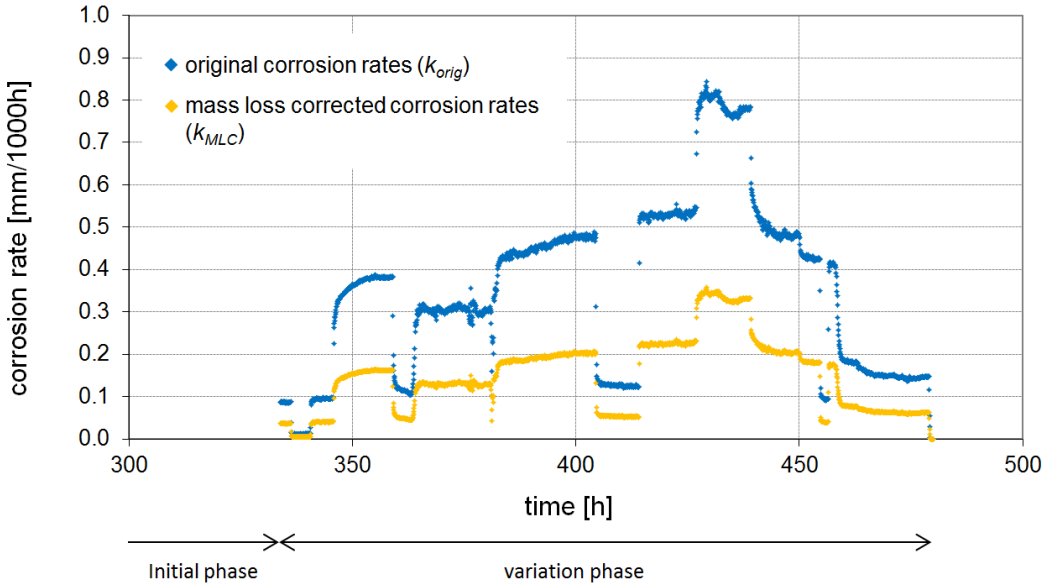

Figure 29: Corrosion rates derived from the online corrosion probe during the variation phase with and without consideration of the mass loss probe (adapted from Paper II)

For the data presented in Figure 29 the mass loss corrected corrosion rates are 55 % lower than the original corrosion rates. The difference results from the different calibration factors *b*. This value of reduction is later on presented for all test runs

performed and is denoted as “mass loss correction”. It is calculated from Eq. 10 and Eq. 11 resulting in:

$$mass\ loss\ correction\ [\%] = 100 \cdot \left(1 - \frac{b_{var}}{b_{total}}\right) \quad \textbf{Eq. 12}$$

In conclusion, when only data from the online corrosion probe are used, the corrosion rates are not correctly determined since the corrosion signal in the initial phase does not represent reality. For this reason, the exclusion of the initial phase is necessary to achieve correct corrosion rates during short-term measurements performed in lab-scale test runs. This is achieved by the application of a mass loss probe in combination with an online corrosion probe. Hereby, the wrong signal from the initial phase is eliminated and does not affect the corrosion rate determination.

It has to be noted that this error can be neglected during long-term measurements lasting several 1000 h but becomes extremely important for short-term measurements lasting only a few 100 h.

4.2.2 Test runs at the test rig (Paper III)

Several studies on high-temperature corrosion of boiler steels reported significant differences in the compositions and the structures of corrosion layers depending on the composition of the steel. Corrosion layers of low-alloyed steels such as 13CrMo4-5 mainly consist of iron oxides [83], [84], whereas for steels containing higher shares of chromium separate layers of iron oxides and chromium oxides were reported [85].

These differences may also influence the “start-up” effect during online corrosion probe measurements. Therefore, one objective of the work presented was to investigate the high-temperature corrosion behaviour of three boiler steels with online corrosion probes and mass loss probes using the new methodology as well as an evaluation of the results based on the new methodology. Within this thesis, the steels 13CrMo4-5, P91 and 1.4541 were evaluated. For this purpose, chemically untreated forest wood chips (referred to as “wood chips”) and waste wood were used as fuels. The waste wood was provided by a local supplier in the area of Graz and mainly consisted of demolition wood (comparable to A1–A3 in accordance with German standards). These test runs were performed at the test rig described in section 3.2.2 and are elaborated in detail in ***Paper III***.

In plants firing chemically untreated wood chips, usually low and medium alloyed steels are used for superheaters. Therefore only 13CrMo4-5 and P91 were investigated for this fuel. In the case of waste wood combustion a higher risk of corrosion is assumed, and therefore only the two higher alloyed steels P91 and 1.4541 were investigated, since they were considered to be of higher relevance in practice. The steels were chosen, since these are steels which are typically used for superheaters in biomass CHP plants. The test run matrix is illustrated in Table 5.

Table 5: Test run matrix

	13CrMo4-5	P91	1.4541
wood chips	x	x	
waste wood		x	x

4.2.2.1 Fuels

For each test run, fuel samples were taken at regular intervals and forwarded to chemical analyses. The resulting fuel compositions are presented in Table 4.

Table 6: Fuel compositions of wood chips and waste wood used for lab-scale measurements (adapted from Paper III)
Explanations: w.b.: wet basis, d.b.: dry basis

		wood chips - 13CrMo4-5		wood chips - P91		waste wood - P91		waste wood - 1.4541	
		mean	std.-dev.	mean	std.-dev.	mean	std.-dev.	mean	std.-dev.
moisture content	wt.% d.b.	31.6	3.9	20.5	1.0	24.0	4.1	27.5	4.4
ash content (550°C)	wt.% d.b.	2.7	1.2	2.8	0.6	21.8	7.1	20.4	6.8
C	wt.% d.b.	48.1	0.4	49.6	0.7	42.1	-	42.8	-
H	wt.% d.b.	6.0	0.1	6.0	0.0	5.1	-	5.2	-
N	wt.% d.b.	0.3	0.1	0.5	0.1	1.7	-	1.7	-
S	mg/kg d.b.	262	70	400	107	1 646	227	1 617	407
Cl	mg/kg d.b.	117	71	95	49	2 494	1 316	1 463	144
Ca	mg/kg d.b.	4 723	1 207	4 795	928	41 280	10 756	38 533	13 158
Si	mg/kg d.b.	3 654	3 009	2 938	1 345	30 940	11 234	27 700	6 975
Mg	mg/kg d.b.	614	193	616	118	4 326	960	4 047	1 374
Al	mg/kg d.b.	615	424	671	212	8 300	2 648	7 430	2 010
Na	mg/kg d.b.	128	92	92	27	2 708	598	2 277	551
K	mg/kg d.b.	1 875	449	2 205	579	4 450	774	4 250	747
Fe	mg/kg d.b.	313	237	390	108	7 660	5 907	5 043	1 707
P	mg/kg d.b.	242	71	428	136	1 102	291	1 129	383
Mn	mg/kg d.b.	88	26	603	387	235	87	208	44
Zn	mg/kg d.b.	15	5	28	10	165	59	195	95
Pb	mg/kg d.b.	4.1	4.6	8.8	0.5	38.0	18.8	15.1	10.1
2S/Cl	mol/mol	7.3	1.5	8.8	0.6	1.7	0.6	2.2	0.5

The mean ash contents of the wood chips were almost the same at 2.6 and 2.8 wt.% for the two test runs. For waste wood, the mean ash contents were 21.8 and 20.4 wt.%. Here, the difference between it and wood chips is striking. Significant shares of impurities such as fine particles and soil were found in the fuel.

K, Na, S and Cl are considered to be the most relevant elements with regard to high-temperature corrosion when firing chemically untreated woody biomass fuels, since they participate in the Cl-induced active oxidation mechanism (see section 2.1.2). Although their concentrations varied to some extent over the test runs, their variations are within the usual range for forest wood chips of good quality of one batch.

Besides K, Na, S and Cl, also the heavy metals Zn and Pb are usually relevant to high-temperature corrosion when firing waste wood. As expected, the heavy metal

concentrations found in the waste wood significantly exceeded those in wood chips (e.g. Zn: 165 and 195 mg/kg d.b. for waste wood compared with 15 and 28 mg/kg d.b. for wood chips). This results in a higher risk of high-temperature corrosion for waste wood due to molten salt corrosion (see section 2.1.3). Furthermore, the molar 2S/Cl ratios for waste wood are lower (1.7 and 2.2) compared to wood chips (7.3 and 8.8), which indicates an increased risk of Cl-induced active oxidation for waste wood (see section 2.1.2).

Generally, it can be stated that the fuel compositions mainly deviated within usual variation ranges. Therefore, significant impacts of changing fuel compositions on the results are not likely. Generally, the potential for high-temperature corrosion is clearly higher for waste wood compared to wood chips due to elevated heavy metal concentrations and lower 2S/Cl ratios.

4.2.2.2 Online corrosion probe measurements

All test runs at the test rig were performed using a combination of a mass loss probe with an online corrosion probe (see section 4.2.1) to determine high-temperature corrosion rates. Figure 30 shows the corrosion (material loss determined with the mass loss probe) measured in mm for the two materials investigated during wood chips combustion. During the initial phase the corrosion followed a paralinear trend, which corresponds with data from literature [30], [45]. For wood chips - 13CrMo4-5 a corrosion of 0.045 mm was found after 312 h, whereas for wood chips - P91 the corrosion was 0.028 mm after 309 h. Hence, P91 clearly showed a better corrosion resistance regarding high-temperature corrosion during the initial phase.

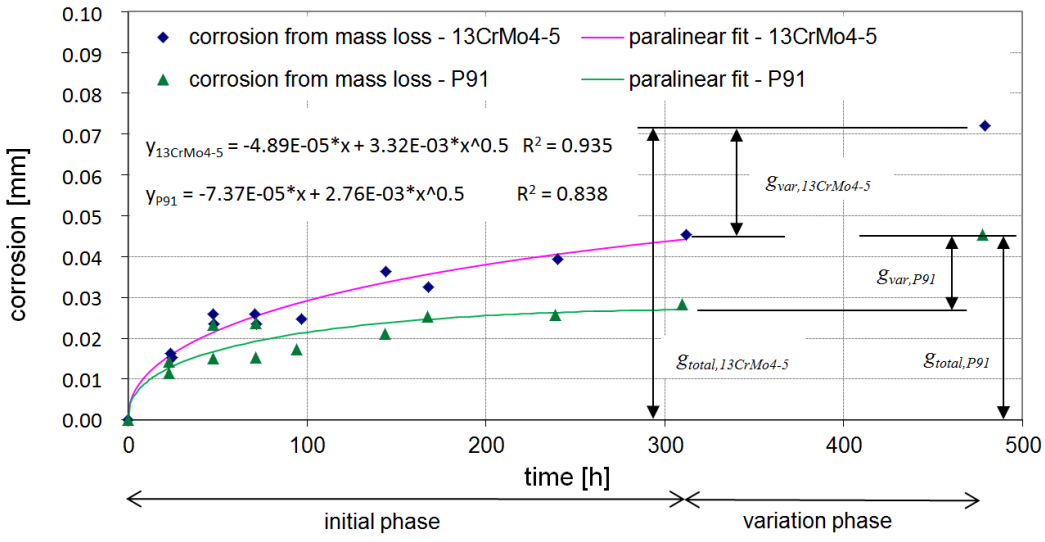

Figure 30: Mass losses determined with the mass loss probe as well paralinear fits of the mass losses during the initial phase of the wood chips test runs (adapted from Paper III)

The results of the waste wood test runs are shown in Figure 31. Here, a corrosion of 0.073 mm was found for P91 after the initial phase, whereas for waste wood – 1.4541 this value decreased to 0.036 mm. As for the wood chips test runs, the higher alloyed steel (in this

case 1.4541) showed a better corrosion resistance which is in accordance with literature [86]. For the waste wood test runs, the paralinear fits generally describe the corrosion trend in the initial phase but are less accurate than for the wood chips test runs.

The most likely reason for the stronger scattering in the case of waste wood is the determination of mass loss in accordance with ASTM G1-03 (see section 3.8.2). During this procedure, the corroded test rings were placed in an acidic solution in an ultrasonic bath in order to remove the corrosion products. For the wood chips test run, a solution of diammonium citrate (ASTM G1-03: C.3.4) was used. However, for the waste wood test runs, the corrosion products were more difficult to remove. Partially, corrosion products tended to stick to the ring surface when the uncorroded steel started to dissolve in places where corrosion products had already been removed. This problem had not been anticipated after the wood chips test runs, and especially for the test run waste wood – P91 less accurate paralinear fits had to be used for data evaluation.

For 1.4541 a pre-test for the removal of corrosion products had been performed. For this purpose, steels rings were oxidised in a muffle furnace and the corrosion products were removed using different solutions. A solution of HNO_3 / HF (ASTM G1-03: C.7.5) was chosen, based on this pre-test. However, the corrosion products from the test run were more difficult to remove than the corrosion products from the pre-test. Again, partial corrosion products tended to stick to the ring surface when the uncorroded steel already started to dissolve. Therefore, a fit with lower accuracy compared to the wood chips test runs had to be used. For future test runs, this methodology should be adapted and thoroughly tested prior to test runs.

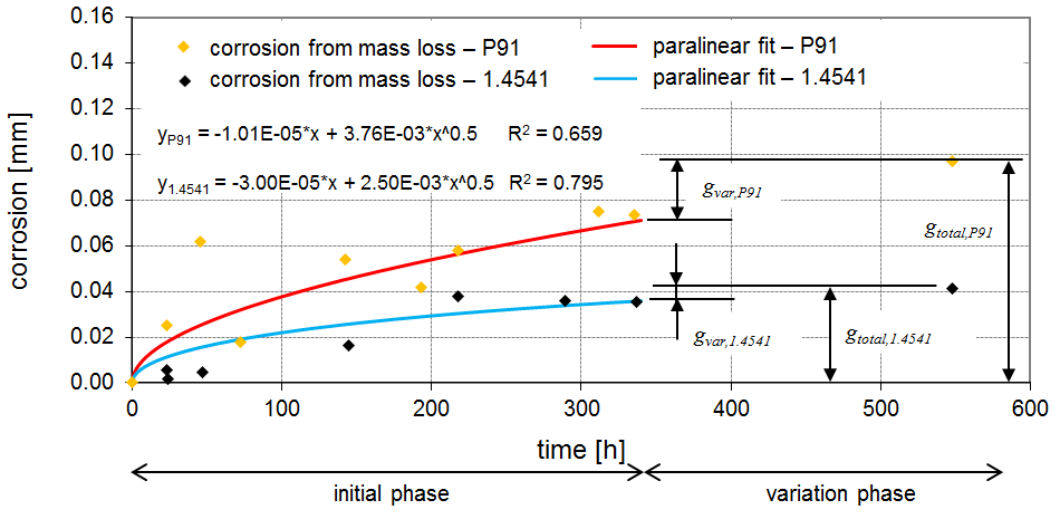

Figure 31: Mass losses determined with the mass loss probe as well as paralinear fits of the mass losses during the initial phase of the waste wood test runs (adapted from Paper III)

Corrosion rates were calculated using the data from the mass loss probe and the online corrosion probe. For all test runs, the original corrosion rates and the mass loss corrected corrosion rates were determined (see section 4.2.1). These corrosion rates as well as the flue gas temperatures and the probe surface temperatures during the variation phases

for the wood chips test runs are plotted in Figure 32. The same data for the waste wood test runs are plotted in Figure 33.

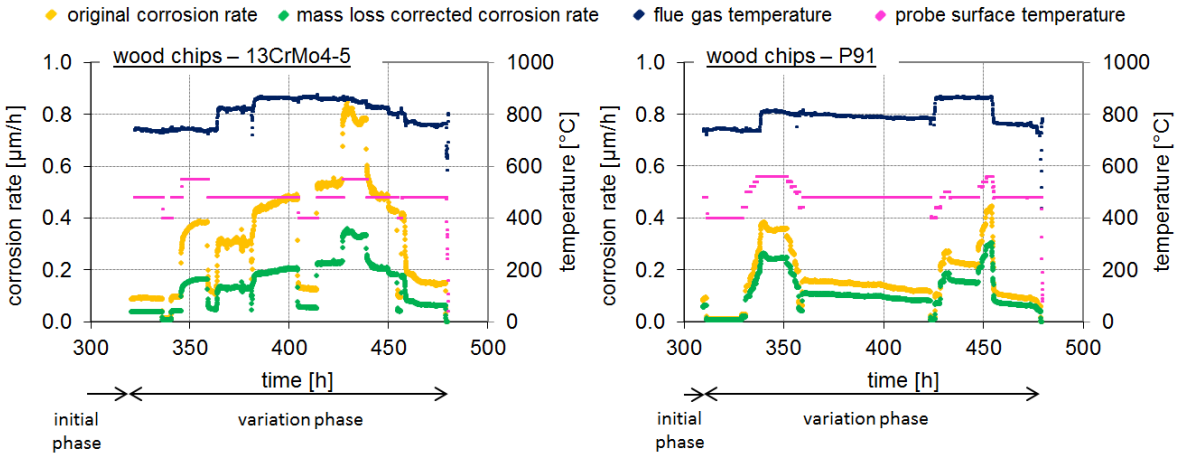

Figure 32: Corrosion rates with and without mass loss correction for the wood chips test runs as well as probe surface and flue gas temperature (adapted from Paper III)

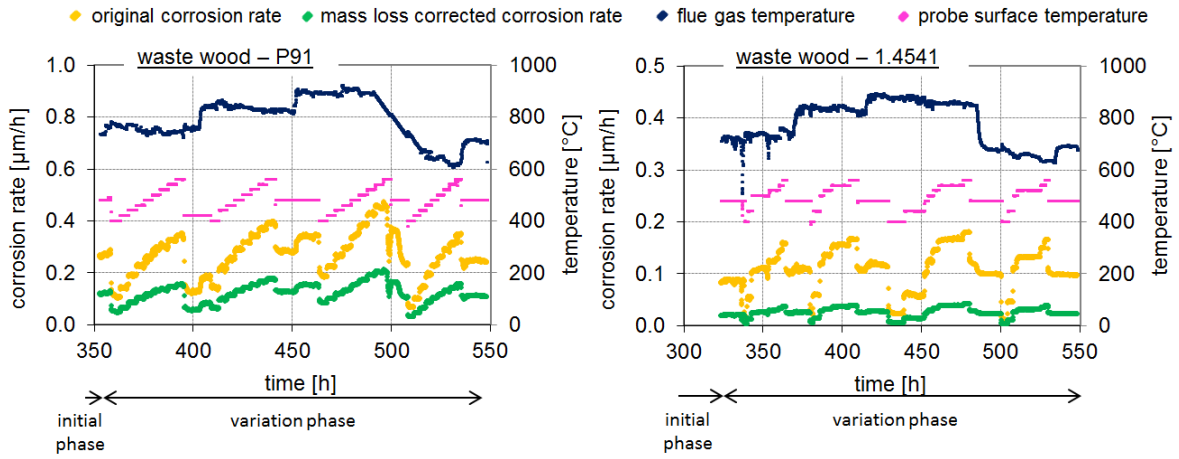

Figure 33: Corrosion rates with and without mass loss correction for the waste wood test runs as well as probe surface and flue gas temperature (adapted from Paper III)

The data plotted in Figure 32 and Figure 33 show that the corrosion rates immediately reflected the variations of the flue gas temperature and the probe surface temperature for all test runs. This shows that the variations influence chemical reactions or transport processes that react very quickly and are detected by the online corrosion probe. This demonstrates the applicability of the online corrosion probe for different fuels and different superheater materials (***Paper III***).

Furthermore, the data show that in all cases original corrosion rates are higher than mass loss corrected corrosion rates. However, the difference is not constant between individual test runs. In order to evaluate this difference, the mass loss correction presented in Eq. 12 (see section 4.2.1) was determined for all test runs.

In Table 7 the mass loss correction is presented for the different test runs. It amounts to values between 32 % and 77 %. The differences in the mass loss correction show that short-term test runs using online corrosion probes without mass loss correction not only result in wrong corrosion rates, but that a comparison of the results is also inaccurate since the mass loss correction (or the start-up error) may differ significantly. Therefore, mass loss correction is necessary in order to accurately compare short-term test runs using online corrosion probes.

Table 7: Mass loss correction determined for the individual test runs

	13CrMo4-5	P91	1.4541
wood chips	55 %	32 %	
waste wood		55 %	77 %

In the following sections, only mass loss corrected corrosion rates are presented and discussed. The corrosion rates determined during the variation phases of each test run were evaluated using the same procedure as applied for the measurement data from the real-scale test runs (see section 4.1). Corrosion rates were determined as mean values for certain flue gas temperatures (+/- 10°C) as well as for certain probe surface temperatures (+/- 1°C). The mean values as well as standard deviations of corrosion rates for certain flue gas and probe surface temperatures for the fuel wood chips are presented in Figure 34, whereas the results for waste wood can be found in Figure 35.

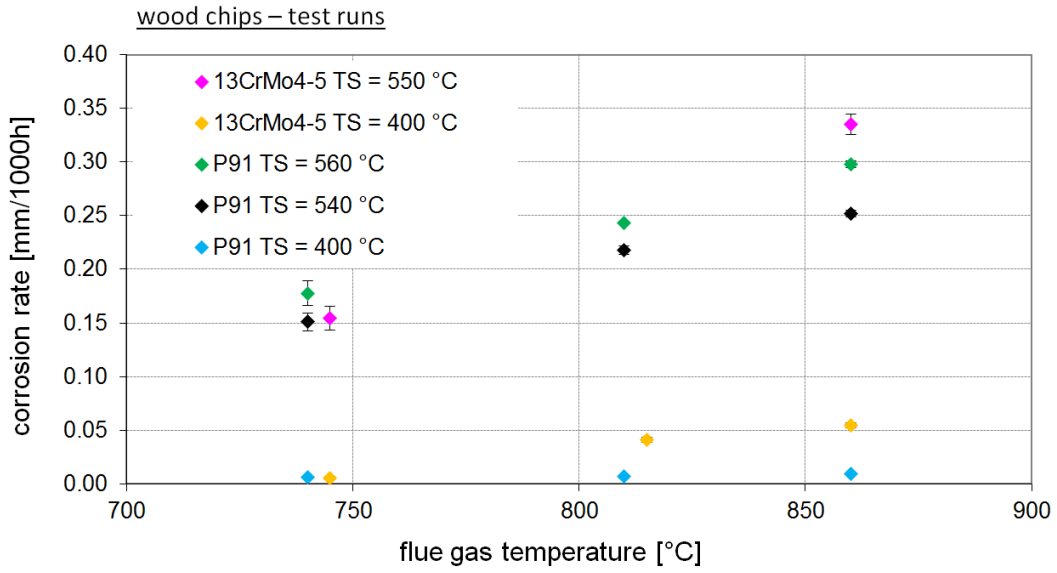

Figure 34: Corrosion rates dependent on the flue gas temperature for certain probe surface temperatures (adapted from Paper III)

Explanations: corrosion rates are mean values at certain flue gas temperatures (+/- 10°C) and certain corrosion probe temperatures (+/- 1°C); error bars show the standard deviations; data for 13CrMo4-5 adapted from: [1]

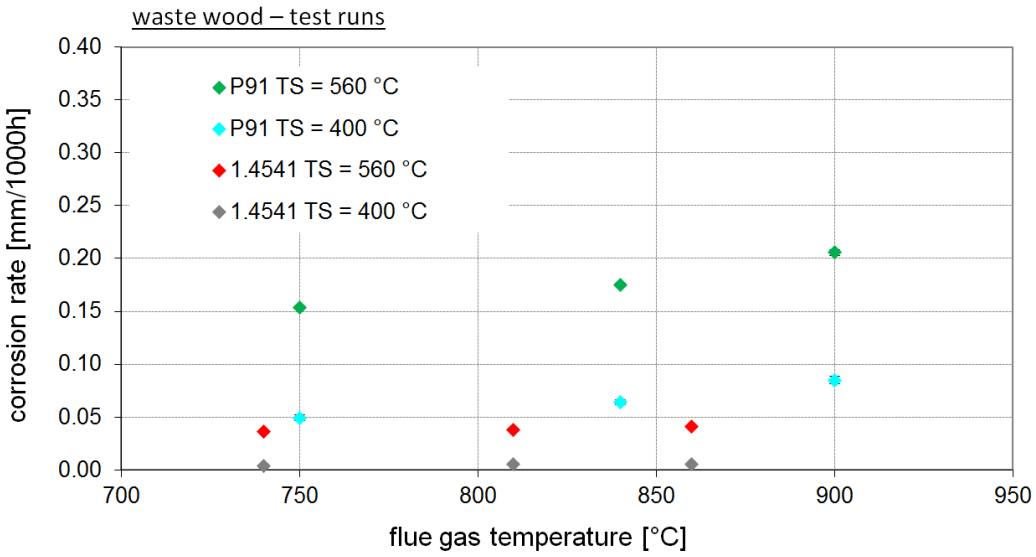

Figure 35: Corrosion rates dependent on the flue gas temperature for certain probe surface temperatures (adapted from Paper III)
Explanations: corrosion rates are mean values at certain flue gas temperatures (+/- 10°C) and certain corrosion probe temperatures (+/- 1°C); error bars show the standard deviations

The general trends found during the real-scale measurements were an increase in the corrosion rates at increased probe surface temperatures as well as increased flue gas temperatures (see sections 4.1.1.1 and 4.1.2.1). These general trends were also observed during all test runs performed at the test rig. However, the extent of the influencing temperatures on the corrosion rates differed substantially for the individual test runs.

For the data presented in Figure 34 and Figure 35, flue gas temperatures differed between the individual test runs. In order to be able to compare the data and to evaluate the trends, the data need to be fitted. As stated in section 4.1.1.1, the dependency of high-temperature corrosion rates on the flue gas temperature is typically described via an Arrhenius function, which has an exponential character. Such correlations were found and reported in MSW incinerators (e.g. [24], [37]) as well as in biomass combustion plants (e.g. [87]). Since a detailed mathematical description of corrosion rates was not the aim of this thesis and the data presented in Figure 34 and Figure 35 are not sufficient to derive an exponential equation, a linear correlation was used. The trends derived are only used for data comparison and must not be used to extrapolate the data. Based on the linear fits, corrosion rates were determined at T_{FG} = 750°C and T_{FG} = 850°C and the increase of the corrosion rates from T_{FG} = 750°C to 850°C was evaluated.

Wood chips test runs

The fits as well as the corrosion rates and the increase of the corrosion rates are presented in Table 8.

Table 8: Evaluation of corrosion rates for the wood chips test runs
Explanations: T_S: probe surface temperature [°C]; k: corrosion rate [mm/1000h];
A, B: constants in the linear fit

super-heater steel	T_S [°C]	linear fit $k = (A \cdot T_{FG} + B)$	k at T_{FG} = 750°C [mm/1000h]	k at T_{FG} = 850°C [mm/1000h]	Δk between T_{FG} = 750°C and 850°C [mm/1000h]	Increase of k from T_{FG} = 750°C to 850°C [%]
13CrMo4-5	400	$A = 4.32 \cdot 10^{-4}$ $B = -0.315$	0.009	0.052	0.043	469
13CrMo4-5	550	$A = 1.57 \cdot 10^{-3}$ $B = -1.016$	0.162	0.319	0.157	97
P91	400	$A = 2.55 \cdot 10^{-5}$ $B = -0.013$	0.006	0.009	0.003	42
P91	560	$A = 9.98 \cdot 10^{-4}$ $B = -0.562$	0.186	0.286	0.100	54

The different dependencies of the corrosion rates on the temperatures can be seen when comparing the corrosion rates for 13CrMo45 and P91 of the wood chips test campaign, for example, at the probe surface temperature of T_S = 400°C. In this case, the corrosion rate between T_{FG} = 750°C and 850°C increased by 469 % for 13CrMo45 and by 42 % for P91. At a higher probe surface temperature of T_S = 550°C (13CrMo4-5) or 560°C (P91), the corrosion rate between T_{FG} = 750°C and 850 °C increased by 97 % for 13CrMo4-5 and by 54 % for P91. These data show that the corrosion rates of the lower alloyed steel 13CrMo4-5 are significantly more affected by increasing flue gas temperatures compared to P91.

When absolute corrosion rates are compared, 13CrMo4-5 and P91 show a comparable resistance to high-temperature corrosion at T_{FG} = 750°C. This applies to T_S = 400°C as well as to T_S = 550°C (13CrMo4-5) or T_S = 560°C (P91). At the higher flue gas temperature of T_{FG} = 850°C, however, the corrosion rates of 13CrMo4-5 exceed those of P91. Therefore, it can be concluded that P91 has a higher resistance to high temperature corrosion at high flue gas temperatures in the range of 850°C, but there is no significant difference at lower flue gas temperatures in the range of 750°C.

Waste wood test runs

Different dependencies of the corrosion rates on the influencing temperatures were also found in the waste wood test runs and they are presented in Table 9. At a probe surface temperature of T_S = 400°C, the corrosion rate of P91 between T_{FG} = 750°C and 850°C increased by 49 %. For 1.4541 the increase only amounted to 36 %. At higher probe surface temperature of T_S = 560°C the corrosion rate between T_{FG} = 750°C and 850°C increased by 22 % for P91, and by 11 % for 1.4541. Comparable to the wood chips test

runs, the corrosion rates of lower alloyed steel, in this case P91, are more strongly affected by increasing flue gas temperatures.

Table 9: Evaluation of corrosion rates for waste wood test runs
Explanations: T_S: probe surface temperature [°C]; k: corrosion rate [mm/1000h];
A, B: constants in the linear fit

super-heater steel	T_S [°C]	linear fit $k = (A \cdot T_{FG} + B)$	k at T_{FG} = 750 °C [mm/1000h]	k at T_{FG} = 850 °C [mm/1000h]	Δk between T_{FG} = 750 °C and 850 °C [mm/1000h]	Increase of k from T_{FG} = 750 °C to 850 °C [%]
P91	400	$A = 2.31 \cdot 10^{-4}$ B = -0.126	0.048	0.071	0.023	49
P91	560	$A = 3.38 \cdot 10^{-4}$ B = -0.103	0.151	0.185	0.034	22
1.4541	400	$A = 1.50 \cdot 10^{-5}$ B = -0.007	0.004	0.006	0.002	36
1.4541	560	$A = 3.94 \cdot 10^{-5}$ B = -0.007	0.036	0.040	0.004	11

The absolute values of the corrosion rates determined during the waste wood test runs, showed significantly lower corrosion rates for 1.4541 compared to P91. The highest corrosion rate at T_S = 560°C and T_{FG} = 850°C for 1.4541 was 0.040 mm/1000h which was still below the lowest corrosion rate for P91 T_S = 400°C and T_{FG} = 750°C at 0.048 mm/1000h. This shows that 1.4541 has a significantly higher resistance against high-temperature corrosion than P91.

Evaluation of P91 for the wood chips and the waste wood test run

For P91, corrosion rates obtained for wood chips combustion and waste wood combustion were generally in the same range. However, the rates showed different dependencies on the temperatures. At low probe surface temperatures (T_S = 400°C), the rates were higher for waste wood than for wood chips. At T_S = 560°C, however, the rates were lower for waste wood than for wood chips. For T_S = 400°C and T_{FG} = 750°C, the corrosion rates determined were 0.006 mm/1000h for wood chips and 0.048 mm/1000h for waste wood. At T_S = 560°C, the corrosion rates were 0.186 mm/1000h for wood chips and 0.151 mm/1000h for waste wood. This shows that the influence of the probe surface temperature was significantly higher for wood chips combustion, which was also found in earlier work [53].

A possible reason for the difference is a different dominating corrosion mechanism. As discussed in the analyses of the corrosion probes in section 4.2.2.4, hot corrosion type II is a likely corrosion mechanism for waste wood combustion, which is not the case for wood chips combustion. P91 contains 8.75 wt.% Cr which is usually not enough for the

formation and maintenance of a protective Cr_2O_3 layer on the surface of the material. The minimum Cr concentration for the formation of such a layer is, typically, 10 wt.%. Hence, an oxide layer containing chromium oxide as well as iron oxides will be formed in the event of corrosion for P91. The formation of such a corrosion layer may result from Cl-induced active oxidation as well as from hot corrosion type II. For waste wood combustion, Cl-induced active oxidation as well as direct oxidation of the steel by oxygen from the flue gas are possible.

4.2.2.3 Deposit probe measurements

In order to characterize the deposit formation, deposit probe measurements were performed for all test runs similar to the measurements performed in real-scale (sections 4.1.1.2 and 4.1.2.2). Deposits were sampled at probe surface temperatures of 480°C and 560°C (or 550°C for 13CrMo4-5) over a period of 2 h. The deposit samples were analysed regarding their chemical composition by means of SEM/EDX at three positions of the test ring (windward, windward +50°, leeward). The results of the analyses are presented in Figure 18.

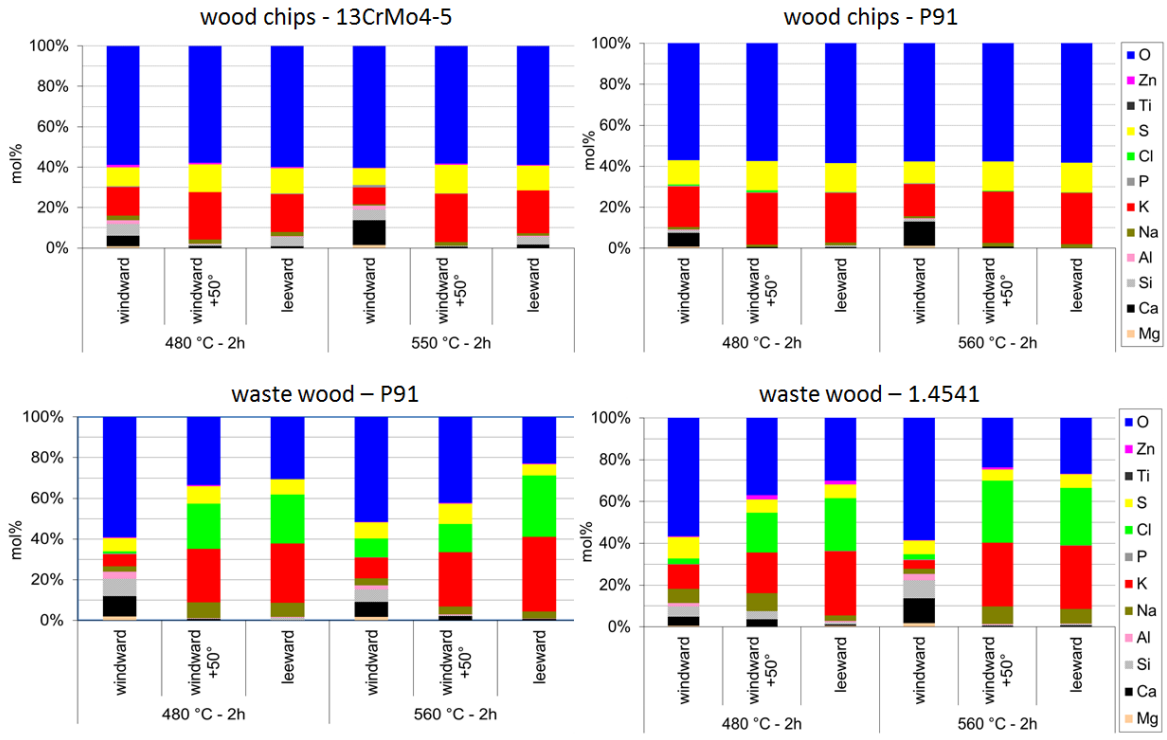

Figure 36: Results of SEM/EDX analyses of the deposits sampled at different positions of the deposit probe. (adapted from Paper III).
Explanations: The caption of each analysis characterizes the sampling point, the surface temperature of the test ring and the sampling time

The deposits sampled during the wood chips test runs mainly consisted of K and S, their ratio indicating the presence of K_2SO_4. On the windward side, higher amounts of Ca and Si as well as Mg were found, compared to the windward +50° and the leeward position. These elements are typically found in coarse fly ashes which are deposited by internal

impaction [72]. This deposition process mainly forms deposits on the windward side. The deposits sampled during the wood chips - 13CrMo4-5 test run contained higher shares of Si compared to the wood chips - P91 test run, which resulted from slight differences in fuel composition. Cl was only found in minor concentrations with a maximum concentration of 0.9 mol% in the deposits sampled at 480°C during the wood chips – P91 test run. This indicates that the condensation temperature of the gaseous alkali chlorides was between 480°C and 550°C.

The deposits sampled during the waste wood test runs were formed to a large extent of K and S. On the windward side, the deposits contained higher shares of Ca, Si and Mg from coarse fly ashes. Furthermore, K and Na as well as S and Cl were found on the windward side. This indicates the presence of K- and Na-chlorides as well as K- and Na-sulphates. The deposit compositions on the windward +50° and the leeward position mainly consisted of K and Na as well as S and Cl (K-, Na-chlorides and K-, Na-sulphates). The high shares of Na and Cl (up to 30.3 mol% Cl) differed considerably from the deposits from wood chips test runs. Another relevant difference was a share of up to 2.0 mol% Zn in the deposits on the windward +50° and the leeward side of the waste wood test runs. In the deposits of the wood chips test runs, the maximum Zn concentration was 1.0 mol%. Although Zn and Na cannot be accurately separated during EDX analyses (at 12 kV – see section 3.8.3) this finding indicates higher shares of Zn in the deposits of the waste wood test runs. Zn is important regarding corrosion, since it may decrease the melting point of ashes and thereby cause higher corrosion rates due to hot corrosion type II [21], [58], [88], [89].

In order to evaluate possible molten phases, the SEM pictures were evaluated. For this purpose, deposits sampled during the wood chips test runs and deposits sampled during the waste wood test runs were compared. Examples of the findings are shown in Figure 37 using deposit samples from the wood chips – P91 and the waste wood – P91 test run. Figure 37 shows the windward side and the leeward side at 480°C and at 560°C probe surface temperature.

It can be seen that all deposits sampled during the wood chips test run are formed from individual, solid particles. The shape of the deposits is similar for both probe surface temperatures (480°C and 560°C) and does not indicate any molten phases. The shape of the deposits sampled during the waste wood test run at 480°C is similar to the one from the wood chips test run. At 560°C, however, molten and sintered phases are visible. The deposits on the windward side consist of larger particles, which are sintered or molten on their surface. On the leeward side, a compact layer on the surface of the deposit ring is visible. This layer shows cracks, which are typically formed during the cooling of the probe when the deposit probe is removed from the hot flue gas.

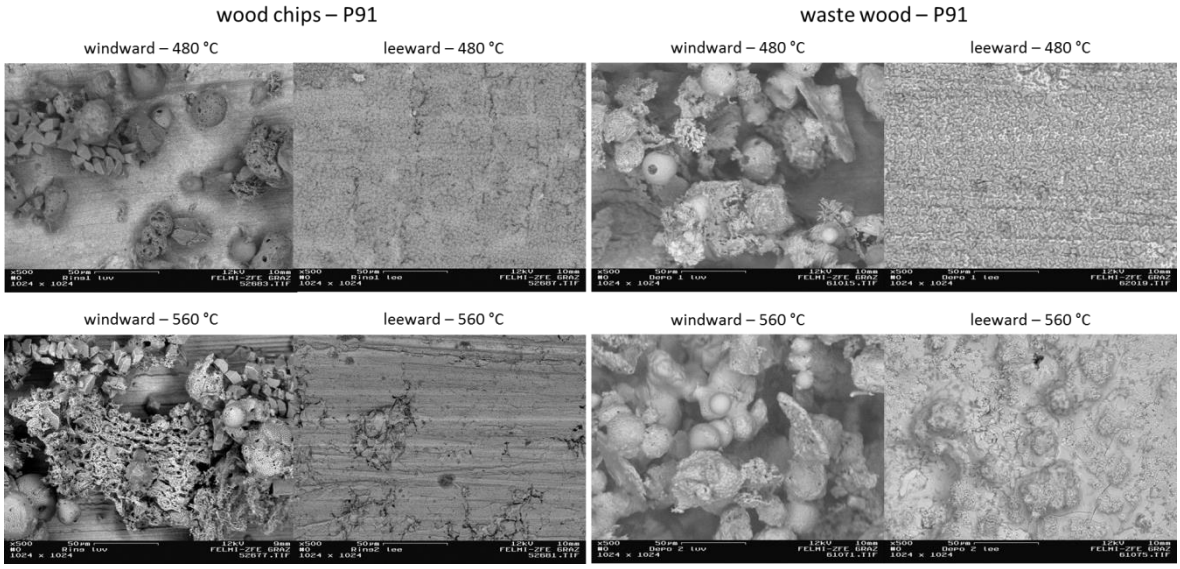

Figure 37: SEM pictures of deposits sampled with the deposit probe

The SEM pictures show that deposits originating from waste wood combustion contained molten phases at 560°C probe surface temperature but not at 480°C. This indicates a melting point between 480°C and 560°C. In the deposits from wood chips combustion no molten phases were found. This agrees with findings from lab-scale work of van Lith [90] in which corrosion processes at conditions representing waste wood fired boilers were investigated. In her thesis, molten deposits were found at 500°C.

Summing up, the deposits sampled during the waste wood test runs contained higher shares of Al, Zn, Na and Cl compared to the wood chips test runs. The main influence on corrosion processes results from Cl, which may cause higher corrosion rates due to Cl-induced active oxidation, as well as from Zn, which may decrease the melting point of ashes and thereby cause higher corrosion rates due to hot corrosion type II. Molten deposits were confirmed by visual inspection of deposits at a probe surface temperature of 560°C with a melting point between 480°C and 560°C.

The chemical composition of the deposits sampled showed no significant differences between the two test runs with either fuel (wood chips or waste wood). Therefore, the deposit analyses validated the comparability of the test runs with each fuel regarding the chemical composition of deposits.

4.2.2.4 Analyses of online corrosion probe rings (Paper III, Paper IV)

The probe rings of the online corrosion probe applied in the lab-scale test runs were analysed by means of SEM/EDX in order to gain more information on the possible corrosion mechanisms prevailing. Within the test runs, different fuels as well as different superheater steels were investigated. Therefore, the analyses also provided information on the differences in deposit chemistry and the corrosive attack of the material.

SEM/EDX element mappings were performed on the windward side and the leeward side of the probes. The size and position of the SEM pictures were chosen in order to make all relevant layers visible (deposit layer, corrosion layer, uncorroded material) as already illustrated for the analyses of the rings from the real-scale test runs (see Figure 19, section 4.1.1.3).

Wood chips – 13CrMo4-5

The mappings presented in Figure 38 show the results of the analyses of the corrosion probe rings from the wood chips - 13CrMo4-5 test run.

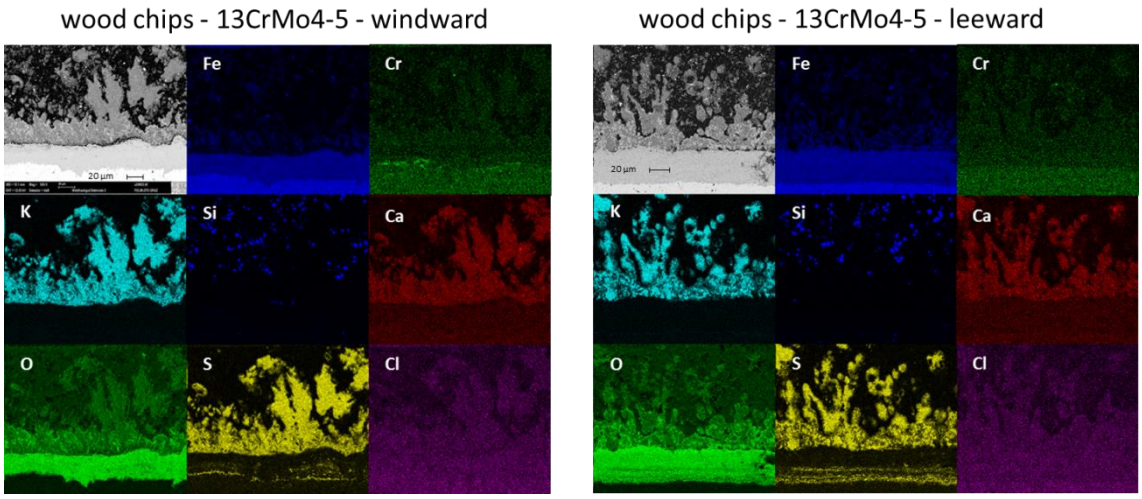

Figure 38: SEM/EDX element mappings of a corrosion probe ring from the wood chips – 13CrMo4-5 test run (adapted from Paper III)

The deposit layer of the corrosion probe ring from the wood chips – 13CrMo4-5 test run mainly consisted of K, Si, Ca and S as well as O. These results indicate the presence of K- and Ca-sulphates as well as Ca- and Si-oxides. The corrosion layer was one compact layer consisting of Fe and O as well as small concentrations of Cr, which results from the low concentration of Cr in the steel (see section 3.3). The chemical composition of the corrosion front is of special interest regarding the corrosion mechanisms prevailing. For wood chips – 13CrMo4-5, an enrichment of S was found at the corrosion front. Furthermore, no Cl was found, which would indicate Cl-induced corrosion to be of significant relevance. These results are in line with the results from SEM/EDX analyses of the wood chips test runs in the real-scale plant (section 4.1.1.3) where also no Cl but S was found at the corrosion front.

The elements mappings revealed no relevant differences between the windward side and the leeward of the corrosion probe ring.

Wood chips – P91

In Figure 39 the element mappings from the wood chips – P91 test run are presented. In order to gain additional information about the chemical compositions of the individual

layers, spot and area analyses of the corrosion probe rings were made. They are presented in Figure 40. These analyses had not been performed for the wood chips – 13CrMo4-5 test run.

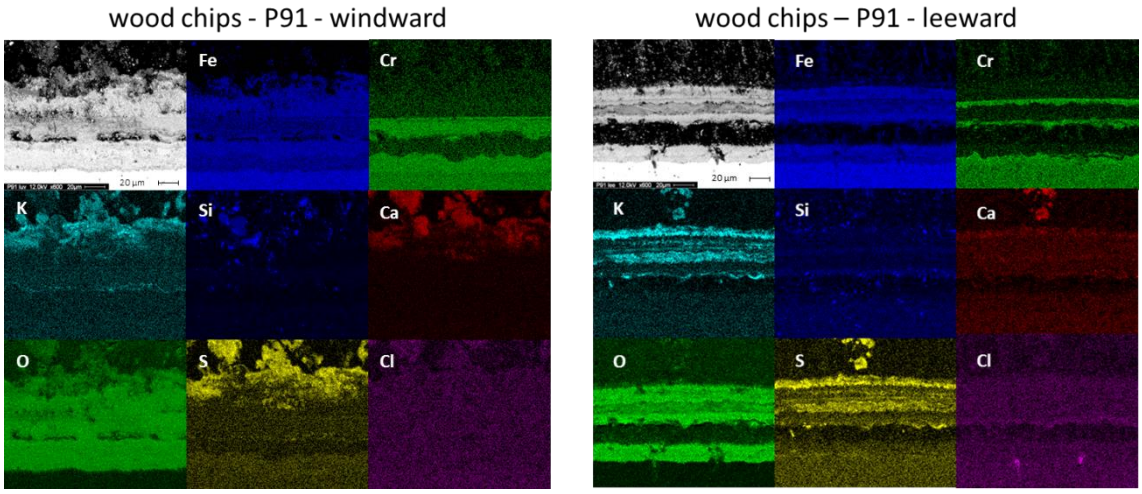

Figure 39: SEM/EDX element mappings of the corrosion probe rings from the wood chips – P91 test run (adapted from Paper III)

The chemical compositions of the deposits are comparable to the deposits from the wood chips – 13CrMo4-5 test run. They mainly consist of K, Si, Ca and S as well as O, which indicates K- and Ca-sulphates as well as Ca- and Si-oxides. The area analyses of the deposits strongly indicate the presence of K- and Ca-sulphates by the ratios of K and Ca to S (Figure 40 windward: areas 5-7; leeward: areas 6 and 7). The remaining deposits prevail as oxides since no other anions were found. The comparability with the wood chips – 13CrMo4-5 deposits is in agreement with the deposit probe measurements, where the deposit compositions determined for wood chips – 13CrMo4-5 and wood chips – P91 were also comparable.

For wood chips - P91 the corrosion layer consisted of different sub-layers which were alternately Cr-rich or Fe-rich (Figure 39). The separation of Fe and Cr most likely resulted from the higher affinity of Cr to O compared with Fe to O [21], [84], [91]. The area analyses in Figure 40 showed that Cr-rich layers contained up to 22 mol% Cr (windward: area 3) whereas Fe-rich layers contained less than 1 mol% Cr (windward: area 4, leeward: areas 2 and 5). The separated sublayers were most likely formed during the temperature variations which caused spallation. Within the corrosion layer on the leeward side the deposit elements K and S were found, which can be seen in the element mappings (Figure 39) and was confirmed by area analyses (Figure 40: leeward area 3).

On the corrosion front, only the elements from the steel (Fe and Cr) as well as O were found. Therefore, no conclusions regarding a possible corrosion mechanism were drawn.

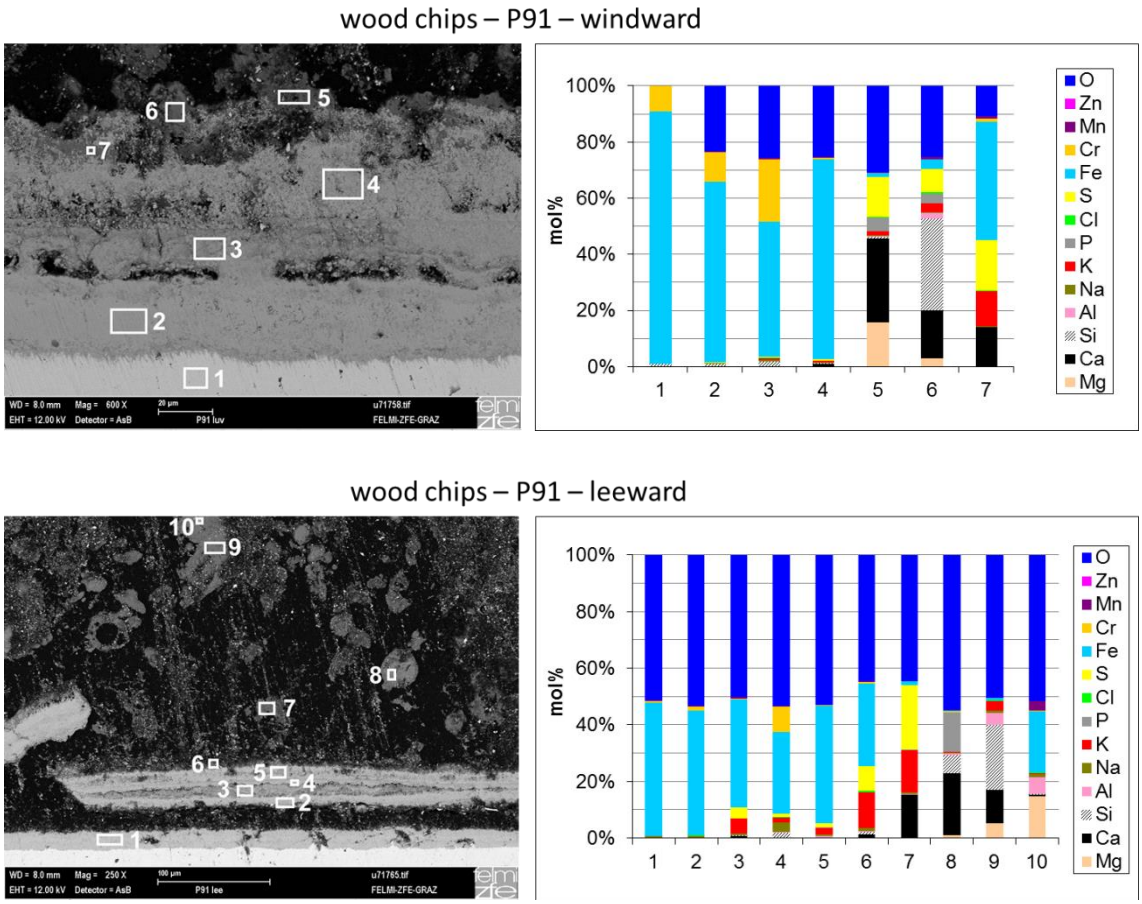

Figure 40: SEM/EDX spot and area analyses of a corrosion probe ring from the wood chips – P91 test run

Waste wood – P91

Figure 41 shows the element mappings from the waste wood – P91 test run. The deposits mainly consisted of K, Si, Ca and S. The area analyses presented in Figure 42 confirmed these elements, their ratio indicating K- and Ca sulphates as well as Si- and Mg-oxides (windward areas 7 and 8, leeward area 7). The shape of the deposits, especially on the leeward side indicated that melting or sintering of the deposits had occurred. Molten deposits are in agreement with the results of the deposit probe measurements (section 4.2.2.3) where molten deposits were confirmed at probe surface temperatures of 560°C. Since the maximum probe surface temperature of the online corrosion probe was also 560°C, melting of the deposits is plausible.

Comparable to the wood chips – P91 test run, the corrosion layer in the case of waste wood – P91 also showed some spallation. This is especially visible on the leeward side, where an inner Cr-depleted corrosion layer (Figure 42: leeward area 2) is separated from an outer layer (areas 4 and 5) containing about 10 mol% Cr. The crack between these layers is filled with deposits (Si, K, S). As concluded for the wood chips – 13CrMo4-5 test

run, the spallation was most likely caused by the temperature variations of the online corrosion probe. The element mapping from the leeward side shows Cl within the corrosion layer although no Cl was found in the deposits. This is assumed to be a result of the temperature variations occurring during the measurements. Since Cl was found in lower layers, it must have been in the deposits too. Due to the high probe surface temperatures up to 560°C, this Cl could have evaporated (***Paper IV***).

Cl was also found at the corrosion front. This indicates Cl-induced corrosion to be a relevant corrosion process. On the windward side, a severe attack of the ground material occurred, which is visible in Figure 41 in the Fe, O and Cl mappings. The area analyses (Figure 42: windward areas 2 and 3) showed only the presence of ring materials (Fe and Cr) and Cl. However, after a discussion of the results with experts during the review of ***Paper IV*** such an extreme corrosive attack was considered highly unlikely.

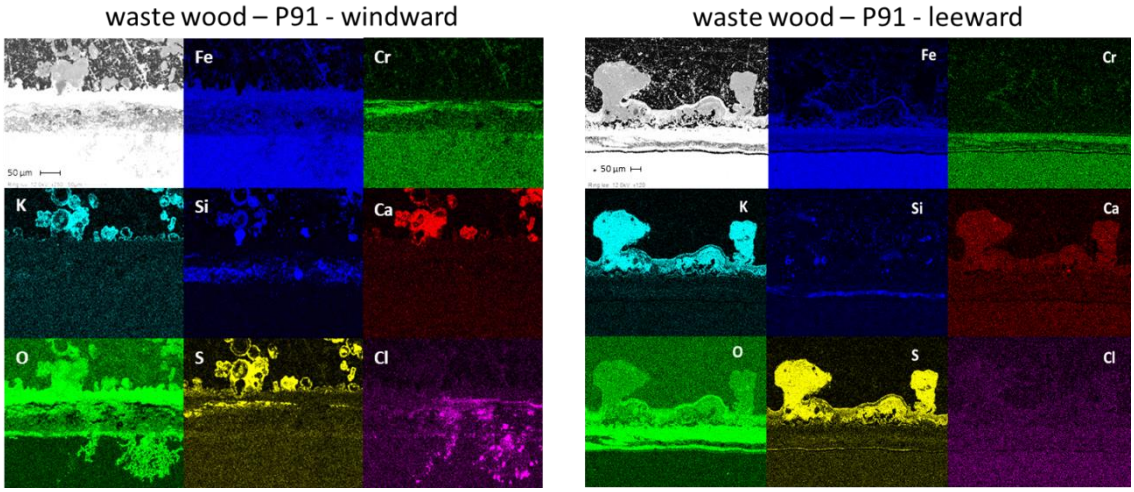

Figure 41: SEM/EDX element mappings of the corrosion probe rings from the waste wood – P91 test run (adapted from Paper III)

It is assumed that the severe corrosion might have occurred during the sample preparation. Metal chlorides are known to be highly hygroscopic and may therefore alter the sample. Salmenoja [55] reported hygroscopic interfaces between the base metal and the corroded scale supporting this assumption. However, the assumption could not be verified since the samples were not available any more at that time which would have allowed additional analyses. Nevertheless, it has to be noted, that a careful and adequate handling of corrosion samples, especially with regard to moist atmospheres is important. The samples have to be stored in a desiccator immediately after the measurements. Furthermore, short storage times between sample preparation and analyses should be realized.

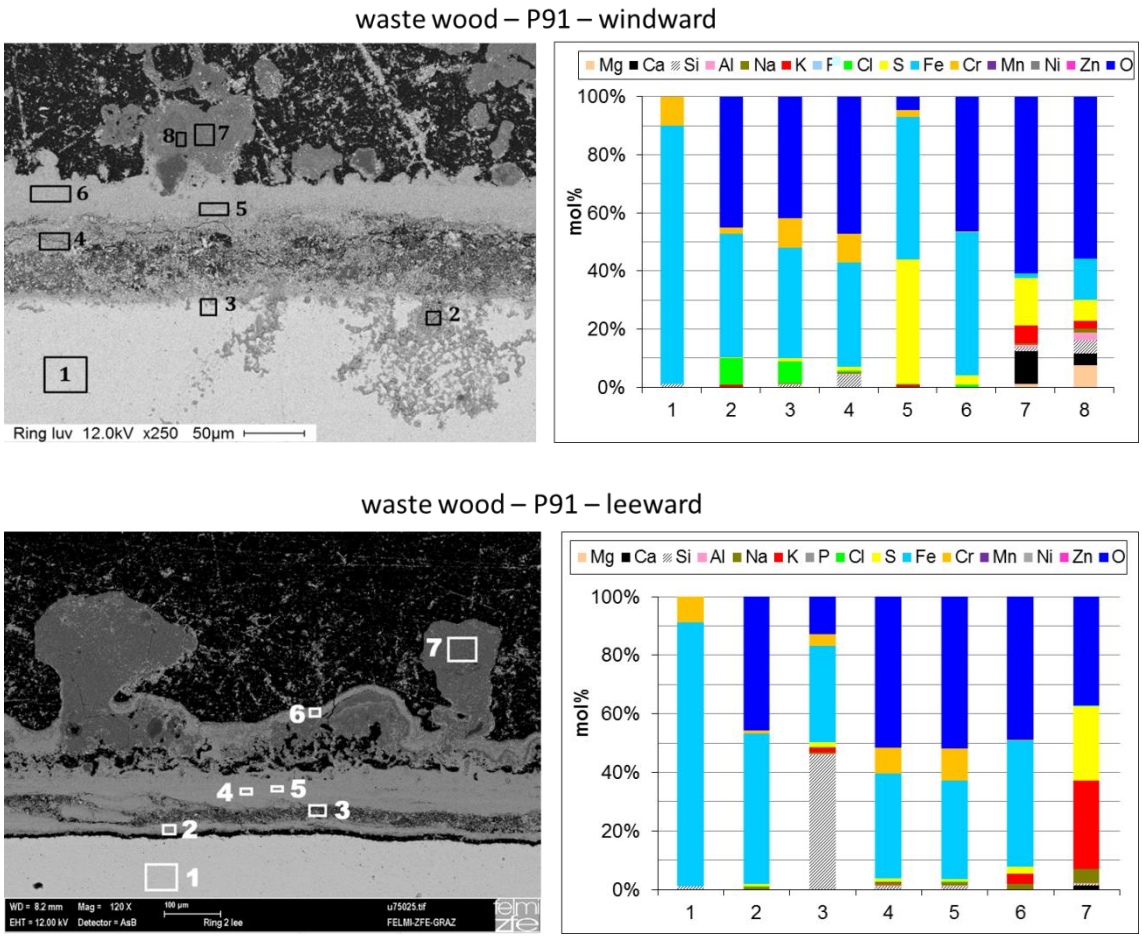

Figure 42: SEM/EDX spot and area analyses of a corrosion probe ring from the waste wood – P91 test run

Waste wood – 1.4541

The element mappings of the corrosion probe rings from the waste wood – 1.4541 test run are presented in Figure 43. The area analyses are presented in Figure 44.

The chemical composition of the deposit layer found in the waste wood – 1.4541 test run is comparable to one from waste wood – P91; it mainly consists of K, Si and S as well as small amounts of Ca. Their ratio indicates K-and Ca-sulphates and Si-oxides (Figure 44: windward areas 12, leeward areas 7 and 8). Furthermore, Zn was found in the deposits (Figure 44: leeward area 8). Although Zn and Na cannot be accurately separated by EDX analyses at 12 kV, the large concentration of 11 mol% indicates that at least some Zn was contained in the deposits. The shape of the deposits (Figure 44: windward area 12, leeward areas 7 and 8) indicates that melting or sintering of the deposits had occurred. Zn in the deposits explains the molten deposit phases, which were also found on the corrosion probe rings from the waste wood – P91 test run and which were confirmed by the deposits probe samples (section 4.2.2.3, Figure 37).

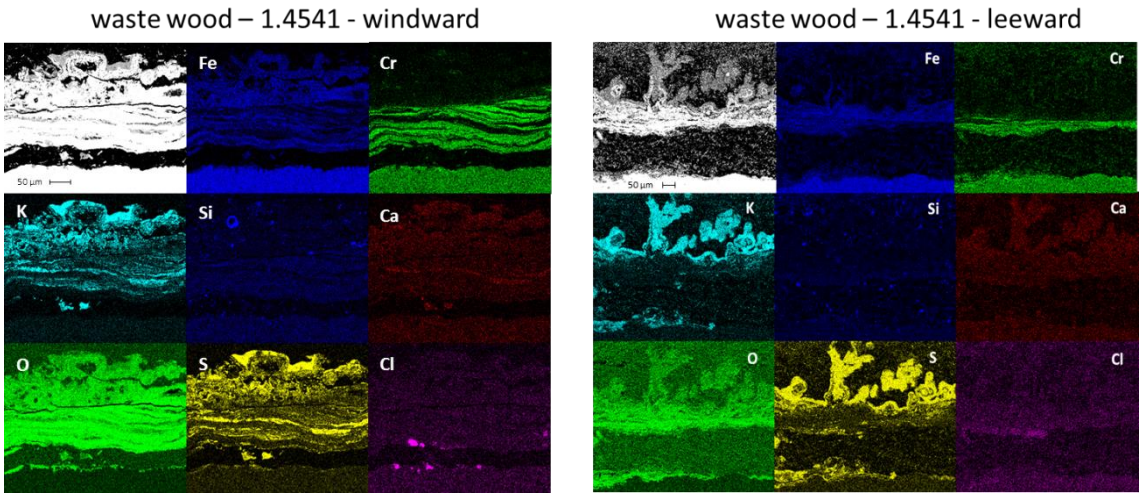

Figure 43: SEM/EDX element mappings of the corrosion probe rings from the waste wood – 1.4541 test run (adapted from Paper III)

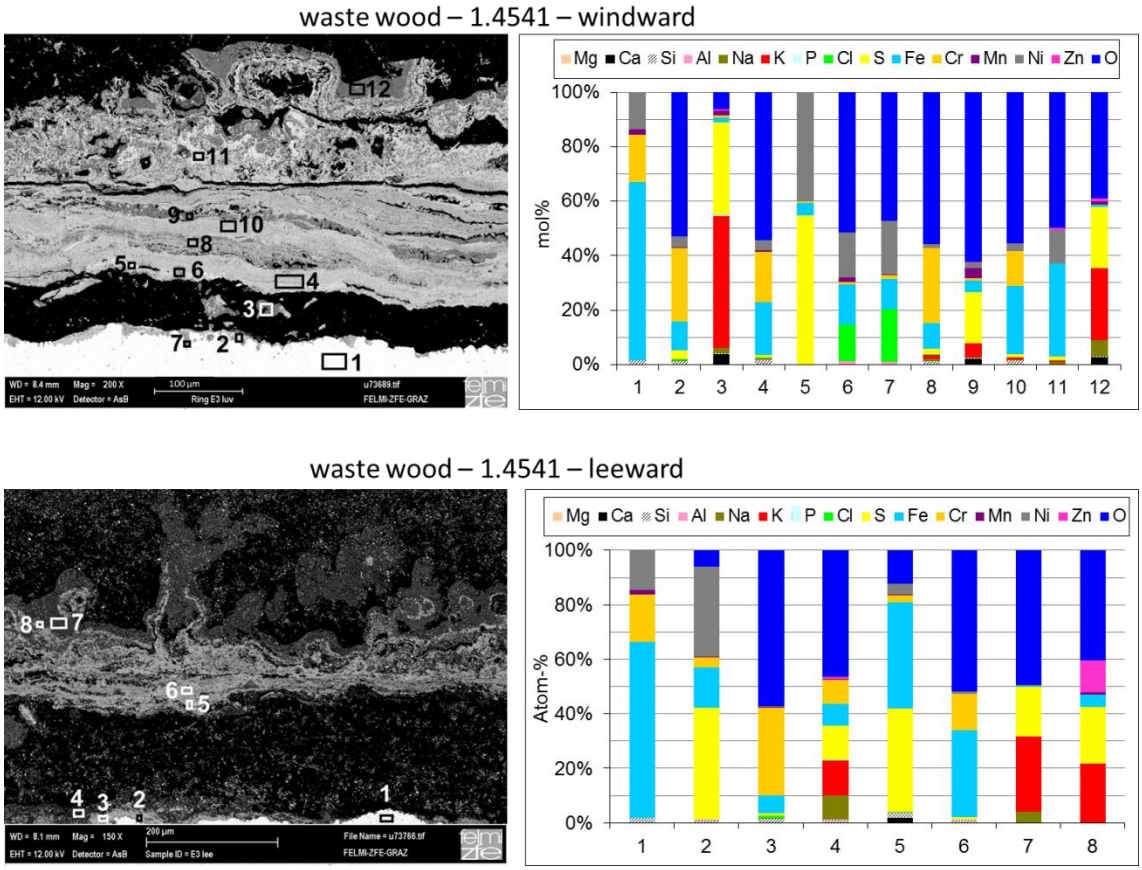

Figure 44: SEM/EDX spot and area analyses of a corrosion probe ring from the waste wood – 1.4541 test run

The corrosion layer, especially on the windward side, contained multiple sublayers which are clearly noticeable as Cr-rich and Fe-rich layers in Figure 43. The cracks between these

sublayers contain large shares of deposition elements, especially K and S (Figure 44: windward area 9).

On the inside of the corrosion layer as well as on the corrosion front, the analyses showed Cl-rich areas without any other elements from the deposits (Figure 44: windward areas 6 and 7). This finding supports a Cl-induced corrosion mechanism suggesting an attack of the ground material by Cl, which forms Fe-chlorides that are subsequently oxidized. Furthermore, S was found at the corrosion front in combination with Fe, Cr and Ni as well as low O concentrations, suggesting the presence of metal sulphides (Figure 44: windward area 5, leeward areas 2 and 5). In this, a participation of S in the corrosion process is suggested. Possible processes are the reaction of SO_2 with the steel. However, this reaction is unlikely for stainless steel [3]. Furthermore, S may be present as FeS or FeS_2 due to the sulphation of metal chlorides resulting from Cl-induced active oxidation [79], [80]). Also hot corrosion type II is likely to have occurred, since this corrosion process can dissolve the protective oxide of stainless steels. Within this process, pyrosulphates and alkali metal trisulphates are formed, which cause corrosion and form metal sulphides [4].

5 Summary, conclusions and recommendations

5.1 Evaluation of methods

Within this thesis, newly developed online corrosion probes were applied in biomass fired boilers to systematically investigate high-temperature corrosion. The measurements were conducted in real-scale plants based on grate combustion as well as in a lab–scale test rig which was also based on grate combustion. Within all test runs, plausible corrosion rates were determined and the applicability of online corrosion probes in biomass combustion plants was demonstrated.

Online corrosion probes require a conductive layer on their surface for measurements to be conducted. This layer is formed from ash deposits and corrosion products as soon as the probe is exposed to the flue gas. When a fully developed layer has been formed, the measurement signal represents the real corrosion rate. However, during the build-up of this layer (the initial phase), the measurement signal does not represent the actual corrosion rate. Since the corrosion rate is calculated from the measurement signal subsequent to the test run and uses the integral over the whole measurement signal, the wrong signal during the initial phase causes an error in the corrosion rate determination. This “start-up” error can be neglected in the course of long-term measurements lasting several 1000 h but can significantly influence the results during short-term measurements lasting only several 100 h.

The real-scale measurements lasted for at least 3000 h. Therefore, the start-up error was neglected for the calculation of corrosion rates from the measurement signal. The lab-scale measurements however, were performed for only about 500 h. In order for these test runs to reflect, or come close to, real-life conditions, the start-up error could not be neglected. For this purpose, a methodology was developed enabling reliable determination of corrosion rates with online corrosion probes during short-term test runs. The methodology was based on the combination of a newly developed mass loss probe with an online corrosion probe. Its evaluation is included in section 5.1.2.

In the following sections, specific conclusions for the real-scale test runs, the lab-scale test runs and the analyses of corrosion probes are presented.

5.1.1 Real-scale measurements

Within the scope of the work presented, real-scale measurements were conducted using two online corrosion probes in parallel at two positions in the radiative sections of biomass CHP plants (grate furnaces with water-tube steam boilers). Soot blowing was not investigated as an influencing parameter during these test runs, because no soot blowers were installed at the positions of the online corrosion probe measurements. Test runs were performed in one plant firing chemically untreated wood chips and in one plant firing a mix of 50 % chemically untreated wood chips, 45 % waste wood of categories A1-A3 and 5 % waste wood of category A4 in accordance with German standards. Within each of the test runs, the influence of the probe surface temperature and of the flue gas

temperature on the corrosion rate was investigated. Probe surface temperatures were varied within a range of 400°C to 560°C whereas flue gas temperatures were investigated in the range between 730°C and 930°C in the wood chips fired CHP plant and in the range between 730°C and 900°C in the waste wood fired CHP plant. In these test runs, the high-temperature corrosion behaviour of the low alloyed superheater steel 13CrMo4-5 was investigated.

Conclusions

The measurements revealed immediate reactions of the online corrosion signal to changes in probe surface temperatures and flue gas temperatures.

Generally, higher temperatures of the probe surface and the flue gas resulted in increased corrosion rates. For probe surface temperatures, these correlations were determined over longer periods by measurements conducted in both plants. In this way it was possible to establish a clear correlation between probe surface temperatures and corrosion rates.

A specific influence of the flue gas temperatures on corrosion rates was only ascertained during the test runs in the wood chips fired CHP plant. In this case, the data were evaluated over longer periods (weeks) and then served to establish a correlation between flue gas temperature and corrosion rate. The data obtained in the waste wood fired CHP plant showed increasing corrosion rates corresponding to increasing flue gas temperatures, too. However, a clear trend was only found for short intervals (days). In an extended evaluation (weeks), the influence of the flue gas temperature was found to be of minor significance. A possible explanation can be found in the fuel composition, which was changing significantly during the test run. These changes most likely resulted in different corrosion rates at similar probe and flue gas temperatures. Additionally, the SEM/EDX analyses of the online corrosion probes revealed multiple corrosion layers detached from the probe itself. This indicated a detachment of the corrosion layers during the measurements, which also influenced the measurement signal. These influencing factors also affected the correlation between corrosion rate and probe surface temperature. The correlation in this case is assumed to have resulted from the significantly stronger influence of the probe surface temperature on the corrosion rate, compared to the influence of the flue gas temperature (determined for short intervals).

The application of two online corrosion probes in parallel provides the advantage of conducting measurements at different flue gas temperatures. For the measurements in the wood chips fired CHP plant, the corrosion rates measured by the two online corrosions probes showed a distinctive dependency on the flue gas temperature. This dependency was found for both online corrosion probes with good agreement of the values for overlapping flue gas temperatures. Therefore, the parallel application of two probes provides the advantage of covering a larger range of flue gas temperatures within one test run. In the waste-wood fired CHP plant no clear correlation between the flue gas temperature and the corrosion rate was determined. Hence, also the data from the two online corrosion probes could not be combined.

The corrosion rates determined within the test runs were too high when compared with the practical experience of boiler manufactures and plant operators. The most likely reason may be the variations in the probe surface temperature between 400°C and 560°C. These caused spallation of the oxide layers as well as of the deposits (summed up in section 5.1.3). After spallation, it was possible for corrosive agents to attack the ground material, which resulted in higher corrosion rates compared with superheater tubes in a steady-state operation plant. Hence, the absolute corrosion rates are not directly applicable. But the correlations can be applied nonetheless, e.g. to estimate the increase in the corrosion rate when increasing the steam temperature.

The measurements performed in the real-scale CHP plants demonstrated the applicability of online corrosion probes in biomass fired boilers and provided measurement data on corrosion rates at real plant operation conditions. However, variations in fuel composition as well as limited control of influencing parameters and unexpected shut-downs constituted restraints. Therefore, the determination of the influence of single parameters on the corrosion rate was often not possible.

Recommendations

Online corrosion probes demonstrated their applicability in biomass fired boilers, and they provide a possibility to determine corrosion rates within a certain range of probe surface and flue gas temperatures. However, the corrosion rates determined were significantly higher than the experience of the plant operators showed. This was assumed to result from variations in the probe surface temperature. Therefore, the recommendation is to apply a mass loss probe, which is operated at a constant probe surface temperature, in parallel with the online corrosion probe. In this way, the corrosion rate at steady state operation can be determined and used as a reference value for the data obtained with the online corrosion probe.

Furthermore, online corrosion probes are recommended for the monitoring of corrosion rates at constant probe surface temperatures. This application is of interest if changes in the corrosion rate are expected, due to changes in the fuel used or due to changes in operating conditions. They facilitate immediate evaluation of the corrosion rate due to the combustion of the new fuel or to the changed operating conditions before any damage to the superheaters due to corrosion occurs.

The gathering of data for the development of models to simulate corrosion is not recommended in real-scale test runs. One the one hand it is usually not possible to change individual parameters (e.g. flue gas temperature) without also changing other parameters (e.g. boiler load). Furthermore, operating conditions and fuel compositions can strongly vary and often cannot be controlled. Also, unexpected shutdowns can occur, all of which makes it difficult to get accurate measurement data.

Therefore, it would appear important to perform online corrosion probe measurements for the generation of data used for model development within lab-scale test runs, which

can be operated in well-defined conditions, allow the use of more homogeneous fuels and enable the variation of individual parameters of interest.

5.1.2 Lab-scale measurements

First measurements in the test rig using wood chips showed that the general trend of corrosion rates increasing with increasing probe surface temperatures as well as with increasing flue gas temperature agreed with the results obtained in the real-scale test runs. However, since lab-scale measurements cover a shorter time span (about 500 h) than real-scale measurements (several 1000 h), the start-up error (summed up in section 5.1) occurring during online corrosion probe measurements must not be neglected.

Therefore, a new methodology was developed based on a mass loss probe which is applied in parallel with the online corrosion probe. In accordance this methodology, the test runs are divided into two phases. Phase 1 is the initial phase, in which the build-up of a fully developed layer on the online corrosion probe occurs. After the initial phase, the measurement signal from the online corrosion probe is directly proportional to the real corrosion rate. In phase 2, the variation phase, the influencing parameters - probe surface temperature and flue gas temperature - are varied to determine their influence on the corrosion rate. The mass loss probe allows the determination of the mass loss during the variation phase, which is subsequently used to calculate corrosion rates from the measurement signal of the online corrosion probe. In this way, the wrong measurement data from the initial phase are excluded, and the start-up error does not influence the results. These values are referred to as “mass loss corrected corrosion rates”, whereas the rates determined without consideration of the mass loss probe are referred to as “original corrosion rates”. The difference between the corrosion rates is referred to as “mass loss correction” (see section 4.2.1).

Short-term lab-scale measurements (about 500 h) were conducted to investigate the corrosion behaviour of the steels 13CrMo4-5 and P91 during the combustion of chemically untreated wood chips. Furthermore, the steels P91 and 1.4541 were investigated during the combustion of waste wood.

Conclusions

The new methodology was used for all lab-scale measurements presented in this thesis. For all test runs, the values for mass loss correction were determined since different combinations of biomass fuels and superheater steels may result in different types of corrosion which may influence the start-up error.

The measurements demonstrated that the values of mass loss correction ranged from 32 % (for wood chips – P91) up to 77 % (for waste wood – 1.4541). This means that corrosion rates determined by means of the online corrosion probe differed between 32 % and 77 % from reality due to the different start-up errors.

On the one hand these results show that the new methodology constitutes a proper evaluation method for short-term online corrosion probe measurements. On the other

hand they clearly show that a comparison of short-term online corrosion probe measurements for different biomass fuels and different superheater materials is inaccurate without taking the start-up error into consideration.

The calculation of corrosion rates from the measurement signal is based on the determination of the mass loss from mass loss rings. This method is also applied to the mass loss probe. For this purpose, all corrosion products have to be removed from the mass loss ring without removing any uncorroded material. In the present case, the corrosion products were dissolved in acidic solutions in accordance with ASTM G1-03. This step constitutes a possible source of error since corrosion products may tend to stick to the uncorroded material, although uncorroded steel is already being dissolved. This behaviour was found to be dependent on the fuel used and on the superheater steel used. Therefore, the removal of corrosion products has to be thoroughly tested prior to a measurement campaign.

The corrosion rates determined for different superheater steels during the combustion of wood chips and waste wood were correlated with probe surface temperatures and flue gas temperatures. Beside the dependency of the corrosion rate on the probe surface temperature, and in contrast to the real-scale waste wood measurements, also a clear dependency on the flue gas temperature was possible over longer intervals for all test runs. Here, the principal objective of the lab-scale test runs, a detailed investigation of influencing factors on high-temperature corrosion at more stable conditions compared to a real-scale plant, was successfully achieved.

Although the general trends were comparable, the corrosion rates obtained from the lab-scale test runs exceeded the ones from the real-scale test runs. One possible reason is a larger amount of coarse fly ash particles in the flue gas of real-scale plants. These particles are usually formed of Ca, Si and Mg which do not participate in high-temperature corrosion mechanisms. Therefore, they could form a protective layer on the surface of the online corrosion probes in real-scale plants and thereby lead to lower corrosion rates. However, this potential reason was not investigated in detail within this thesis and hence represents an important topic for future work.

Recommendations

Short-term online corrosion probe measurements require the consideration of the start-up error since it significantly influences corrosion rates. Performing these measurements without such a methodology is not recommended. The application of a mass loss probe constitutes a proper methodology for evaluating short-term measurements with online corrosion probes.

In order to accurately determine mass loss by removing corrosion products from mass loss rings, the removal method has to be tested prior to test runs to ensure that corrosion products can be completely removed without removing any uncorroded material.

5.1.3 SEM/EDX analyses of online corrosion probes

Online corrosion probes allow the control of the probe surface temperature by cooling it with pressurized air. In this way, a spectrum of probe surface temperatures can be investigated within a single testing campaign as was done within the research for this paper. In order to evaluate the corrosion processes, the deposits and corrosion products on the online corrosion probes were analysed subsequent to the test run by means of SEM/EDX.

Conclusions

Due to the variations of the probe surface temperatures performed during the test runs, the deposit compositions as well as the compositions of corrosion products were most likely altered. This altering of the chemistry was confirmed by deposit sampling with a deposit probe at constant probe surface temperatures close to the positions of the online corrosion probes. Analyses of these deposits showed small concentrations of chlorine in the deposits sampled in the wood chips fired CHP plant as well as in the deposits sampled in the test rig during the wood chips test runs. Since no chlorine was found in the deposits on the online corrosion probes, it was concluded that the deposits had been altered. At high probe surface temperatures, already deposited chlorides might have evaporated. On the other hand, at times of low probe surface temperatures increased condensation of chlorides might have occurred. This was concluded for the real-scale test runs (see section 4.1.1.3) as well as for the lab-scale test runs (see section 4.2.2.4).

Despite this limitation, the SEM/EDX analyses allow an evaluation of the deposits for the temperature range investigated, e.g. if molten deposits occurred. Especially in combination with deposit probe measurements and SEM/EDX analyses of these deposits, such conclusions can be drawn.

An evaluation of the corrosion products revealed a spallation of the corrosion layers during all test runs. This effect most likely occurred due to probe surface temperature variations. Therefore, the corrosion layer differs from a corrosion layer which is formed in a real-scale plant under conditions of steady-state operation. Hence, conclusions on the formation of corrosion layers in real-scale plant are limited. Nonetheless, the SEM/EDX analyses performed within this work allowed a qualitative comparison of the different steels used in the different test runs.

The chemistry at the corrosion front is of special interest since it allows an evaluation of the corrosion mechanisms prevailing. However, as already stated for the deposit chemistry, the temperature variations performed during the test runs cause a limitation regarding the value of the results. Similar to the chemical compositions of the deposits, also the chemistry at the corrosion front is altered by temperature variations. Hence, the corrosion mechanisms in steady-state operated plants may deviate from the corrosion mechanisms derived from the SEM/EDX analyses. Furthermore, possible changes in the corrosion mechanism occurring within the temperature variations from 400°C to 560°C cannot be determined.

Nonetheless, the SEM/EDX analyses allow conclusions whether the corrosion process is dominated e.g. by Cl or S. Furthermore, the type of corrosion can be determined (e.g. trough-shaped corrosion, uniform corrosion or pitting).

Recommendations

Although variations of the probe surface temperature alter the chemistry and structure of deposits and corrosion products, SEM/EDX analyses of online corrosion probes subsequent to test runs should be performed. These analyses allow an evaluation of deposits formed in the temperature range investigated and allow a comparison of corrosion products from different test runs. Furthermore, they allow a first evaluation of the dominating corrosion mechanism.

In order to gain specific results for a certain probe surface temperature, measurements with a corrosion probe (or a mass loss probe) operated at a constant probe surface temperature should be performed. For these measurements, a simpler probe compared to the online corrosion probe can be used since no online measurements data are required. By means of SEM/EDX analyses of such a probe, the deposit formation, the formation of a corrosion layer as well as specific information on the corrosion mechanism will be gained.

Since the corrosion process on a probe operated at constant probe surface temperatures would be comparable to a superheater tube applied in a real-scale plant under steady-state operation, also the corrosion rate should be comparable. The application of this probe in parallel with an online corrosion probe would allow the determination of the corrosion (or the mass loss of a test ring) which could be used as a reference value with regard to the data from the online corrosion probe.

5.2 Outcome of measurements – Evaluation of results

5.2.1 Fuels

Within the work presented in this thesis, chemically untreated wood chips and waste wood (A1-A4 in accordance with German standards) were used as fuels. The most significant general difference regarding high-temperature corrosion is a significantly lower molar 2S/Cl ratio in waste wood (1.7 – 2.2) compared to wood chips (6.0 – 8.8). Therefore, the risk of Cl-induced active oxidation is higher for waste wood.

Furthermore, waste wood contains higher concentrations of heavy metals. This is of relevance to the possible occurrence of hot corrosion type II. Deposits in biomass fired boilers typically contain alkali sulphates (K_2SO_4 and Na_2SO_4). In general, the melting temperatures of these sulphates are too high for melting to occur. However, the presence of heavy metals in deposits can significantly reduce the melting temperature of deposits due to the formation of eutectics with relatively low melting points, even below 500°C. Therefore, the risk of hot corrosion type II is significantly higher when firing fuels with elevated heavy metal contents, such as waste wood.

5.2.2 Real-scale measurements

The real-scale measurements in a wood chips fired CHP plant provided data for corrosion rates of 13CrMo4-5 dependent on probe surface temperatures (T_S) between 400°C – 560 °C and of flue gas temperatures (T_{FG}) between 710°C – 950°C. Within these temperature ranges, corrosion rates from 0.02 – 0.18 mm/1000h were determined. The corrosion rates showed a strong dependence on the probe surface temperature but only a minor dependence on the flue gas temperature. Within these test runs no dependency on the flue gas velocity was established.

Corrosion rates of 13CrMo4-5 in the waste wood fired CHP plant were determined for T_S = 400°C - 560°C and T_{FG} = 730°C - 900°C and resulted in corrosion rates ranging from 0.05 to 0.6 mm/1000h. During these measurements only a minor dependency on the flue gas temperature was determined, and only the probe surface temperature could be correlated with the corrosion rates. Also, the flue gas velocity had no measureable influence on the corrosion rate. The significantly higher corrosion rates, compared with the wood chips fired CHP plant, most likely resulted from increased concentrations of Cl (or lower ratios of 2S/Cl) as well as from elevated heavy metal contents (Zn, Pb) in the fuel.

The corrosion rates determined within the measurements were too high when compared with the practical experience of the plant operators, as already discussed in the evaluation of methods (section 5.1.1). However, the correlations can be applied using data from experience, e.g. to estimate the increase in the corrosion rate when increasing the steam temperature

5.2.3 Lab-scale measurements

The lab-scale measurements were performed using the new methodology developed within this work, which uses a mass loss probe in parallel to an online corrosion probe. During the lab-scale measurements, the corrosion rate trends in the initial phase of each test run were determined. These trends followed a paralinear rate law in all test runs performed. Together with the determination of the corrosion rate trends in the initial phase, the mass loss correction was determined for each test run (see section 4.2.1). In the following section, only the mass loss corrected corrosion rates presented in section 4.2.2.2 are discussed.

Corrosion rates of the steels 13CrMo4-5 and P91 were determined for the combustion of chemically untreated wood chips. For the combustion of waste wood, the corrosion rates of the steels P91 and 1.4541 were determined. The corrosion rates were determined for T_S = 400°C - 550°C (13CrMo4-5) or 560°C (P91 and 1.4541) and for T_{FG} = 740°C - 900°C. The flue gas temperatures at the position of the online corrosion probe differed between the individual test runs. In order to be able to compare the data, the corrosion rates were fitted. By this, a comparison of corrosion rates at similar flue gas temperatures was achieved. In the following sections the results are briefly summarized on the basis of

selected probe surface and flue gas temperatures in order to illustrate themost relevant findings.

Within the test runs with chemically untreated wood chips, 13CrMo4-5 and P91 showed a comparable resistance to high-temperature corrosion at T_{FG} =750°C. This applies to T_S = 400°C (13CrMo4-5: k = 0.009 mm/1000h; P91: k = 0.006 mm/1000h) as well as to T_S = 550°C (13CrMo4-5: k = 0.162 mm/1000h) or T_S = 560 °C (P91: k = 0.186 mm/1000h). At the higher flue gas temperature of T_{FG} = 850°C, however, the corrosion rates of 13CrMo4-5 exceeded the ones of P91 (e.g. at T_S = 400°C; 13CrMo4-5: k = 0.319 mm/1000h; P91: k = 0.286 mm/1000h). Therefore, it was concluded that P91 has a higher resistance to high temperature corrosion at high flue gas temperatures above 850°C but no significant difference was noted at lower flue gas temperatures up to 750°C.

The values of the corrosion rates determined during the waste wood test runs showed significantly lower corrosion rates for 1.4541 compared to P91. The highest corrosion rate at T_S = 560 °C and T_{FG} = 850 °C for 1.4541 was 0.040 mm/1000h, which was still below the lowest corrosion rate for P91 at T_S = 400 °C and T_{FG} = 750 °C with 0.048 mm/1000h. This shows that 1.4541 has a significantly higher resistance to high-temperature corrosion than P91.

P91 was used for wood chips combustion and waste wood combustion. Hence, a direct comparison of the corrosion rates is possible. In general, the corrosion rates were in the same range. However, the rates showed different dependencies on the probe surface temperature. At T_{FG} = 750°C and low probe surface temperatures (T_S = 400°C), the rates were higher for waste wood combustion (k = 0.048 mm/1000h) than for wood chips combustion (k = 0.006 mm/1000h). At T_{FG} = 750°C and T_S = 560°C, however, the rates were lower for waste wood combustion (k = 0.0151 mm/1000h) than for wood chips combustion (k = 0.186 mm/1000h). This shows that the influence of the probe surface temperature was significantly higher for wood chips combustion, which was also found in earlier work [53].

These results show that different superheater steels may show different dependencies on influencing factors such the fuel used and the probe surface temperature. Therefore, making general suggestions for superheater steels is hardly possible; they need to be evaluated specifically for certain boundary conditions. The method developed within this work provides a basis for making this evaluation.

5.2.4 Corrosion mechanisms

As pointed out in the evaluation of methods (see section 5.1.3), due to the variations of the probe surface temperatures performed within the test runs, the conclusions that can be drawn from the SEM/EDX analyses of online corrosion probes are limited. However, in combination with the deposits probe measurements possible corrosion mechanisms were determined.

For chemically untreated wood chips, analyses of the online corrosion probe did not clarify the high-temperature corrosion mechanisms with any certainty since no Cl, which would indicate active Cl-induced oxidation, was found. However, S was found at the corrosion front in some cases (real-scale test run with 13CrMo4-5, lab-scale test run with 13CrMo4-5) which indicates a role of S in the corrosion process. S may participate in the direct reaction of gaseous SO_2 with the steel as well as in the sulphidation of metal chlorides formed during Cl-induced active oxidation. Since the deposit probe measurements conducted in real-scale as well as in lab-scale revealed low concentrations of Cl in the deposits sampled at 480°C, Cl-induced active oxidation is also possible.

Based on these findings, it is suggested that the corrosion mechanism during wood chips combustion is a combination of Cl-induced oxidation, direct oxidation of the steel by oxygen from the flue gas as well as possibly a direct reaction of SO_2 with the steel.

For waste wood combustion, elevated levels of S and Cl were found at the corrosion front. Furthermore, significant concentrations of Cl were found in the deposit in the real-scale as well as in the lab-scale test runs. This suggests that Cl-induced active oxidation is a relevant mechanism.

Additionally, sintered or molten deposit layers were confirmed by SEM/EDX analyses of the corrosion probes. Molten deposits were also confirmed by SEM pictures of the deposits sampled during waste wood combustion. The melting of deposits was most likely caused by the presence of alkali sulphates in combination with heavy metals in deposits. Here, eutectics with relatively low melting points, even below 500°C are likely to have been formed. This suggests that hot corrosion type II is also a relevant corrosion mechanism in the case of waste wood combustion.

5.2.5 Corrosion resistance of the steels investigated

13CrMo4-5 was investigated for wood chips combustion. 13CrMo4-5 is a low alloyed steel, mainly consisting of Fe (about 97 wt.%). Hence, Fe is the relevant reacting element, which cannot form a passivating layer. In this case, Cl-induced active oxidation, hot corrosion type II, but also a direct oxidation of the iron by oxygen from the flue gas as well as possibly a direct reaction of SO_2 with the iron are potential corrosion mechanisms affecting 13CrMo4-5.

P91 is a medium alloyed steel containing 8.75 wt.% Cr. This Cr content is usually not enough for the formation and maintenance of a complete passivating Cr_2O_3 layer on the surface of the material, which lies typically at 10 wt.% . Hence, in the case of P91, an oxide layer containing chromium oxides as well as iron oxides will be formed in the event of corrosion. Therefore, the direct reaction of Fe as well as of Cr is relevant to this steel. The corrosion rates determined for P91 were only slightly lower compared to 13CrMo4-5 for the case investigated. Even though the Cr content is not high enough for a full passivating layer, the slightly better corrosion resistance can most likely be explained by the relevant Cr content (8.75 wt.%) and the generally better corrosion resistance of Cr compared with Fe.

1.4541 contains 18 wt.% Cr, which leads to the formation of a passivating Cr_2O_3 layer. Therefore, the penetration of the passivating layer by corrosive agents, or the dissolution of the layer, are key reactions during the corrosion process. While the penetration of an intact passivating layer is hardly possible, dissolution of the Cr_2O_3 layer is generally possible during Cl-induced active oxidation as well as by hot corrosion type II. This dissolution can subsequently lead to the formation of pores and cracks, which enable a penetration of the corrosion layer by the corrosive agents S, Cl and O. Since the investigations performed showed that corrosion occurs under the conditions investigated, it is concluded that dissolution and, as a consequence, a penetration of the Cr_2O_3 layer takes place. However, the corrosion rates determined show that 1.4541 has a significantly higher resistance to high-temperature corrosion than P91 in the case investigated.

5.2.6 Application of results

As already discussed in the evaluation of methods (section 5.1.2), the corrosion rates determined within the lab-scale test runs as well as the ones determined in real-scale are higher than the rates obtained from the practical experience of plant operators. However, the data can be used to evaluate the impact of a change of an influencing factor, e.g. the increase of the probe surface temperature (representing the steam temperature in a steam boiler).

The findings may be used, for instance, as a basis to evaluate if the corrosion rate at is still acceptable at an increased steam temperature. Also the application of a superheater at a position with a higher flue gas temperature can be evaluated regarding the risk of high-temperature corrosion using the data gathered within this work.

An example of such an application is shown for waste wood combustion with the superheater steel P91 based on the measurements in the test rig (section 4.2.2).

- An increase in the probe surface temperature (representing the steam temperature) from 400°C to 560°C at a flue gas temperature of 750°C, increases the corrosion rate by a factor of 3.2 (from 0.05 mm/1000h to 0.15 mm/1000h according to the data from the lab-scale test runs).
- If the superheater is exposed to a flue gas temperature of 850°C instead of 750°C at a probe surface temperature of 400°C, the corrosion rate increases by a factor of 1.4 (from 0.05 mm/1000h to 0.07 mm/1000h according to the data from the lab-scale test runs).

Furthermore, a comparison of corrosion rates for different superheater steels is possible. An example of this is shown for waste wood combustion with the superheater steels P91 and 1.4541 based on the measurements in the test rig:

- For a probe surface temperature of 560°C and a flue gas temperature of 750°C, the corrosion rate can be reduced by a factor of 3.8 by the application of 1.4541 (k = 0.04 mm/1000h) instead of P91 (k = 0.15 mm/1000h).

This application example shows that the work performed within the scope of this thesis forms a basis for the choice of appropriate steam parameters and appropriate flue gas temperatures occurring at superheaters. Since higher alloyed superheater materials usually show better corrosion resistance but are typically more expensive, the work also forms a basis for the correct material selection for superheater tubes. However, a consideration of costs was not part of this work and is the concern of plant manufacturers.

5.2.7 Realisation of increased steam temperatures in future CHP plants

The results of the survey conducted at the beginning of this work showed that, in 2012, 540°C constituted the upper limit of steam temperatures in biomass fired water-tube steam boilers. The majority of plants were equipped with superheaters made from low alloyed superheater steels. In this case, a maximum steam temperature of 500 °C was determined. Based on the results of measurements performed within this work it is concluded that increased steam temperature are generally feasible if the proper type of steel is selected for the superheaters.

For wood chips combustion, the use of low alloyed steels is not recommended to achieve these increased steam temperatures since their application is limited to approximately 560°C material temperature in continuous operation. Within this thesis, higher alloyed superheater materials generally showed better corrosion resistance throughout the temperatures ranges investigated. P91 showed only slightly better corrosion resistance than 13CrMo4-5 at flue gas temperatures above 850°C. However, at flue gas temperatures below 750°C, comparable corrosion rates were found. Hence, P91 is not considered an appropriate choice to achieve steam temperatures above 540°C.

Although a higher alloyed steel such as 1.4541 was not investigated for wood chips combustion within this research, waste wood combustion corrosion rates were determined for stainless steel 1.4541 as well as for P91. At a material temperature of 560°C the corrosion rates of 1.4541 were between 4.2 to 4.6 times lower than the corrosion rates of P91.

Based on the possible corrosion mechanisms (see section 5.2.4), the conclusion is that 1.4541 will also show a significantly higher corrosion resistance in the case of wood chips combustion. Hence, the application of a heat resistant stainless steel such as 1.4541 can be recommended for wood chips combustion to realise steam temperatures above 540°C in future biomass-fired water-tube steam boilers.

Furthermore, 1.4541 can also be recommended for waste wood combustion to increase steam temperatures compared to the current state. Since the corrosion rates determined within this work are higher than actual values determined by plant operators, an estimation of achievable maximum temperatures is not possible from the data available. However, the application of a superheater material which has at least the corrosion resistance of heat resistant stainless steel is considered necessary to achieve steam temperatures of 540°C or higher for waste wood combustion systems.

6 Future work / Outlook

The work performed provides data on high-temperature corrosion rates and their dependence on influencing factors. However, the values for the corrosion rates obtained are higher than the known corrosion rates in real boilers. The most likely reason is the variation of the probe surface temperature performed during the test runs. The application of a mass loss probe which is operated at constant probe surface temperatures and applied in parallel with an online corrosion probe would allow the determination of the corrosion rate at steady state operations. This corrosion rate could serve as a reference value for the data obtained with the online corrosion probe. The application of the proposed methodology is planned for future test runs.

The application of a mass loss probe operated at constant probe surface temperatures will also allow the investigation of deposits and corrosion products; it will also furnish specific information on the corrosion mechanism for a certain/specific probe surface temperature. This information was only available to a limited extent from the online corrosion probes due to the temperature variations.

Within the lab-scale measurements, the evaluation of mass loss for different superheater steels was determined as a possible source of error which may affect the accuracy of results. For future work, the methodology for the removal of corrosion products will have to be thoroughly tested prior to test runs. Therefore, different methods for the removal of corrosion products will be tested.

Furthermore, the differing corrosion rates determined within lab-scale measurements and real-scale measurements need to be determined. One possible difference is the amount of coarse fly ash particles in the flue gas, which is typically higher in real-scale plants. These particles are usually formed of Ca, Si and Mg which do not participate in high-temperature corrosion mechanisms and could therefore form a protective layer on the surface of the online corrosion probes resulting in lower corrosion rates. In order to ascertain corrosion rates closer to real-scale applications, this issue will be investigated further.

Within this thesis corrosion rates for certain combinations of biomass fuels and superheater steels were determined. In future research activities, also more detailed investigations into the effect of additives of high-temperature corrosion should be conducted in order to allow the use of cheap low quality fuels while reducing corrosion (and ash deposition) risks. To this end, special additives which are available at low cost such as residues from industrial processes are of interest. For future test runs, the application of recycled gypsum and coal fly ash is planned.

7 Bibliography

[1] European Comission, “EUR-Lex homepage: Access to European Union law,” [Online]. Available: http://eur-lex.europa.eu/legal-content/EN/TXT/PDF/?uri=CELEX:52015DC0080&from=EN. [Accessed 16 08 2015].

[2] S. Retschitzegger, T. Brunner, I. Obernberger and B. Waldmann, “Assessment of Online Corrosion Measurements in Combination with Fuel Analyses and Aerosol and Deposit Measurements in a Biomass Combined Heat and Power Plant,” *Energy & Fuels,* vol. 27, no. 10, pp. 5670-5683, 2013.

[3] R. Antunes and M. de Oliveira, “Corrosion in biomass combustion: A materials selection analysis and its interaction with corrosion mechanisms and mitigation strategies,” *Corrosion Science,* vol. 76, pp. 6-26, 2013.

[4] D. O. Albina, “Theory and experience on corrosion of waterwall and superheater tubes of waste-to-energy facilities,” PhD thesis, Columbia University, New York, USA, 2005.

[5] H. Nielsen, F. Frandsen, K. Dam-Johansen and L. Baxter, “The implications of chlorine-associated corrosion on the operation of biomass-fired boilers,” *Pogress in Energy and Combustion Science,* vol. 26, no. 3, pp. 283-298, 2000.

[6] C. Schroer and J. Konys, “Rauchgasseitige Hochtemperatur-Korrosion in Müllverbrennungsanlagen - Ergebnisse und Bewertung einer Literaturrecherche,” Forschungszentrum Karlsruhe GmbH, Karlsruhe, 2002.

[7] W. Sharp, “SUPERHEATER CORROSION IN BIOMASS BOILERS: Today’s Science and Technology,” Technical report, 2010.

[8] R. W. Bryers, “Fireside slagging, fouling, and high-temperature corrosion of heat-transfer surface due to impurities in steam-raising fuels,” *Progress in Energy and Combustion Science,* vol. 22, no. 1, pp. 29-120, 1996.

[9] T. Blomberg, “Correlation of the corrosion rates of steels in a straw fired boiler with the thermodynamically predicted trend of KOH(g) in the flue gases,” *Biomass and Bioenergy,* vol. 39, pp. 489-493, 2012.

[10] F. J. Frandsen, “Utilizing biomass and waste for power production - a decade of contributing to the understanding, interpretation and analysis of deposits and corrosion products,” *Fuel,* vol. 84, no. 10, pp. 1277-1294, 2005.

[11] L. A. Hansen, H. P. Nielsen, F. J. Frandsen, K. Dam-Johansen, S. Harlyck and A. Karlsson, “Influence of deposit formation on corrosion at a straw-fired boiler,” *Fuel*

Processing Technology, vol. 64, no. 1-3, pp. 189-209, 2000.

[12] H. P. Michelsen, F. Frandsen, K. Dam-Johansen and O. H. Larsen, "Deposition and high temperature corrosion in a 10 MW straw fired boiler," *Fuel Processing Technology,* vol. 54, no. 1-3, pp. 95-108, 1998.

[13] S. B. Hansen, P. A. Jensen, F. J. Frandsen, H. Wu, B. Sander, J. Wadenbäck and P. Glarborg, "Deposit probe measurements in Danish grate and pulverized fuel biomass power boilers," in *Proceedings Impacts of Fuel Quality on Power Production and Environment*, 2012.

[14] O. H. Larsen and N. Henrisken, "Ash Deposition and High Temperature Corrosion at Combustion of Aggressive Fuels," in *Int. Conf. on Power Plant Chemical Technology*, 1997.

[15] S. van Lith, F. J. Frandsen, M. Montgomery, T. Vilhelmsen and S. A. Jensen, "Lab-scale Investigation of Deposit-induced Chlorine Corrosion of Superheater Materials under Simulated Biomass-firing Conditions. Part 1: Exposure at 560 °C ," *Energy & Fuels,* vol. 23, no. 7, pp. 3457-3468, 2009.

[16] M. Montgomery, S. A. Jensen, U. Borg, O. Biede and T. Vilhelmsen, "Experiences with high temperature corrosion at straw-firing power plants in Denmark," *Materials and Corrosion,* vol. 62, no. 7, pp. 593-605, 2011.

[17] M. Montgomery, A. Karlsson and O. H. Larsen, "Corrosion Investigations at Masnedø Combined Heat and Power Plant Part VI," Technical University of Denmark, Lyngby , 2001.

[18] H. Nielsen, L. Baxter, G. Sclippab, C. Morey, F. Frandsen and K. Dam-Johansen, "Deposition of potassium salts on heat transfer surfaces in straw-fired boilers: a pilot-scale study," *Fuel,* vol. 79, no. 2, pp. 131-139, 2000.

[19] H. P. Nielsen, F. J. Frandsen and K. Dam-Johansen, "Lab-Scale Investigations of High-Temperature Corrosion Phenomena in Straw-Fired Boilers," *Energy & Fuels,* vol. 13, no. 6, pp. 1114-1121, 1999.

[20] Y. Alipour, "High temperature corrosion in a biomass-fired power boiler - Reducing furnace wall corrosion in a waste wood-fired power plant with advanced steam data," Licentiate Thesis, KTH Royal Institute of Technology, Stockholm, 2013.

[21] D. Bankiewicz, "Corrosion behaviour of boiler tube materials during combustion of fuels containing Zn and Pb," PhD thesis, Abo Akademi, Turku, 2012.

[22] W. Sharp, L. Douglas and J. R. Keiser, "Energy from Biomass - Lessons from European Boilers," Sharp Consultant, Columbia, MD, USA, 2011.

[23] I. Obernberger and T. Brunner, “Deposition und Korrosion in Biomassefeuerungen,” in *Tagungsband zum VDI-Seminar 430504 "Beläge und Korrosion in Großfeuerungsanlagen"*, 2004.

[24] S. Maisch, B. Waldmann, R. Warnecke, R. Haider and S. Horn, “Quantifizierte Korrosionsgeschwindigkeit in Abhängigkeit der Rohrwand- und Rauchgastemperatur,” in *VDI-Fachkonferenz - Feuerung und Kessel - Beläge und Korrosion - in Großfeuerungen*, 2010.

[25] A. Atkinson, “Transport processes during the growth of oxide films at elevated temperature,” *Rev. Mod. Phys.,* vol. 57, pp. 437-470, Apr 1985.

[26] Y. Kawahara, “Evaluation of high-temperature corrosion life using temperature gradient corrosion test with thermal cycle component in waste combustion environments,” *Materials and Corrosion,* vol. 57, no. 1, pp. 60-72, 2006.

[27] S. Retschitzegger, T. Gruber, T. Brunner and I. Obernberger, “Improvement of the accuracy of short-term corrosion probe measurements by addition of a mass-loss probe,” *Fuel Processing Technology,* vol. 137, pp. 148 - 156, 2015.

[28] F. Haider, M. Ziegler, S. Maisch, B. Waldmann, C. Deuerling and R. Warnecke, “Online Corrosion Monitoring - Auswertung ausgewählter Ereignisse,” in *VDI – Fachkonferenz, Feuerung und Kessel - Beläge und Korrosion - in Großfeuerungsanlagen*, 2012.

[29] L. Johansson, J. Svensson, J.Pettersson, C.Pettersson and N. Folkesson, “Beneficial effects of sulphur additions on superheater corrosion - Results from laboratory exposures and field studies,” in *Verfahrenstechnik und Konstruktion in Grossfeueranlagen* , Frankfurt , 2007.

[30] P. Kofstad, High Temperature Corrosion, ELSEVIER APPLIED SCIENCE PUBLISHERS LTD, 1988, ISBN: 1851661549.

[31] Thyssen-Krupp, *Werkstoffblatt TK 1.7335,* Mülheim a. d. Ruhr: THYSSENKRUPP MATERIALS INTERNATIONAL GMBH, 2008.

[32] S. Retschitzegger, T. Brunner and I. Obernberger, “Untersuchung von Frischdampfparametern,” Technical report, BIOENERGY 2020+, Graz, 2011.

[33] C. B. Petersen, “Germany's first 100% straw-fired CHP plant,” 2012. [Online]. Available: http://www.bwe.dk/download/press_pdf/press20121201_en.pdf. [Accessed 19 10 2016].

[34] B.-J. Skrifvars, R. Backman, M. Hupa, K. Salmenoja and E. Vakkilainen, “Corrosion of

superheater steel materials under alkali salt deposits Part 1: The effect of salt deposit composition and temperature," *Corrosion Science,* vol. 50, no. 5, pp. 1274-1282, 2008.

[35] Siemens, "Siemens commissions record-high-efficiency 750MW steam power plant Lünen in Germany," Siemens, 2013. [Online]. Available: www.siemens.com/press/en/pressrelease/?press=/en/pressrelease/2013/energy/power-generation/ep201312013.htm&content[]=EP&content[]=PG. [Accessed 14 12 2015].

[36] C. Pettersson, "KCl-Induced High Temperature Corrosion of the Austenitic Fe-Cr-Ni Alloys 304L and Sanicro 28 at 600 °C," *Corrosion Science,* pp. Vol. 48, 6. 1368-1378, 2006.

[37] B. Waldmann, "Korrosion in Anlagen zur thermischen Abfallverwertung: elektrochemische Korrosionserfassung und Modellbildung," PhD thesis, Augsburg University, Augsburg, 2007.

[38] S. Maisch, "Identifikation und Quantifizierung von korrosionsrevlevanten Parametern in Müllverbrennungsanlagen mittels Charakterisierung der deponierten Partikel und elektrochemischer Online-Messungen," PhD thesis, Augsburg University, Augsburg, Germany, 2011.

[39] F. Haider, S. Horn, B. Waldmann and R. Warnecke, "Quantifizierung des Korrosionsdiagramms auf der Basis von Messungen mit der Augsburger Korrosionssonde," in *VDI-Wissensforum, Beläge und Korrosion*, 2008.

[40] D. Farrell and B. Robbins, "On-Line Monitoring of Furnace Corrosion," *OMMI,* vol. 3, August 2004.

[41] D. Farrell and B. Robbins, "ON-LINE MONITORING OF FURNACE WALL AND SUPERHEATER," in *39th Corrosion Science Symposium*, University of Northumbria at Newcastle, U.K, 1998.

[42] J. Beutler, K. Davis, T. Shurtz, D. Bai, R. Jafari and W. Cox, "Real-time Corrosion Monitoring during Co-firing of Accordant Energy's ReEngineered Feedstock," in *Proceedings of "Impacts of Fuel Quality on Power Production"*, Snowbird, Utah, USA, 2014.

[43] DIN 50 900, Begriffe der Korrosion, Teil 1: Allgemeine Begriffe. Grundlagen und Ziele der Begriffsnorm – Ein Rückblick nach fünfjährigem Bestehen dieser Norm.," *Materials and Corrosion,* pp. 33-36, 1981.

[44] Richardson, Shreir's Corrosion, Vols. Vol. 1-4, Elsevier Science, ISBN: 9780444527882, 2009.

[45] P. Gellings and K. Tostmann, Korrosion und Korrosionsschutz von Metallen: eine Einführung, München, Germany: Carl Hanser Verlag; ISBN: 3-446-12594-9, 1981.

[46] H. Grabke, E. Reese and M. Spiegel, "The effects of chlorides, hydrogen chloride, and sulfur dioxide in the oxidation of steels below deposits," *Corrosion Science,* vol. 37, no. 7, pp. 1023-1043, 1995.

[47] M. Schütze, Protective oxide scales and their breakdown, D. Holmes, Ed., John Wiley & Sons, 1997.

[48] M. Schütze, "Fundamentals of High Temperature Corrosion," in *Corrosion and Environmental Degradation*, Weinheim, Germany, Wiley VCH; ISBN: 9783527299713, 2000, pp. 67-130.

[49] T. Brunner, F. Biedermann, W. Kanzian, N. Evic and I. Obernberger, "Advanced Biomass Fuel Characterization Based on Tests with a Specially Designed Lab-Scale Reactor," *Energy & Fuels,* pp. 5691-5698, 23 July 2013.

[50] D. Vaughan, H. Krause and W. Boyd, Chloride corrosion and its inhibition in refuse firing. Ash Deposits and Corrosion Due to Impurities in Combustion Gas, New York: Hemisphere Publishing Corporation, 1978.

[51] K. Kautz and J. Tichatschke, "Zusammenhänge zwischen Rauchgasverhältnissen, Kesselbelastung und Korrosionen in einer kommunalen Müllverbrennungsanlage," *VGB Kraftwerkstechnik,* pp. 249-263, 1972.

[52] H. Asteman and M. Spiegel, "Investigation of the HCl (g) attack on pre-oxidized pure Fe, Cr, Ni and commercial 304 steel at 400°C," *Corrosion Science,* vol. 49, p. 3626–3637, 2007.

[53] T. Gruber, K. Schulze, R. Scharler and I. Obernberger, "Investigation of the corrosion behaviour of 13CrMo4-5 for biomass fired boilers with coupled online corrosion and deposit probe measurements," *Fuel,* vol. 144, pp. 15-24, 2015.

[54] P. Sommersacher, T. Brunner and I. Obernberger, "Fuel Indexes: A Novel Method for the Evaluation of Relevant Combustion Properties of New Biomass Fuels," *Energy & Fuels,* p. 11, 2011.

[55] K. Salmenoja, "Field and laboratory studies on chlorine-induced superheater corrosion in boilers fired with biofuels," PhD-thesis, Abo Akademi, Turku, 2000.

[56] C. P. O'Hagan, B. O'Brien, F. Griffin, B. Hooper, S. Leen and R. Monaghan, "Porosity-Based Corrosion Model for Alkali Halide Ash Deposits during Biomass Co-firing," *Energy & Fuels,* vol. 29, pp. 3082-3095, 2015.

[57] R. Riedl, J. Dahl, I. Oberberger and M. Nardoslawsky, “Corrosion in fire tube boilers of biomass combastion plants,” *Proceedings of the China international corrosion control conference '99,* Vols. -, pp. 1-5, 1999.

[58] M. Spiegel, “Salt melt induced corrosion of metallic materials in waste incineration plants,” *Materials and Corrosion,* vol. 50, no. 7, pp. 373-393, 1999.

[59] R. A. Rapp, “Hot corrosion of materials: a fluxing mechanism?,” *Corrosion Science ,* vol. 44, no. 2, pp. 209-221, 2002.

[60] Y. S. Zhang and R. A. Rapp, “Solubilities of alpha-Fe2O3 and Fe3O4 in Fused Na2SO4 at 1200 K,” *Journal of The Electrochemical Society,* vol. 132, no. 10, pp. 2498-2501, 1985.

[61] C. Bernsteiner, “Online-Monitoring von Korrosionsvorgängen in Biomasse-befeuerten Anlagen,” BSc thesis, Graz University of Technology, Graz, 2013.

[62] K. Tostmann, Korrosion - Ursachen und Vermeidung, Wiley-VCH, ISBN: 9783527302031, 2001.

[63] C. Deuerling and B. Waldmann, “Innovative Messtechnik zur kombinierten Korrosions- und Materialforschung im Kraftwerksbereich,” in *Proceedings of the 43. Kraftwerkstechnisches Kolloquium*, Dresden, Germany, 2011.

[64] T. Mitchell, D. Voss and E. Butler, “The observation of stress effects during the high temperature oxidation of iron,” *Journal of Matrials Sicence,* vol. 17, pp. 1825-1833, 1982.

[65] ASTM, G1 - 03. Standard Practice for Preparing, Cleaning, and Evaluating Corrosion Test Specimens,” 2011.

[66] EN, 14774-1:2009: Solid biofuels. Determination of moisture content. Oven dry method. Total moisture. Reference method., Published: January 2010.

[67] EN, 14780:2011: Solid biofuels. Sample preparation., Published: June 2011.

[68] EN, 14775:2009: Solid biofuels. Determination of ash content., Published: March 2010.

[69] EN, 15104:2011: Solid biofuels. Determination of total content of carbon, hydrogen and nitrogen. Instrumental methods., Published: February 2011.

[70] EN, 15290:2011: Solid biofuels. Determination of major elements. Al, Ca, Fe, Mg, P, K, Si, Na and Ti., Published: February 2011.

[71] EN 15296:2011: Solid biofuels. Conversion of analytical results from one basis to another., Published: February 2011.

[72] T. Lauren, “Methods and instruments for characterizing deposit buildup on heat exchangers in combustion plants,” Licentiate Thesis, Abo Akademi, Abo/Turku, Finland, 2008.

[73] J. Krook, A. Mårtensson, M. Eklund and C. Libiseller, “Swedish recovered wood waste: linking regulation and contamination,” *Waste Management,* pp. Vol 8 (3), pp. 638–648, 2008.

[74] Mar Edoa, “Assessment of chemical and material contamination in waste wood fuels – A case study ranging over nine years,” *Waste Management,* pp. Volume 49, 311–319, 2016.

[75] STANDARDKESSEL-LENTJES, “Project no. SES-CT-2033-502679, BIOASH, Ash and aerosol related problems in biomass combustion and co-firing, Deliverable D16, Evaluation of test runs at the large-scale combustion unit of SKG at Elsterwerda,” 2007.

[76] T. Gruber, K. Schulze, R. Scharler, B. Waldmann, F. Haider and I. Obernberger, “Development of an empirical model to describe the local high temperature corrosion risk of 13CrMo4-5 steel in biomass CHP plants regarding the fuel wood chips,” in *Proceedings Impacts of Fuel Quality on Power Production and Environment*, 2012.

[77] F. Gesmundo, D. Young and S. Roy, “The High Temperature Corrosion of Metals in Sulfidizing-Oxidizing Environments: A Critical Review,” *High Temperature Materials and Processes,* vol. 8, pp. 149-190, 2011.

[78] J. Gilewicz-Wolter, “Study of iron oxidation in sulfur dioxide atmospheres by means of the 35S Radioisotope,” *Oxidation of metals,* vol. 11, no. 2, pp. 81 - 91, 1977.

[79] B. Waldmann, “PhD-thesis: Korrosion in Anlagen zur thermischen Abfallverwertung : elektrochemische Korrosionserfassung und Modellbildung,” Augsburg University, Augsburg, Germany, 2007.

[80] H.-H. Reichel and U. Schirmer, “Waste incineration plants in the FRG: Construction, materials, investigation on cases of corrosion,” *Materials and Corrosion,* vol. 40, no. 3, pp. 135-141, 1989.

[81] M. Westen-Karlsson, “Assessment of a Laboratory Method for Studying High Temperature Corrosion Caused by Alkali Salts,” Licentiate Thesis, Abo Akademi, Abo/Turku, Finland, 2008.

[82] H. Evans, “Stress effects in high temperature oxidation of metals,” *International Materials Reviews,* vol. 40, pp. 1-40, 1995.

[83] Y. Li, M. Spiegel and S. Shimada, “Corrosion behaviour of various model alloys with NaCl–KCl coating,” *Materials Chemistry and Physics,* vol. 93, p. 217–223, 2005.

[84] J. Lehmusto, D. Lindberg, P. Yrjas, B.-J. Skrifvars and M. Hupa, “The role of potassium in high temperature corrosion of superheater steels,” in *Proceedings Impacts of Fuel Quality on Power Production and Environment*, 2012.

[85] M. Uusitalo, P. Vuoristo and T. Mäntylä, “High temperature corrosion of coatings and boiler steels below chlorine-containing salt deposits,” *Corrosion Science,* vol. 46, no. 6, pp. 1311-1331, 2004.

[86] R. Antunes, “Corrosion in biomass combustion: A materials selection analysis and its interaction with corrosion mechanisms and mitigation strategies,” *Corrosion Science,* pp. 76, 6–26, 2013.

[87] T. Gruber, “CFD-based modeling approaches for high-temperature corrosion in biomass fired boilers,” PhD thesis, Graz University of Technology, Graz, 2015.

[88] S. van Lith, C. Buchardt and F. J. Frandsen, “Lab-Scale Investigation of the Potential for Corrosion of Deposits,” CHEC Research Centre, Technical University of Denmark, Lyngby, Denmark, 2007.

[89] D. Bankiewicz, “Corrosion behaviour of boiler tube materials during combustion of fuels containing Zn and Pb,” 2012.

[90] S. van Lith, C. Buchardt and F. J. Frandsen, “Lab-Scale Investigation of the Potential for Corrosion of Deposits,” 2007.

[91] G. Yurek, J. Hirth and R. Rapp, “The formation of two-phase layered scales on pure metals,” *Oxidation of Metals,* vol. 8, no. 5, pp. 265-281, 1974.

[92] S. Enestam, P. Björklund, N. Engblom, M. Hamaguchi, M. Rautanen and H. Wallmo, “Energy trends – Recent and future fuel related challenges,” in *Proceedings Impacts of Fuel Quality on Power Production and Environment*, Snowbird, Utah, USA, 2014.

[93] M. Jöller, “Sulfation Modelling of aerosol formation and behaviour in fixed-bed biomass combustion systems, , Graz, 2008,” PhD thesis, Graz University of Technology, Graz, 2008.

[94] M. Montgomery and T. Vilhelmsen, “Experiences with high temperatures corrosion at straw-fired power plants in Denmark,” *Materials and Corrosion,* vol. 62, no. 7, pp.

593-605, 2011.

[95] M. Montgomery, A. Karlsson and O. H. Larsen, “Corrosion Investigations at Masnedo Combined Heat and Power Plant Part VI,” 2001.

[96] M. Spiegel, “Salt melt induced corrosion of metallic materials in waste incineration plants,” *Materials and Corrosion,* vol. 50 (7), no. 7, pp. 373-393, 1999.

8 Annex

8.1 Scientific journal papers